MASTER

GA-5033

RESEARCH ON GRAPHITE

Annual Report April 1, 1963 through March 31, 1964

By
R. J. Price
J. L. White

March 1965
[DTIE Issuance Date]

General Atomic Division
General Dynamics Corporation
San Diego, California

UNITED STATES ATOMIC ENERGY COMMISSION • DIVISION OF TECHNICAL INFORMATION

DISCLAIMER

This report was prepared as an account of work sponsored by an agency of the United States Government. Neither the United States Government nor any agency Thereof, nor any of their employees, makes any warranty, express or implied, or assumes any legal liability or responsibility for the accuracy, completeness, or usefulness of any information, apparatus, product, or process disclosed, or represents that its use would not infringe privately owned rights. Reference herein to any specific commercial product, process, or service by trade name, trademark, manufacturer, or otherwise does not necessarily constitute or imply its endorsement, recommendation, or favoring by the United States Government or any agency thereof. The views and opinions of authors expressed herein do not necessarily state or reflect those of the United States Government or any agency thereof.

DISCLAIMER

Portions of this document may be illegible in electronic image products. Images are produced from the best available original document.

LEGAL NOTICE

This report was prepared as an account of Government sponsored work. Neither the United States, nor the Commission, nor any person acting on behalf of the Commission:

A. Makes any warranty or representation, expressed or implied, with respect to the accuracy, completeness, or usefulness of the information contained in this report, or that the use of any information, apparatus, method, or process disclosed in this report may not infringe privately owned rights; or

B. Assumes any liabilities with respect to the use of, or for damages resulting from the use of any information, apparatus, method, or process disclosed in this report.

As used in the above, "person acting on behalf of the Commission" includes any employee or contractor of the Commission, or employee of such contractor, to the extent that such employee or contractor of the Commission, or employee of such contractor prepares, disseminates, or provides access to, any information pursuant to his employment or contract with the Commission, or his employment with such contractor.

This report has been reproduced directly from the best available copy.

Printed in USA. Price $4.00. Available from the Clearinghouse for Federal Scientific and Technical Information, National Bureau of Standards, U. S. Department of Commerce, Springfield, Va.

USAEC Division of Technical Information Extension, Oak Ridge, Tennessee

GENERAL ATOMIC

DIVISION OF

GENERAL DYNAMICS

JOHN JAY HOPKINS LABORATORY FOR PURE AND APPLIED SCIENCE

P.O. BOX 608, SAN DIEGO 12, CALIFORNIA

GA - 5033
METALS, CERAMICS, AND MATERIALS
(TID - 4500, 38th Ed.)

RESEARCH ON GRAPHITE

ANNUAL REPORT

April 1, 1963, through March 31, 1964

Prepared under
Contract AT(04-3)-167
Project Agreement 12, Task II
for the
San Francisco Operations Office
U.S. Atomic Energy Commission

Work done by:

J. C. Bokros
L. C. Foster
J. O. Gardner
J. E. Knipping
J. M. Pontelandolfo
R. J. Price
J. Schultz
W. M. Schmidt
J. L. White

Report written by:

R. J. Price
J. L. White

PREVIOUS REPORTS IN THIS SERIES

GA-4675—July, August, September, 1963

GA-4901—October, November, December, 1963

CONTENTS

I. INTRODUCTION 1

II. MICROSTRUCTURAL STUDIES 2
2.1. Literature Survey on Micrographic Methods for Graphite . . 2
2.2. Measurement of Preferred Orientation 4
2.3. Quantitative Sensitive-Tint Microscopy 15
2.4. Observations of Pitch Graphitization 15
2.5. Replication Electron Micrography 17
2.6. Fracture Characteristics 27

III. PROCESSING TO ALTER MICROSTRUCTURE 32
3.1. Exploration of Hot-Working Variables 32
3.2. Properties of Hot-Worked Graphites 35
3.3. Fracture Conditions in Hot-Working 44
3.4. X-Ray Diffraction Studies on Hot-Worked Graphite 44
3.5. Preferred Orientation in Hot-Worked Graphite 45
3.6. Recrystallization of Graphite From Liquid Metal 50

IV. RELATION OF PHYSICAL PROPERTIES TO MICROSTRUCTURE 55
4.1. Preferred Orientation 55
4.2. Preferred Orientation and Thermal Expansion 56
4.3. Residual Stresses in an Extruded Graphite Tube 65
4.4. Preferred Orientation and Young's Modulus 68
4.5. Preferred Orientation and Radiation-Induced Dimensional Changes 77
4.6. High-Temperature Deformation Mechanisms 81
4.6.1. Electron Transmission Microscopy 85
4.6.2. High Temperature Compression Test 89
4.6.3. High-Temperature Testing Facility 90

I. INTRODUCTION

The purpose of this research program is to contribute to the basic information on graphite required for a more effective development of graphite-base structural materials for service in high-temperature reactor systems. The approach is based on gaining a more complete knowledge of microstructure in order to understand the structrual behavior of graphitic materials and to guide experimental approaches to improved materials. The program includes work in three related areas of investigation.

A. Characterization of the microstructure of graphitic materials. In addition to the use of conventional metallographic methods, this work includes such studies as quantitative definition of preferred orientation by diffraction methods and investigations of crystal defects by replication and transmission electron microscopy.

B. Exploration of chemical and metallurgical methods for modifying the microstructure of graphite. The initial work has emphasized investigations of the hot-working of graphite and graphite-carbide bodies; studies have also been made of recrystallization by liquid metals.

C. Investigation of the relationship of microstructure to the physical properties of graphitic materials. The principal efforts have been directed to the relation between preferred orientation and such directional properties as thermal expansion and dimensional changes under neutron irradiation. Some work on mechanisms of deformation at high temperatures has also been carried out.

This research program was initiated in July, 1963, and represents a logical outgrowth of investigations on a practical developmental program entitled "Advanced, Graphite-Matrix, Dispersion-Type Fuel Systems" (Contract AT(04-3)-167, Project Agreement 12, Task I).[1, 2]* To a large extent, the initial studies have been aimed at providing basic information in support of the developmental program.

The bulk of the work described in this report has been covered in two quarterly reports.[3, 4]

*References are listed at the end of the report.

II. MICROSTRUCTURAL STUDIES

The microstructural studies are aimed at a general characterization of graphitic materials from the ordinary microscopic scale of pores and filler-binder relationships to the atomic scale of crystal lattice defects. In the initial period of this program, the principal efforts have been devoted to (1) a literature survey on optical and electron micrographic techniques, (2) development and application of methods for the quantitative definition of preferred orientation in polycrystalline graphites, (3) micrographic recognition of the filler and binder constituents in fuel-matrix graphite, (4) replication electron microscopy on hot-worked graphite, and (5) observations of the fracture characteristics of hot-worked graphite. In connection with studies of flow mechanisms of graphite crystals at temperatures in the hot-working range, techniques have also been developed for the observation of dislocations in thin flakes by electron transmission microscopy; this work is described in Section 4.6.

2.1. LITERATURE SURVEY ON MICROGRAPHIC METHODS FOR GRAPHITE

(J. L. White)

The purpose of this literature survey is to gain a full comprehension of micrographic techniques that have been developed or attempted in previous work on graphitic materials, and to define more precisely the significant problems for study by methods currently at hand or readily developed. It is intended to conclude this survey by the preparation of a topical report; the following remarks provide a brief summary of some tentative conclusions.

No comprehensive reviews on the microstructure of graphite have been found. Significant work on optical and replication micrography is being done at several American sites as indicated by Refs. 5 through 14. Recent publications by English workers are noteworthy in demonstrating some success in relating micrographic observations to the physical properties of polycrystalline graphites.[15-17] In general, the microstructure of graphitic materials is markedly more complex than that of conventional metallurgical materials, and the state of development of micrographic technique is accordingly less advanced. The most serious micrographic difficulties are concerned with the vast range of hardnesses of graphitic and carbonaceous materials and the retention of edge detail in pore structures,

as well as such problems of interpretation as the absence of well-defined grain boundaries in ordinary polycrystalline bodies and the existence of a fine structure the details of which are beyond the resolution of ordinary optical methods.

Extensive discussions appear in the literature on the differing roles of filler and binder in respect to the physical properties of graphitic bodies.[18,19] Since these constituents in the finished graphitic body are both composed essentially of graphite crystallites and differ only in being fossils of different carbonaceous starting materials, considerable difficulty has been encountered in obtaining adequate definition of the relationships between these constituents in the microstructures of commercial polycrystalline graphites. This micrographic problem appears to be responsible for the limited progress in understanding the mutual effects of binder and filler during graphitization of the pitch binder and the resulting effects on the ultimate physical properties of finished graphite bodies.

Owing to the layer-lattice structure and accompanying anisotropic properties of the graphite crystal, the matter of preferred orientation in polycrystalline graphite bodies assumes a greater importance than it does in the most anisotropic metal systems. Although optical techniques such as polarized light or sensitive-tint micrography provide qualitative indications of preferred orientation,[11] quantitative studies by these methods are lacking. A satisfactory quantitative definition of the preferred orientation of graphitic bodies can be obtained by the methods of X-ray diffraction described in Section 2.2.

Studies by optical microscopy appear to be limited in the sense that a fine structure on a scale of the order of one micron or less is discernible in most graphitic materials, but cannot be studied in detail owing to problems of relief polishing and etching as well as the fact that the fine structure is near the limit of resolution of optical microscopy. Methods of replication electron microscopy[6-8,15,16] are being extensively applied to resolve this fine structure, and some success has been achieved in relating observations of fine delamination microcracks to the properties of thermal expansion[15] and irradiation growth.[16] The major portion of this work has been done on specimens prepared by cathodic etching.[20]

Grain boundaries typical of those found in metals do not appear to occur as a common structure in conventional graphitic materials. Instead the dominant feature at high magnification is a flow pattern involving the apparent bending of graphite planes. In the extreme case, this bending appears as twin boundaries.

Although extensive use is made of mercury porosimetry and other such methods to obtain a qualitative characterization of the pore structure

of graphitic bodies, relatively little has been done to define fully the relation of pore shape to the graphite grains bounding the pore. This information is particularly important to an understanding of mechanisms of permeation by various diffusants.

Adequate reviews exist of methods of specimen preparation, including grinding, polishing, and pore impregnation.[5, 7, 10, 13] Bodies comprising hard and soft constituents present special problems of relief polishing and subsequent removal of polishing debris.

Investigations of the kinetics of the reactions of graphite with corrosive media show that the various carbon and graphite structures display a wide range of reactivities.[21] However, most studies of micrographic etchants have been restricted to the acid dichromate solutions, and there appears to have been little exploration of such techniques as electrolytic polishing and etching or gaseous oxidation.

2.2. MEASUREMENT OF PREFERRED ORIENTATION

(J. C. Bokros, R. J. Price)

Many of the peculiarities of polycrystalline graphite as an engineering material result from the extreme anisotropy of a graphite single crystal. For example, the room-temperature thermal expansion coefficient of a crystal is $27 \times 10^{-6}\,{}^{o}C^{-1}$ in the c-direction and $-1.5 \times 10^{-6}\,{}^{o}C^{-1}$ in the a-direction, while the value of Young's modulus varies by a factor of 100 between different directions in the same crystal. Since all the conventional fabrication techniques for polycrystalline graphites impart a preferred orientation to the crystallites, the properties of the resulting body reflect to a lesser extent the anisotropy of the single crystal. To rationalize the directional properties of a fabricated graphite body it is very important to have quantitative measurements of the preferred orientation, which can vary all the way from near-isotropic to near-single-crystalline, depending on the fabrication technique.

The directional physical properties in a hexagonal crystal such as graphite depend on only one angular parameter--the angle between the direction in question and the c-axis. It follows that to describe fully the preferred orientation of a polycrystal it is only necessary to give the distribution of c-axes relative to specified directions associated with the forming process. It is convenient to use an intensity function I, which is the population density (relative number per unit solid angle) of c-axes in a given direction, normalized to unity in the direction in which most of the c-axes are aligned.

In the case of bodies prepared by pressing, pyrolytic graphite, deposits, etc., the distribution of c-axes is cylindrically symmetrical about one direction, and the intensity function I is the same at any angle ϕ to the pressing direction or to the normal to the plane of the deposit. The high symmetry makes it possible to use a technique developed by Bacon[22] where a single X-ray diffraction photograph is used to obtain a plot of I (ϕ) against ϕ. The experimental setup is shown in Fig. 1. The intensity is measured at various angles θ around the (002) diffraction ring, and the equivalent value of ϕ is worked out from the equation

$$\cos \phi = \cos^2 77^\circ + \sin^2 77^\circ \times \cos \theta. \qquad (1)$$

Values of I(ϕ) are then obtained by normalizing the X-ray intensities to unity at $\theta = 0$, which corresponds to basal planes aligned exactly perpendicular to the pressing direction.

In the current work, this technique was used to measure the preferred orientation in hot-worked graphite and hot-worked graphite-ZrC composites, molded nuclear graphite, and pyrolytic graphite. All these samples possess the necessary cylindrical symmetry. Slices of material about 0.5 mm thick, with the axis of symmetry lying in the plane of the slice, were cut with a high-speed diamond wheel. They were set up on a transmission X-ray camera as shown in Fig. 1; the film cassette was always loaded with two films because it was found that the range of intensities around the (002) ring was too wide to be recorded accurately in a single exposure. The intensities were measured at 10° intervals around the ring, using an automatic recording densitometer. Both the peak intensities and total integrated intensities were measured, but it was found that both methods gave the same result within experimental error. Results for a number of hot-worked specimens are given in Section 3.5. Other preferred orientation curves are shown in Section 4.2.

The texture of graphites extruded in the form of a bar also has cylindrical symmetry about the extrusion axis, except in the outer layer where there may be an additional tendency for basal planes to lie parallel with the wall of the extrusion die. In this case the experimental setup for preferred orientation measurement is shown in Fig. 2. The intensity is measured at 10° intervals around the ring, and the value of ϕ corresponding to any measured θ is worked out from the equation

$$\cos \phi = \sin 77^\circ \times \cos \theta \qquad (2)$$

(77° is correct for CuK_α radiation, where the Bragg angle for the (002) reflection is 13°). In this case I(ϕ) is obtained by normalizing the measured intensities to unity at $\theta = 90^\circ$. An example of a preferred orientation curve for extruded graphite is shown in Fig. 3.

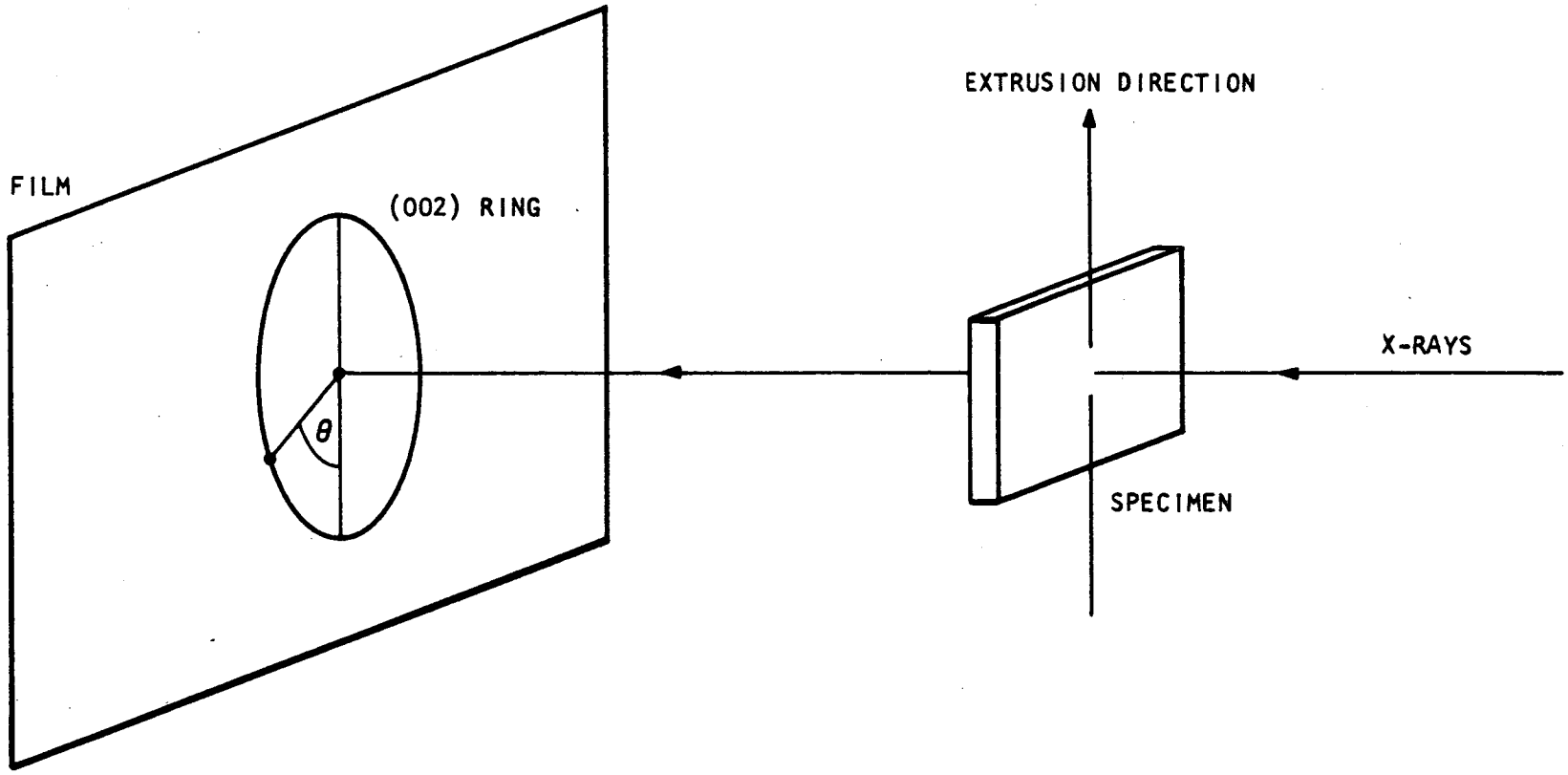

Fig. 1--Experimental setup for preferred orientation measurements on extruded graphite

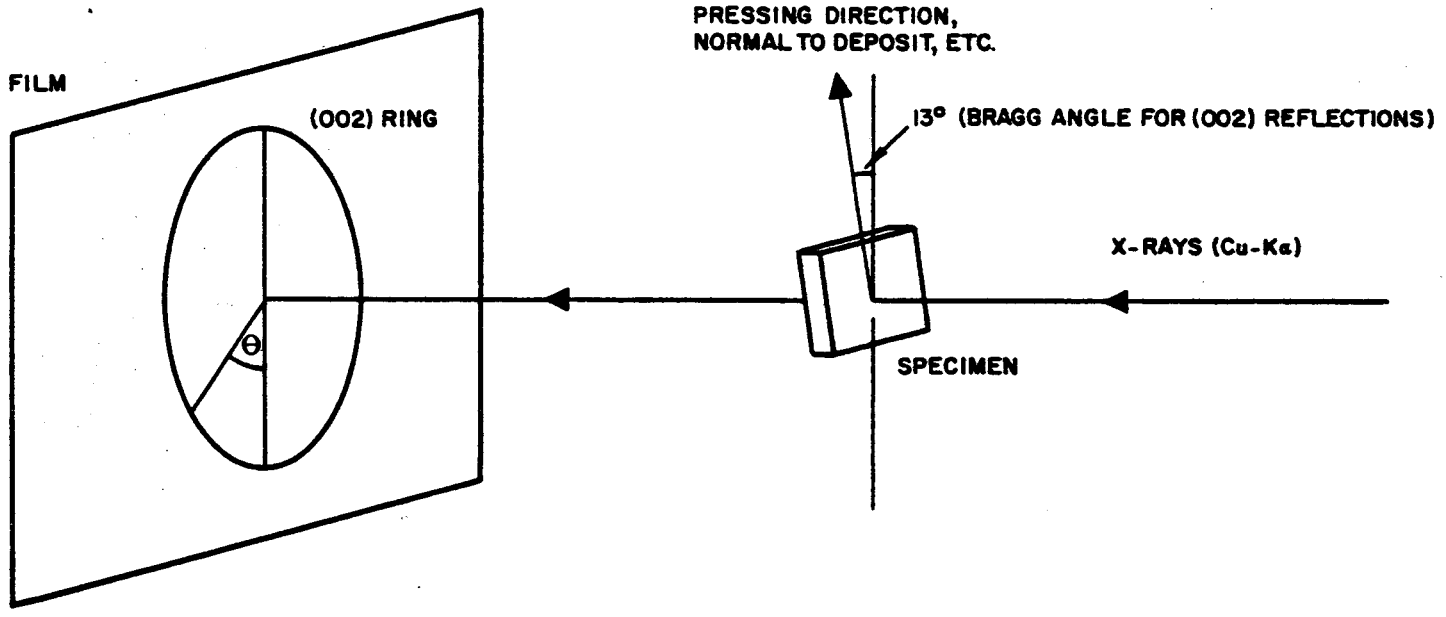

Fig. 2--Experimental setup for orientation measurements on molded, hot-worked, or pyrolytic graphite; 13° inclination correct for Cu-Kα radiation

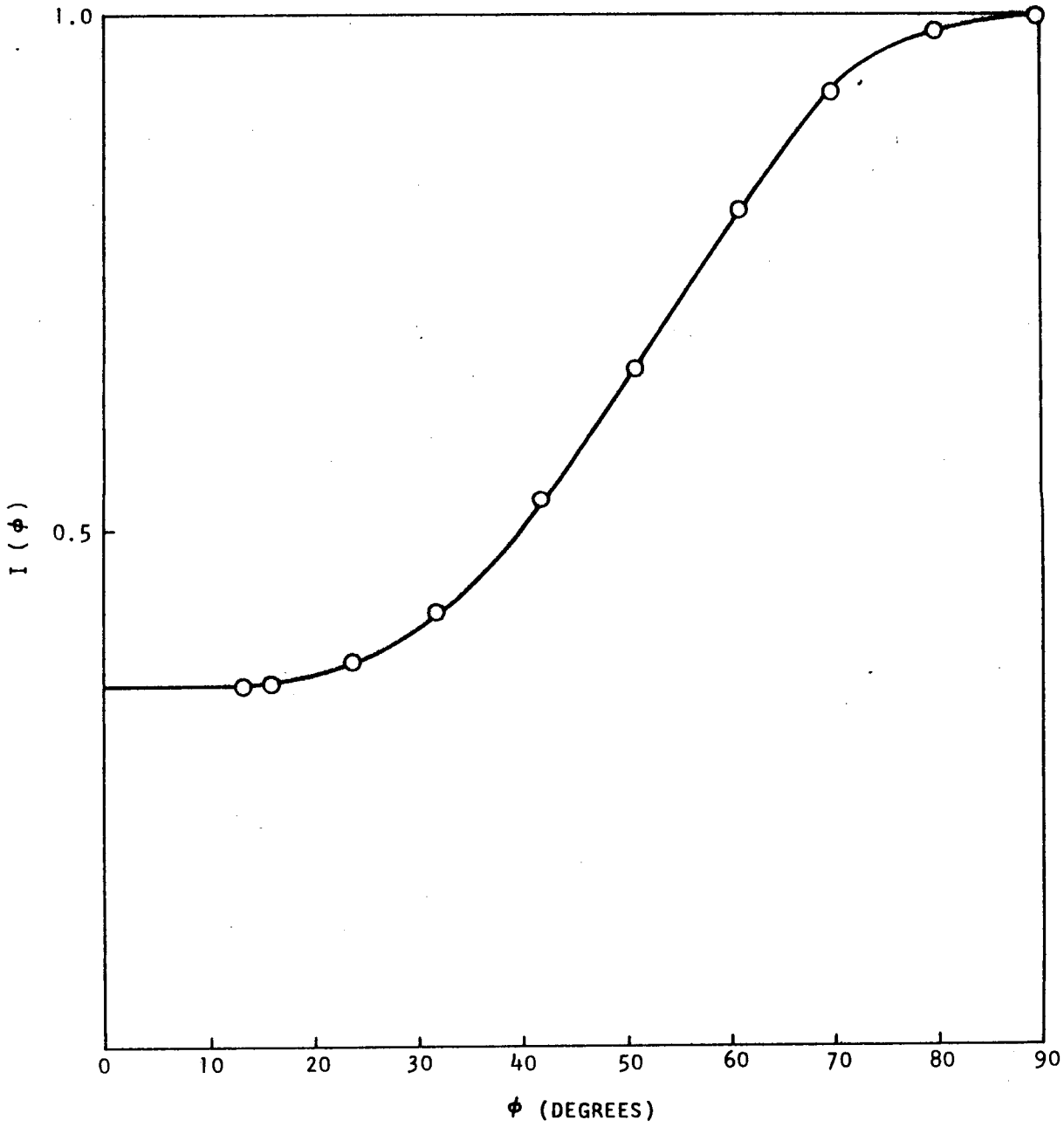

Fig. 3--Preferred orientation curve for extruded needle-coke graphite (EGCR graphite Type NC-8)

Bodies fabricated by other techniques have more complex preferred orientations. When the texture no longer has simple cylindrical symmetry, the intensity function I cannot be plotted as a function of a single angle θ, and it becomes necessary to use a pole figure to represent the distribution of basal plane normals. A good example of this type of body is an extruded tube; the distribution of c-axes in a tube wall may be conveniently represented as contours of equal I on a stereographic projection showing the radial, circumferential, and longitudinal directions.

Such a pole figure could be constructed by the conventional techniques for rolled metal sheets. However, this would involve taking a large number of X-ray photographs and applying laborious absorption corrections to the intensity measurements when the specimen was steeply inclined to the X-ray beam. An alternative technique has been developed in the present program. It is essentially an extension of the Bacon technique to the general case where the texture does not have cylindrical symmetry. It consists of cutting out three samples from the wall of a tube as shown in Fig. 4, and setting each one up in a way similar to that shown in Fig. 1 except that the radial direction now takes the place of the pressing direction. The intensities of the X-ray reflections around the ring are measured for each sample as before and plotted as a function of θ. The transfer of this data to a stereogram is best done graphically. The values of θ on each plot for which I is 0.2, 0.4, etc., are read off and the corresponding points are marked on a stereogram projected in the plane tangent to the tube wall, using the normal geometrical operations for stereographic projections. Data from the three photographs give information about the intensities along the traces shown in Fig. 5. It can be seen that the coverage is fairly complete, particularly in the center of the stereogram, where the contours are closely spaced. More detailed coverage could be obtained by cutting more samples at intermediate angles from the tube wall.

This technique was applied to standard General Atomic extruded tube stock heat-treated at either 2000°C or 2650°C. Figure 6 shows the variation in I along the traces OA and OB in Fig. 5 for one experiment, and complete quadrants of typical pole figures are shown in Fig. 7. It can be seen that there is a tendency for the basal plane normals to align themselves in the radial direction, but the distribution function falls off much more sharply in the plane containing the radial and longitudinal directions than in the plane containing the radial and circumferential directions. This structure may be likened to a pile of sheets of corrugated iron formed into the wall of a tube, with the corrugations lying along the tube (see Fig. 8). The alignment of c-axes along the radial direction in the transverse plane is more pronounced near the inner and outer surfaces of the tube than in the center of the wall, i.e., there is more highly oriented "skin" near the two surfaces. This is probably caused by the

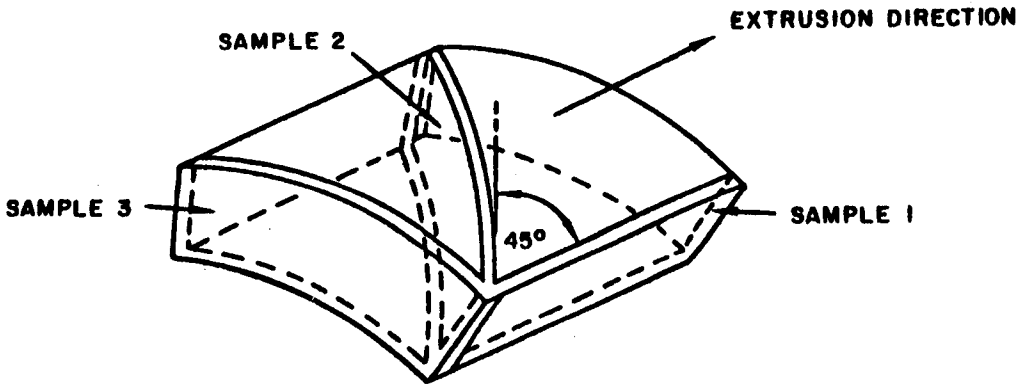

Fig. 4--Preferred orientation curve for extruded needle-coke graphite (EGCR graphite Type NC-8)

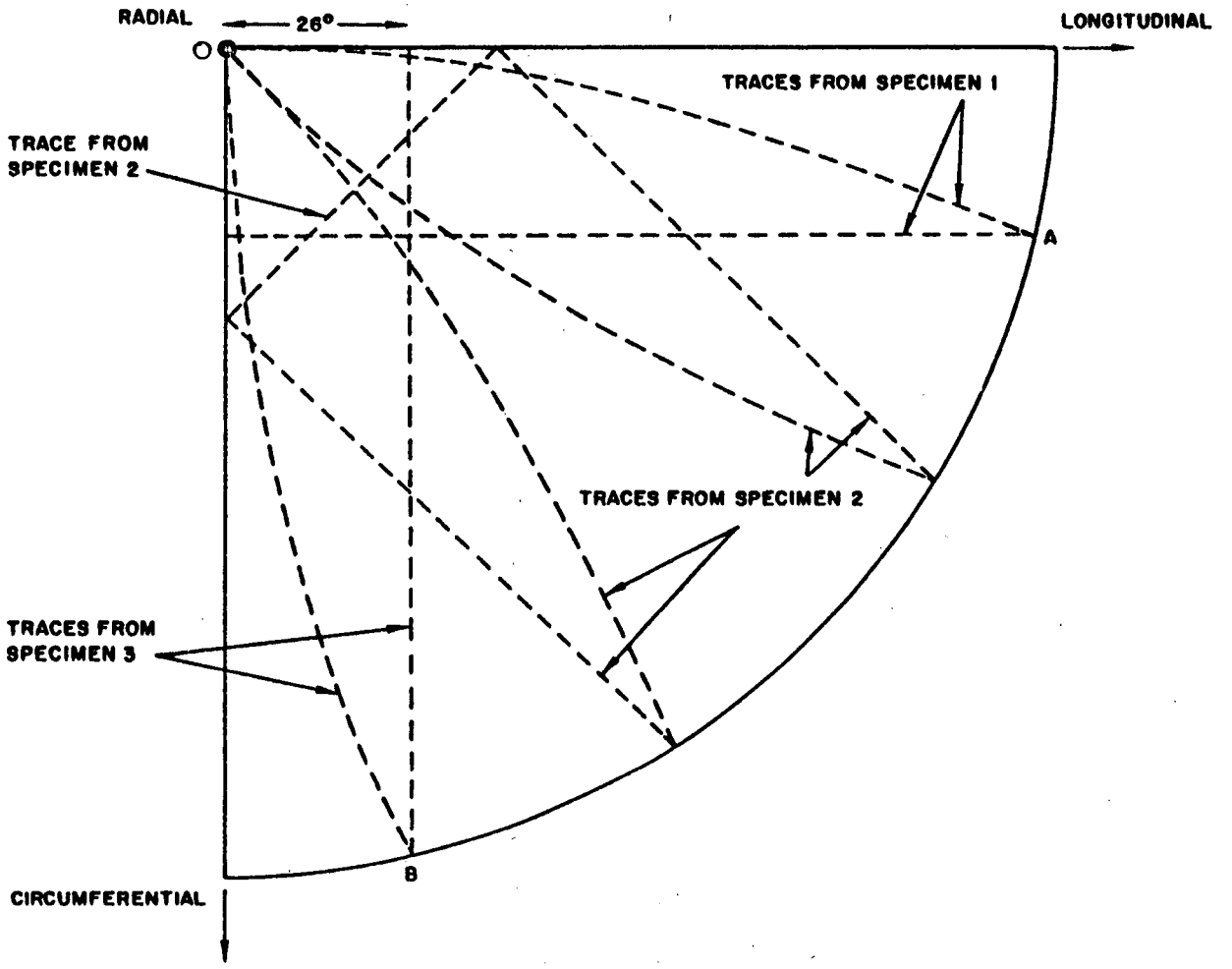

Fig. 5--Stereographic projection of tube wall, showing traces along which data points from X-ray photographs fall.

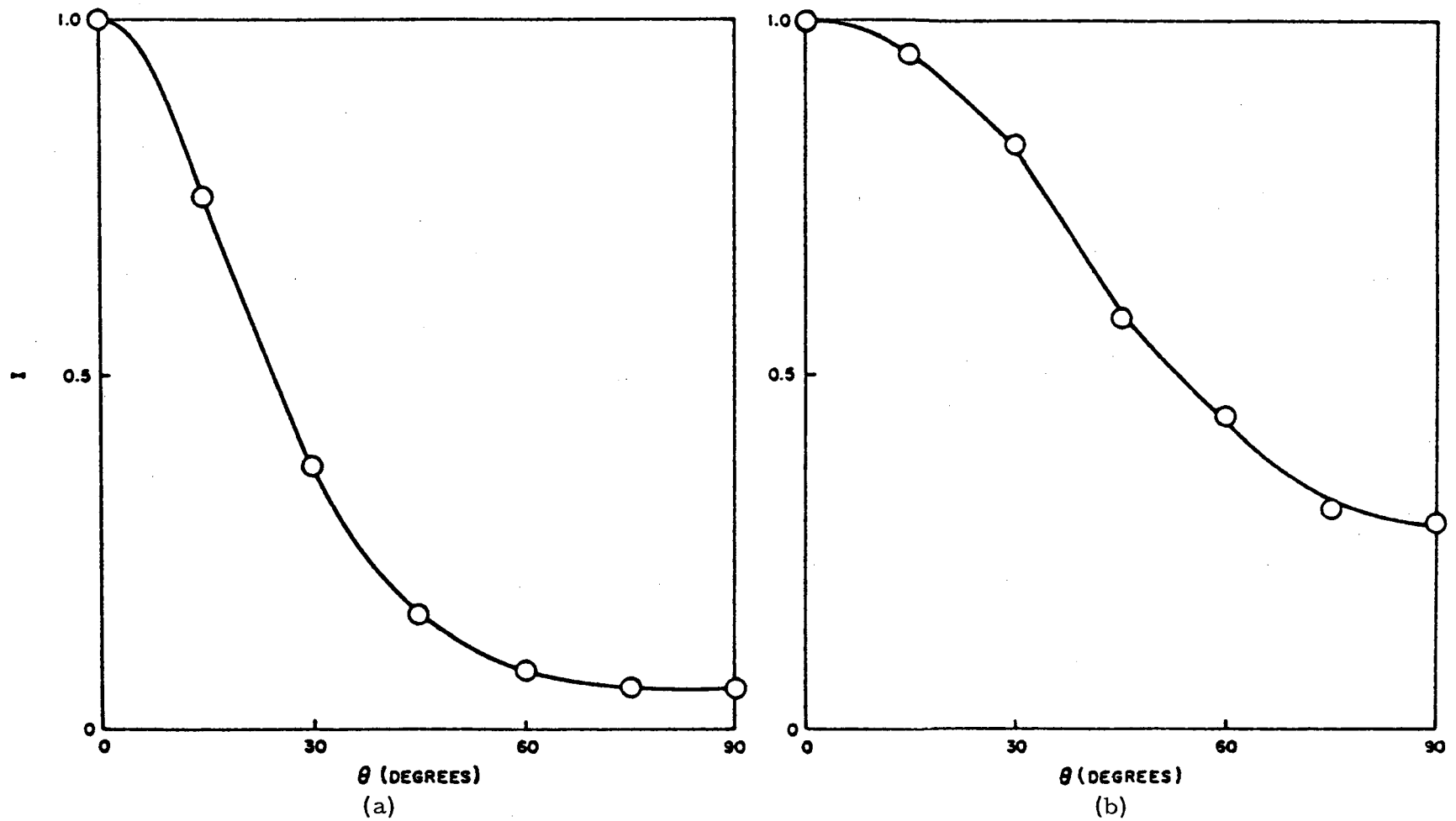

Fig. 6- Variation of normalized c-axis density (I) with angle from 0 along traces OA (a) and OB (b) of Fig. 5 for the middle of the wall of an extruded tube

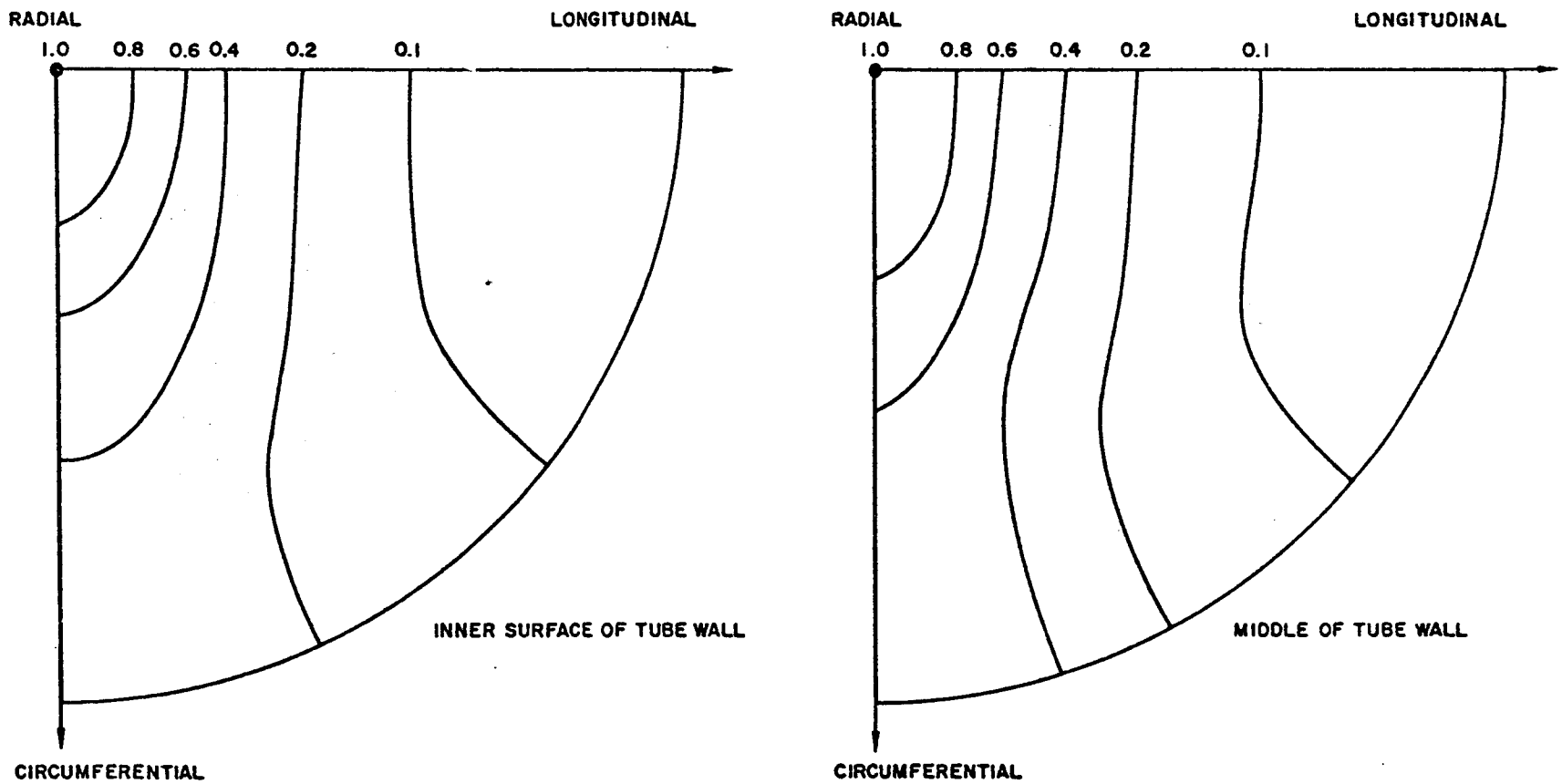

Fig. 7--Pole figures showing the variation of the density of c-axis (I) with orientation in the wall of an extruded graphite tube

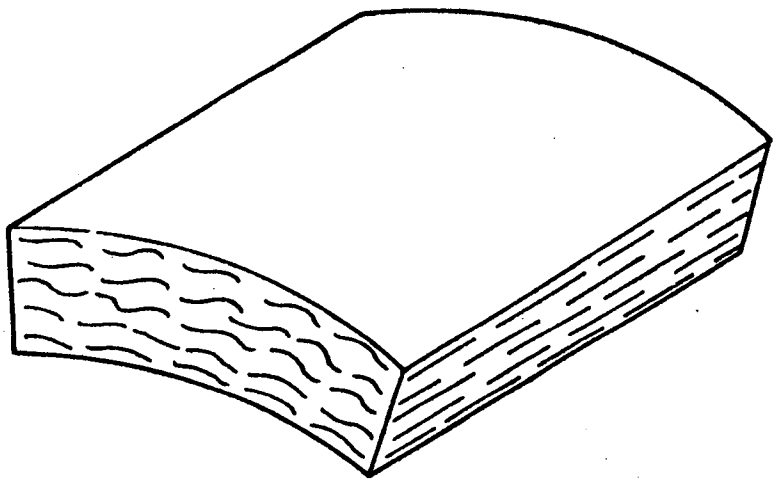

Fig. 8--Schematic illustration of the way the basal planes lie in the wall of an extruded tube

alignment of crystallites during the laminar flow of the pitch past the extrusion dies.

The influence of preferred orientation on the properties of graphitic bodies is discussed in Section IV.

2.3. QUANTITATIVE SENSITIVE-TINT MICROSCOPY
(J. E. Knipping, J. L. White)

Although the diffraction methods for the characterization of preferred orientation are quantitative and unambiguous, these methods are also tedious and do not lend themselves readily to the monitoring of processes. A micrographic method employing elliptically polarized light and termed sensitive-tint microscopy has been used for qualitative indications of preferred orientation in graphitic materials.[10,11] A means of quantifying the sensitive-tint response of a metallographically prepared section is being sought as a simple method for measuring the preferred orientation existing at various points in graphitic materials.

The experimental approach involves the use of suitable filters, a stable light source, and a sensitive photometer with a conventional metallograph. The aim is to measure the light (either blue or red) transmitted to the photometer as a function of specimen orientation on the metallograph stage. The initial work is being done with specimens for which the preferred orientation has previously been measured by X-ray diffraction methods.

The sensitive-tint response for a section of an extruded tube is given in Fig. 9. The preferred orientation in this specimen as measured by X-ray diffraction techniques was given in Fig. 6a. The sensitive-tint response was measured using a tungsten light source with an orange-red filter on a Bausch and Lomb metallograph. The deviations from a sine-wave form and from symmetry over 180° may be due in part to a slight eccentricity in the field of view as the metallograph stage is rotated. On the basis of these indications, further work is proposed to obtain the most suitable photometric conditions and to calibrate the method in terms of the difference between maximum and minimum intensities.

2.4. OBSERVATIONS OF PITCH GRAPHITIZATION
(L. C. Foster, J. E. Knipping, J. L. White)

In order to distinguish the characteristic microstructures of pitch binder as it appears in fuel-matrix graphite, experiments have been designed in which pitch is heat-treated in contact with various graphitic

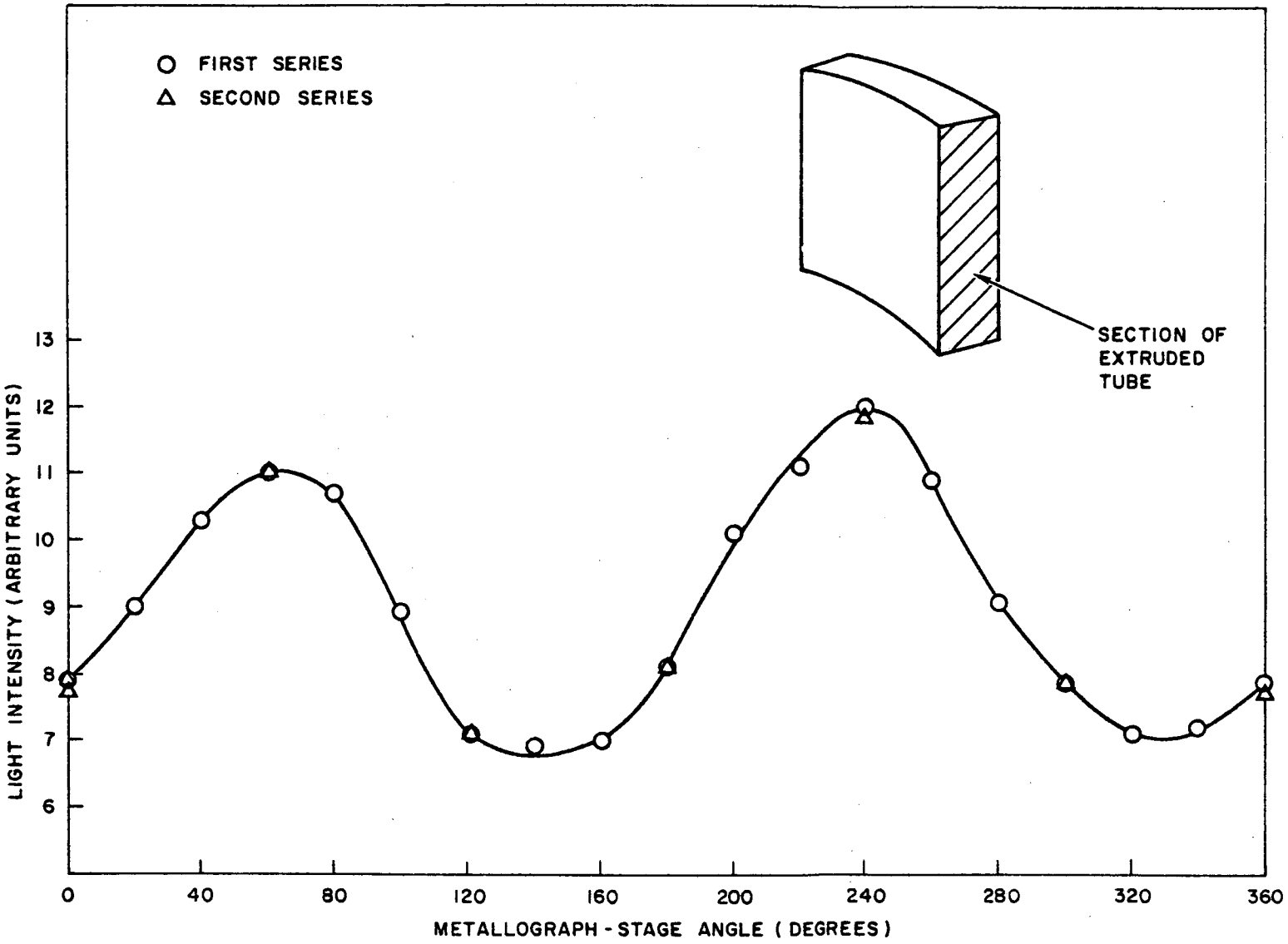

Fig. 9--The sensitive-tint response as a function of metallograph stage angle for a specimen sectioned from the wall of an extruded tube

materials. By means of micrographic observations it is possible to observe how the process of pitch graphitization might affect or be affected by the filler structure.

The results of the first experiment are indicated by the photomicrographs of Figs. 10 and 11. In this experiment a small amount of Barret No. 30 pitch (a pitch binder commonly employed in fuel-matrix graphites prepared at General Atomic) was heated with Madagascar graphite flakes (Asbury Graphite Mills, Inc., grade 3034) at a series of temperatures increasing in steps to finish at 2800°C, where it was held for one hour. At some point in the heat treatment the pitch bubbled to nearly fill the crucible, and on further heat treatment the bubble film was solidified in place. Since a number of graphite flakes were trapped in this film, it was possible to observe the effects of pitch graphitization on individual flakes.

Figure 10 affords a comparison of the pitch structure with that of the AGOT graphite of the crucible wall. The pitch layer gives the sensitive-tint response typical of highly graphitized materials. Although the details of the fine-grain structure of the graphitized pitch are not fully resolved at the magnification of Fig. 10, the pitch layer is clearly distinguished from the filler grain of the AGOT graphite. Large pores are common in the pitch layer, but very few pores smaller than 10 μ were found. Little penetration of pitch into the graphite wall was discernible.

As indicated in Fig. 11, the natural graphite flakes trapped in the bubble film were severely damaged during the heat treatment. The twinned and delaminated structures suggest the action of compressive stress by the pitch film. On etching with $K_2Cr_2O_7$-H_2SO_4, the layer of graphitized pitch was found to etch more rapidly and uniformly than the graphite flakes.

Further investigations of this nature are in progress to learn the effects of heat treatment at various temperatures and with various filler and binder materials. An example of current work in which natural graphite flakes serve as filler and a nongraphitizing material, polymerized furfuryl alcohol, serves as binder is illustrated in Fig. 12. Various heat-treatments from 500°C to 3000°C have been used. Some damage to the graphite flakes was apparent after heat-treatment at 500°C. After heat-treatment to 3000°C, large shrinkage stresses were apparent in the twinned and delaminated structures of the graphite flakes.

2.5. REPLICATION ELECTRON MICROGRAPHY

(J. O. Gardner, J. L. White)

In order to observe in detail the fine structure of polycrystalline graphites, observations by replication electron micrography have been

M 5121-1-16 (250×)

(a) As impregnated and polished

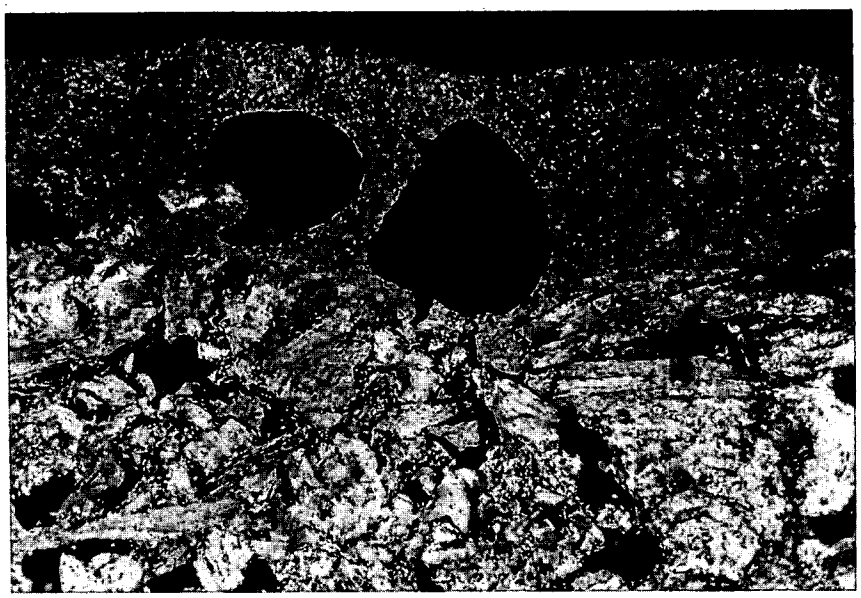

M 5121-1-17 (250×)

(b) As polished and etched

Fig. 10--Structure of a layer of binder pitch (top layer) graphitized in contact with AGOT graphite. Specimen was impregnated with epoxy resin for polishing; etching with $K_2Cr_2O_7$ - H_2SO_4 (30 sec at room temperature) attacks impregnant vigorously and improves microstructural detail

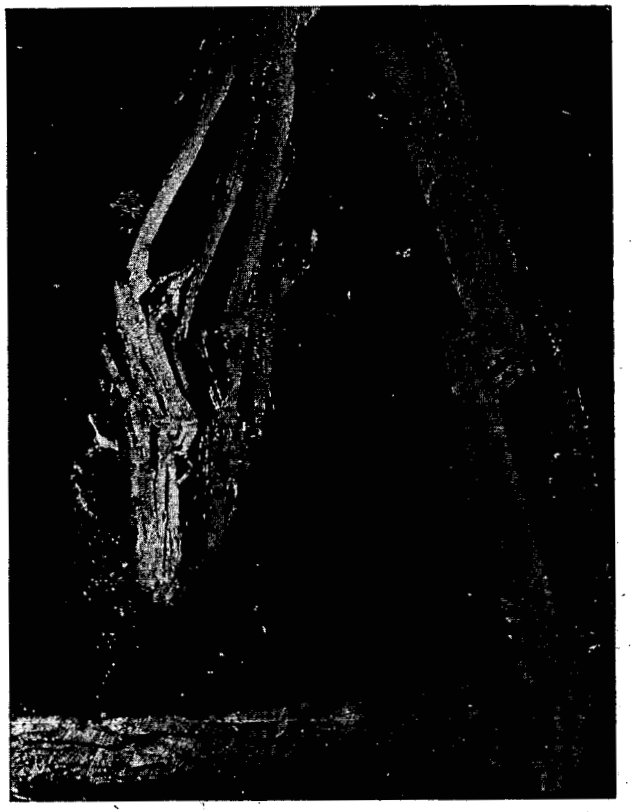

M 5121-1-7 (100×)

(a) As impregnated and polished

M 5121-1-15 (250×)

(b) Same field as at left

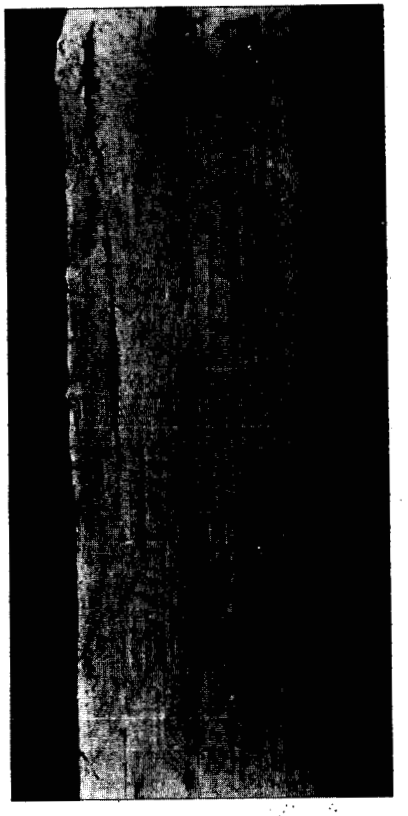

M 5121-1-13 (250×)

(c) Natural flake

Fig. 11--Effects of pitch graphitization on natural graphite flakes entrapped in pitch film. Photomicrograph (c) shows cross section of natural flake in as-received condition

(a) After heat-treatment at 500°C

M-6648 100X

(b) After heat-treatment at 3000°C

M-6663 100X

Fig. 12--Effects of heat-treatment at various temperatures on the structure of Madagascar graphite flakes in a non-graphitizing binder (polymerized) furfuryl alcohol

undertaken on specimens of hot-worked and annealed fuel-matrix graphite. In view of the fact that hot-worked graphite has been characterized by other workers[23, 24] as recrystallized graphite, evidence is being sought for processes of grain nucleation and growth typical of metallurgical recrystallization. It is also desired to learn how the pore structures are affected by possible shearing and shutting mechanisms during hot-working.

The material selected for the initial study was a typical fuel-matrix graphite. The graphite bodies were prepared by hot-pressing graphitized petroleum coke with 10wt-% Barrett No. 30 pitch. The hot-pressing was followed by a vacuum anneal at 1850°C. Two representative specimens are shown in Figs. 13 through 16: one specimen is the annealed matrix graphite and the other specimen has been hot-worked in compression at approximately 2600°C to a strain level of 40%. Each specimen was sectioned longitudinally, i.e., the plane of section is parallel to the direction of hot-pressing or hot-working. Information on the optical microstructure and properties of these materials is given in Refs. 1 and 2 and in Section 3.1 of this report.

Two-stage, negatively shadowed carbon replicas were made from the specimens, which were prepared by metallographic polishing and light etching with $K_2Cr_2O_7$-H_2SO_4 to remove polishing debris. Figures 13 through 16 are electron micrographs selected to show some large pores.

The structures of the replicas are brought out most effectively by stereophotomicrographs. The replicating material has penetrated to varying degrees into small microcracks to form fine ribs whose ends are most heavily shadowed by the palladium metal. These ribs form a general pattern suggesting the "flow patterns" observed optically in coke bodies and some commerical graphites.[5-7] At this scale of magnification the enhancement in preferred orientation imparted by hot-working is not strongly evidenced.

In respect to the microstructure of the graphite, no substantial differences have been found between annealed and hot-worked graphite. As noted in Section 3.4, the diffraction patterns show little difference in degree of graphitization. On the basis of these studies no evidence of grain nucleation or growth has been found to justify description of the hot-working process in terms of recrystallization mechanisms.

The pore structures merit several comments. The planar segments of replica from the large pore cavities are relatively free of microcrack ribs, thus suggesting that the cross section of a large pore (of the order of 10 μ across) has the schematic structure shown in Fig. 17. The orientation of the basal planes parallel with the pore surface is consistent with observations by sensitive-tint microscopy at high magnification.

P 2553 (5000×)

Fig. 13--Fuel-matrix graphite as annealed at 1850°C. Two-stage negatively shadowed carbon replica, longitudinal section

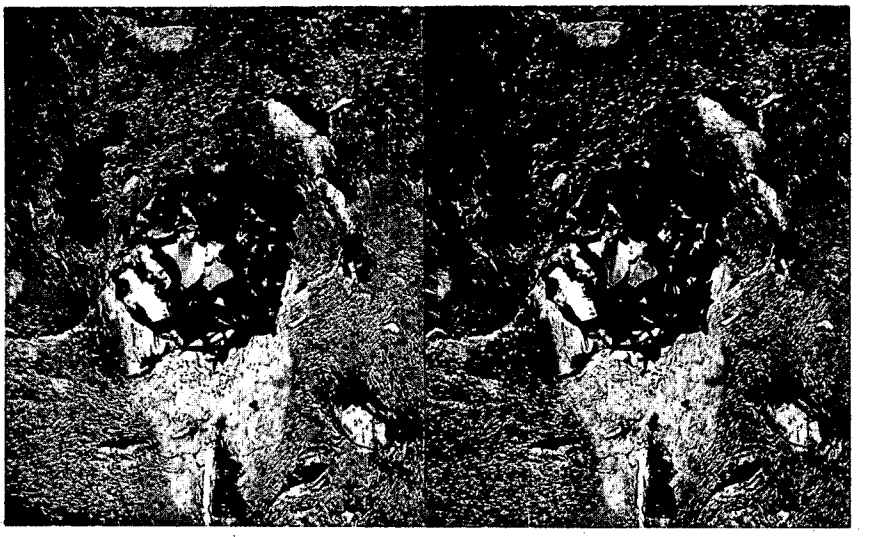

P 2553 (1900×) P 2554 (1900×)

Fig. 14--Fuel-matrix graphite in annealed condition. Stereophotomicrograph of Fig. 13, longitudinal section

P 2539 (5000×)

Fig. 15--Fuel-matrix graphite hot-worked in compression at 2600°C to a strain of 40%. Two-stage, negatively shadowed carbon replica, longitudinal section

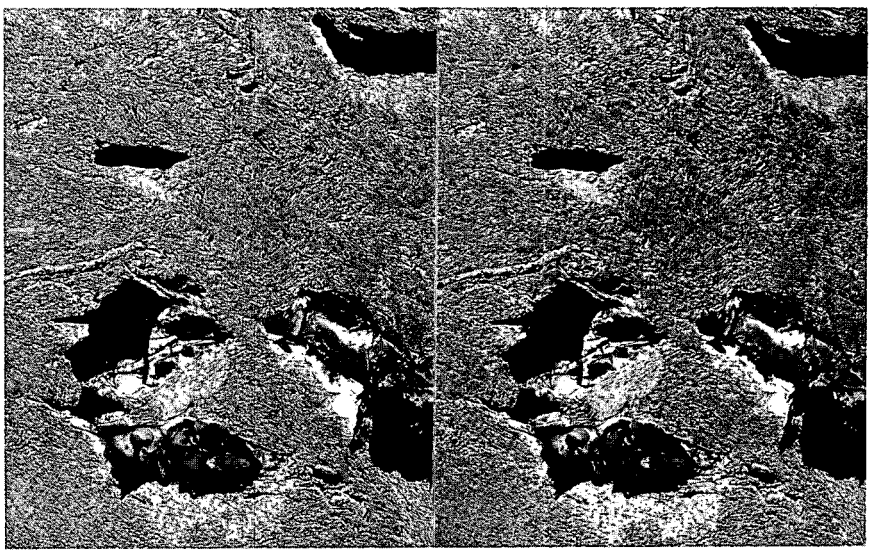

P 2539 (1900×) P 2540 (1900×)

Fig. 16--Fuel-matrix graphite in hot-worked condition. Stereophotomicrograph of Fig. 15, longitudinal section

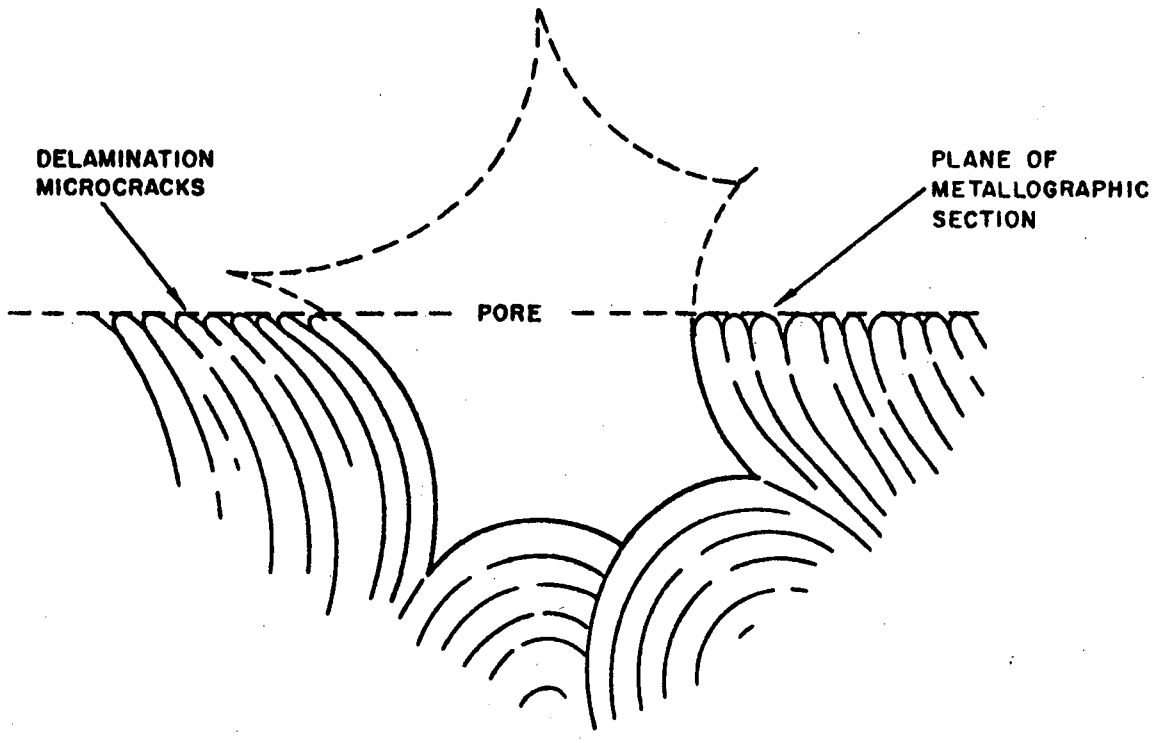

Fig. 17--Schematic cross section of structure in region of large pore (of the order of 10 microns)

Pores of this nature do not seem to exist at smaller sizes; the finer pores appear to consist of relatively narrow planar cracks resulting from delamination processes or imperfect fits between adjoining grains. In the hot-worked graphite the larger pores have been flattened appreciably or closed to a point where they cannot be distinguished from delamination cracks.

It may be noted that the fine structure of the microcracks occurs at an approximate spacing of 1000 Å or less. These fine cracks, which may have been opened up by the mechanical disruption in polishing or by the subsequent etching, thus appear to lie at intervals of the same order as the L_c crystallite dimensions derived from measurements of line-broadening in X-ray diffraction.[25]

2.6. FRACTURE CHARACTERISTICS

(L. C. Foster, J. E. Knipping, J. L. White)

Relatively little work has been reported on the relation between fracture and the microstructure of polycrystalline graphite materials. A simple micrographic method has been developed recently by Jenkins[17] to follow the path of fracture in reactor graphite under tension. A modification of this method is being used to study the fracture characteristics of various types of graphitic materials under compression as well as tension.

A schematic diagram of the bending jig employed in the present work is shown in Fig. 18a. Flat slabs of graphite approximately 1 mm thick are glued to each side of a copper plate, which is of the order of 3 mm thick. Eastman 910 adhesive has been used in the work to date. The strains developed in the specimens on their polished surfaces are calculated from photographs of the bending jig under load, e.g., Fig. 18b.

The present work is illustrated by photomicrographs of hot-worked graphite subjected to stress perpendicular to the preferred orientation of the layer planes, which is the weak direction in this material. The strain level for Figs. 19 and 20 is approximately 1% for compression as well as extension. The specimens were cut from a cylinder of AGOT graphite hot-worked in compression to a true strain of 32%.

The major cracks in Fig. 19a are observed to lie generally perpendicular to the applied stress and tend to run from pore to pore. Observations at higher magnification show that there are many small cracks throughout the specimen and particularly in the regions of the major cracks. The majority of the fractures are delamination-type cracks, i.e., parallel to the layer planes of the grains. The process of failure appears to consist of at least two steps: first, the formation of small delamination cracks, or,

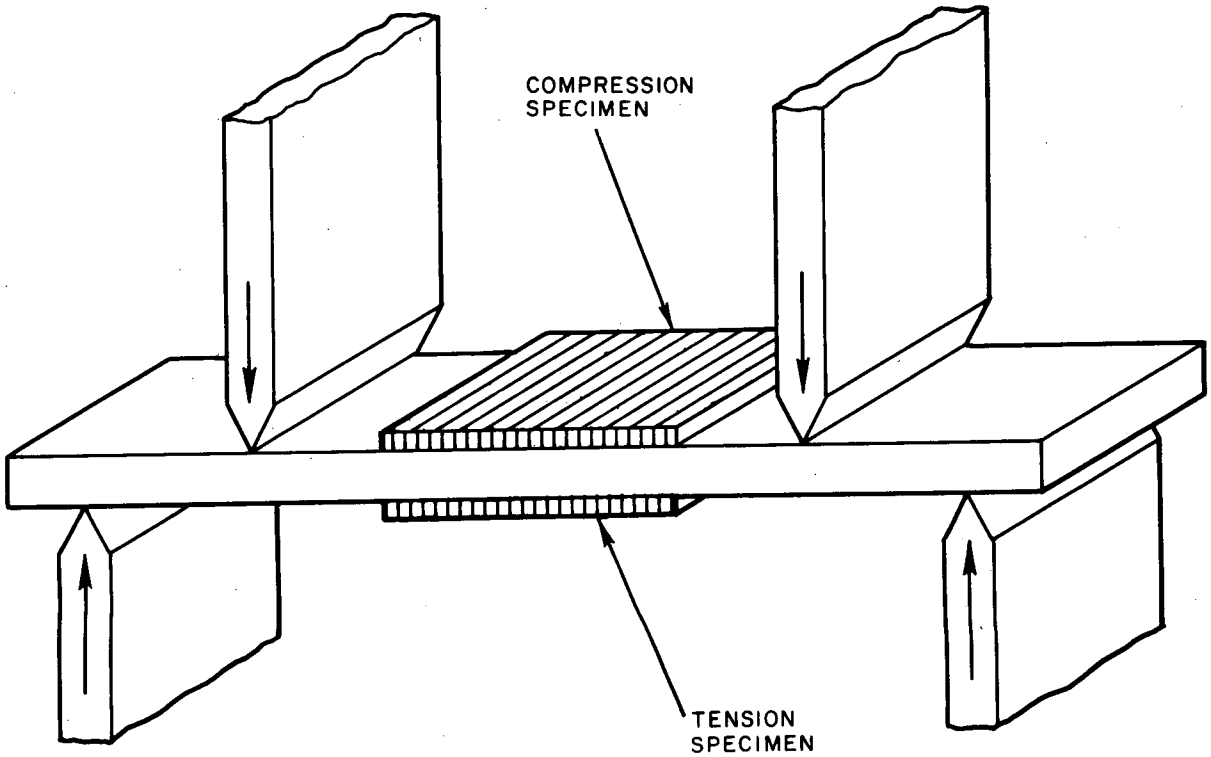

(a)

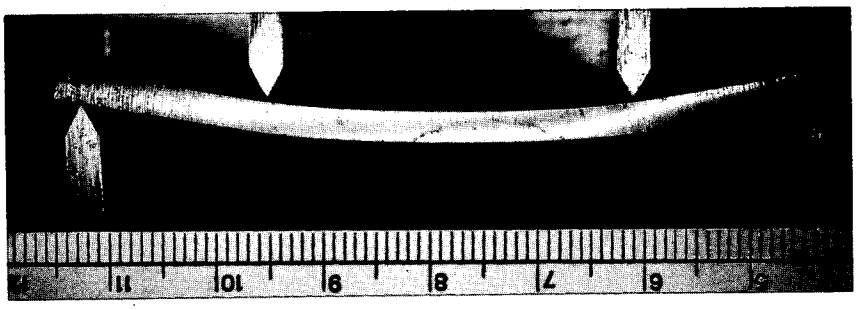

M-5770-2-1

(b)

Fig. 18--Four-point bending jig used to subject thin slabs of graphite to fields of uniform stress: (a) schematic diagram illustrating preferred orientation in hot-worked graphite specimens; (b) photograph of bending jig under load

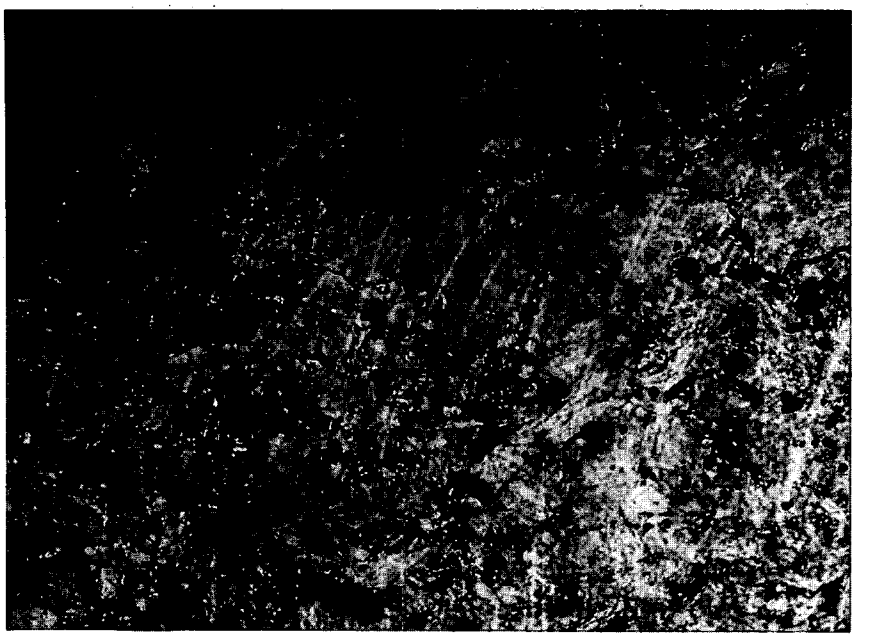

M-6836-1-1 (75×)

(a)

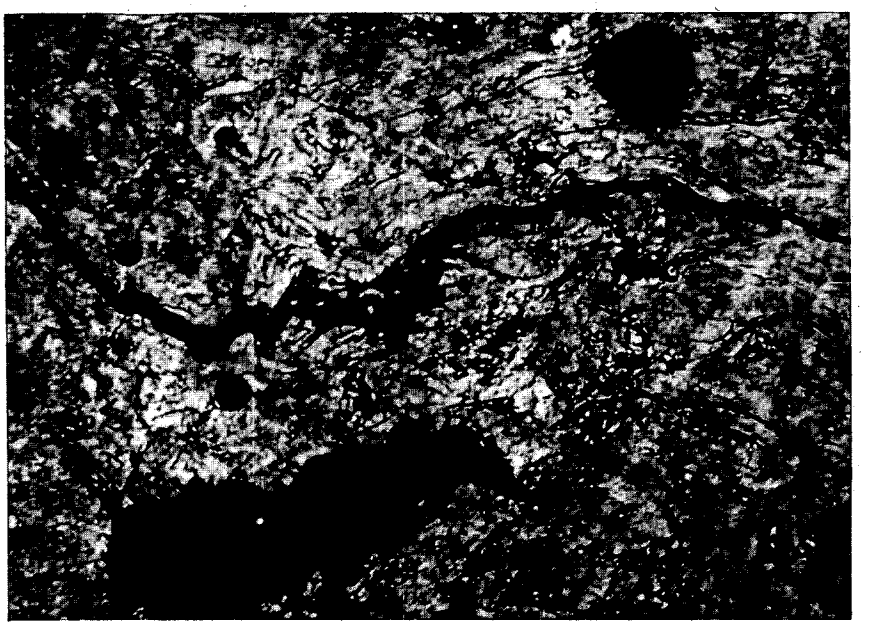

M-6836-1-2 (400×)

(b)

Fig. 19--Surface of hot-worked graphite under 1% strain in tension; applied stress is vertical (oblique light)

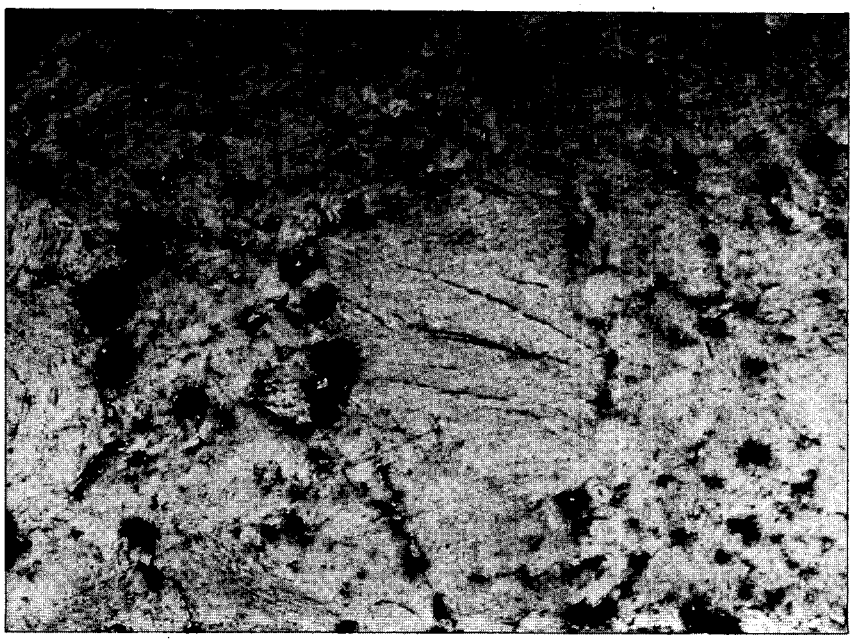

M-6836-2-1 (75×)

(a)

M-6836-2-2 (400×)

(b)

Fig. 20--Surface of hot-worked graphite under 1% strain in compression; applied stress is vertical (oblique light)

more probably, the growth of small cracks already existing as delamination defects or as pores; and second, the formation of major cracks through the overlapping of delamination cracks. The fracture process is completed by the tearing of the laminar material left between overlapping cracks.

Photomicrographs illustrating the same material under compression are shown in Fig. 20. Very few cracks are found at the strain level of 1%, but relief structures stand out most strongly in areas of large grains, while material which appears to be binder shows less tendency to deform.

III. PROCESSING TO ALTER MICROSTRUCTURE

The investigations of processes for the modification of the microstructure of graphite have been devoted primarily to studies of hot-working variables in support of the applied program on advanced graphite-matrix fuel bodies. The initial work on matrix graphite prepared from 10 wt-% pitch and hot-worked to strains of the order of 35% resulted in only modest improvements in the physical properties.[1, 2] It was therefore decided to explore such hot-working variables as strain, pitch content, and preferred orientation in the starting material. In view of the wide range of variables for the hot-working process, only selected exploratory experiments have been conducted for reasons of economy; the measurements of the properties of the hot-worked matrix graphites indicate that favorable results are obtained at higher pitch contents (at least 20 wt-%) and at moderate strain levels (of the order of 50% true strain).

Studies by X-ray diffraction of the crystallite perfection (i. e., degree of graphitization) and of the preferred orientation in hot-worked graphite have also been made and are described in Sections 3. 4 and 3. 5.

Experiments have recently been undertaken to investigate the process of recrystallization of graphite from liquid nickel with a view to understanding the morphology of graphite plates precipitating from liquid media as well as for the preparation of a fully crystalline graphite body.

3. 1. EXPLORATION OF HOT-WORKING VARIABLES

(L. C. Foster, J. M. Pontelandolfo, R. J. Price, J. L. White)

The hot-working device employed in these investigations was developed in connection with the companion program on advanced graphite-matrix fuel systems (Task I) and has been described in previous reports.[1, 2] In connection with that program a temperature-control system has been added to facilitate the hot-working of carbide-bearing systems which have low eutectic temperatures, e. g., UC_2-graphite. This work on temperature control and distribution was extended for purposes of the present program to learn the experimental conditions for the maintenance of the thermal gradients desired for studies of the liquid-metal recrystallization of polycrystalline graphite bodies.

The hot-working investigations on hot-pressed matrix graphite prepared with 10 wt-% pitch have been extended to true compressive strains

of the order of 80%. In order to attain this strain level within a reasonable period, the later stages of the hot-working process were performed at higher temperatures, generally in the neighborhood of 2900°C, since the earlier work[1] demonstrated that most properties of hot-worked graphite were not strongly dependent on the hot-working temperature. The initial stages of hot-working were performed at average specimen temperatures near 2700°C in order that comparisons of the hot-working characteristics could be made with other graphites.

The hot-working curve for a typical warm-pressed graphite prepared with 10 wt-% pitch and oriented such that the hot-working and warm-pressing directions are parallel is given in Fig. 21. Although these curves represent creep under constant load, it should be noted that a substantial portion of the ram displacement is associated with deformation in the load train and that the temperature distribution is not adequate for detailed analysis of the curves in terms of the usual creep parameters. By means of differential deformation experiments,[1] evidence has been obtained for the validity of qualitative comparisons of plasticity under identical hot-working conditions. One purpose of the high-temperature mechanical testing machine currently being set up (see Section 4.6) is to obtain quantitatively significant hot-working data.

In hot-working runs on warm-pressed matrix graphite prepared with 25 wt-% pitch, no difficulty was experienced in reaching strains as high as 80% with hot-working stresses of 6600 psi. No fractures occurred, and the hot-worked specimens were in excellent condition. Somewhat surprisingly, the hot-working characteristics, at least to strains of the order of 35%, were similar to those of 10 wt-% pitch graphite (see Fig. 21).

As pointed out in Section 3.5, the preferred orientation in warm-pressed graphite is of the same sense as that imparted, to a substantially greater degree, by hot-working when the hot-working stress is applied in the same direction as the warm-pressing load. In the interest of seeking more readily hot-worked graphites, the hot-working investigations were extended to extruded cylinders in which the preferred orientation is such that the planes tend to lie parallel with the extrusion direction, which is the axis of the cylinder. The extruded specimens were prepared with 25 wt-% pitch and were hot-worked with the applied stress parallel to the extrusion direction.

Serious difficulties were encountered in hot-working the extruded specimens. Fractures occurred very frequently even at stresses considerably lower than employed in hot-working warm-pressed graphites. In general, the fracture risk appears to be highest at the outset. The fracture surfaces tended to run parallel to the extrusion axis. As indicated by the hot-working curves shown in Fig. 21, the extruded specimens appeared to hot-work more

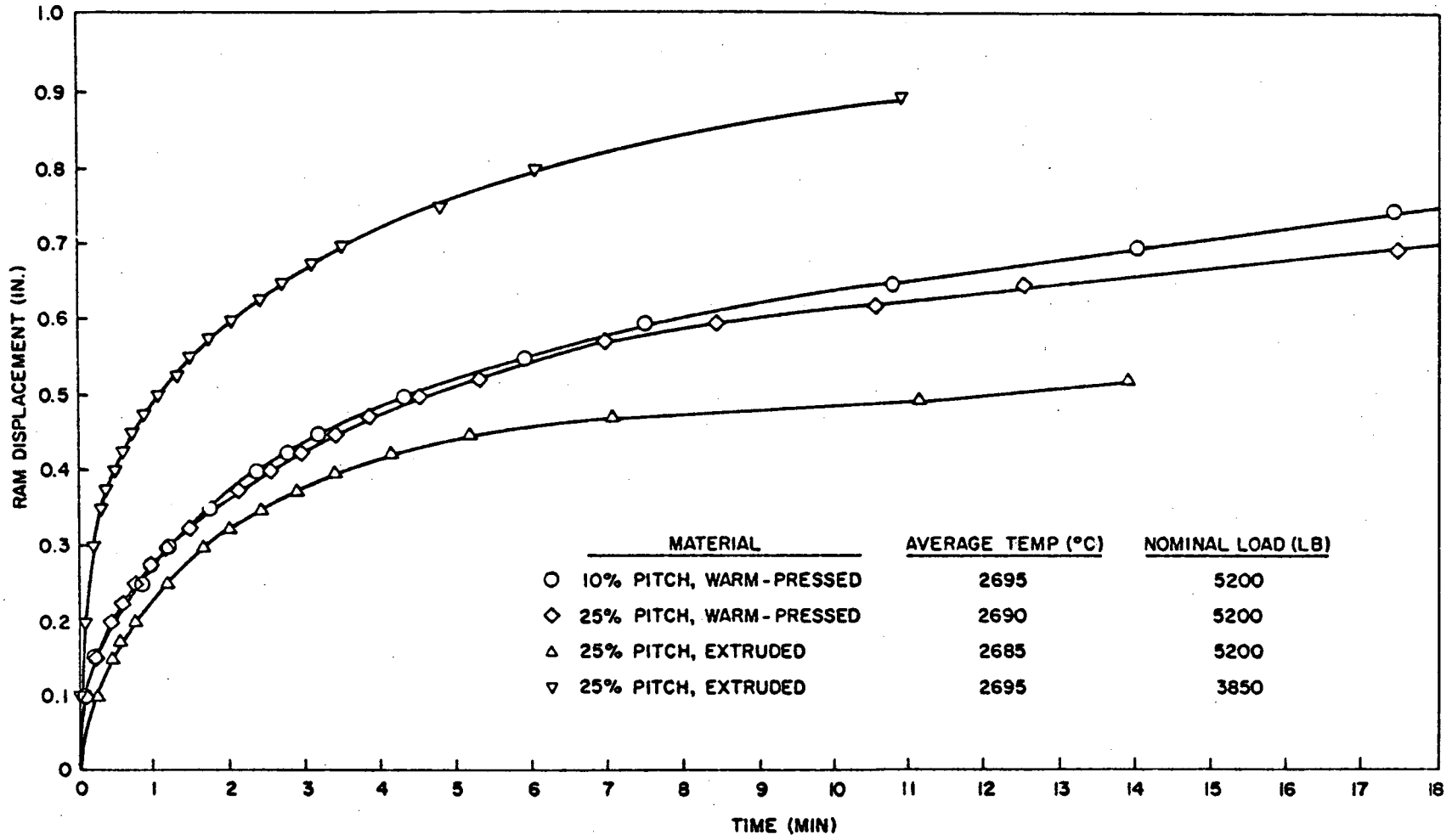

Fig. 21--Hot-working of several matrix graphites in compression. Specimens were cylindrical, 1 in. in diameter by 2 in. in height. Deformation was measured by piston travel of the hydraulic ram. Temperatures are nominal and refer to the average found.

rapidly than the hot-pressed specimens. However, the extruded specimens also showed a strong tendency to deform nonuniformly, i. e., to buckle on one side, and this effect, as well as the lower starting density, is believed to contribute appreciably to the apparent higher plasticity of extruded bodies in hot-working.

The hot-working behavior of extruded graphite suggests that a preferred orientation of opposite sense to that imparted by hot-working is unstable in respect to compressive deformation. This orientation is such as to maximize the risk of twinning reactions leading to delamination cracks running through the graphite grains.[26]

3.2. PROPERTIES OF HOT-WORKED GRAPHITES
(L. C. Foster, J. M. Pontelandolfo, J. L. White)

Measurements of the density, porosity, compressive strength, thermal expansion, and helium permeability have been completed for the three types of hot-worked fuel-matrix graphites discussed in the foregoing section. These materials were prepared using graphitized petroleum coke (GP-38 powder) and pitch binder (Barrett No. 30 pitch) and are labeled as follows: (a) hot-pressed compacts prepared with 10 wt-% pitch; (b) hot-pressed compacts prepared with 25 wt-% pitch; and (c) extruded bodies prepared with 25 wt-% pitch. All bodies were heat-treated in vacuum at 1850°C prior to hot-working. Reference specimens were prepared by annealing at the same temperatures as used in hot-working. Photomicrographs of sections cut longitudinal to the axis of hot-working for hot-pressed bodies are given in Fig. 22.

The results of density and porosity measurements are given in Fig. 23. The porosities were measured by conventional mercury porosimetry, and the values plotted in Fig. 23 refer to the available pore volume for pores greater than 0.086 μ in diameter. Typical porosity spectra are given in Fig. 24 for the hot-pressed matrix graphites. The density tends to saturate or possibly to show a maximum at a strain level near 70% true strain. Densities of the order of 2.05 g/cm^3 were obtained with hot-pressed bodies prepared with 25 wt-% pitch; the extruded bodies were the least dense at all strain levels. These saturation effects were also observed in the porosity data, although commencing at somewhat lower strain levels. The reduction in porosity on hot-working appears in two ways: a reduction in the predominant pore size and a reduction in the volume of pores at any given size. Porosities as low as 2% ($d > 0.086\ \mu$) were observed for hot-pressed bodies prepared with 25 wt-% pitch.

Measurements of the crushing strength were made for specimens cut both parallel with, and perpendicular to the direction of hot-working. The data for the three groups of specimens are summarized in Fig. 25. In all cases the strength in the perpendicular direction decreases with increasing

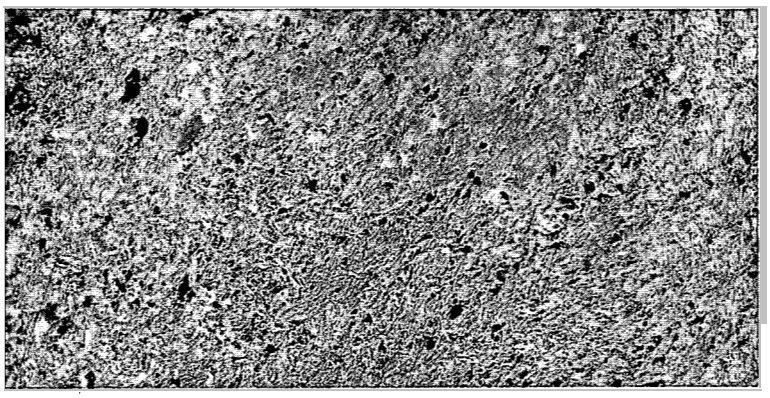

M 3927-1-1 (50×)

(a) Matrix graphite, 10 wt-% pitch, annealed at 2500°C

M 3925-1-1 (50×)

(b) Matrix graphite, 10 wt-% pitch, hot-worked to 69% strain, finishing temperature 2900°C

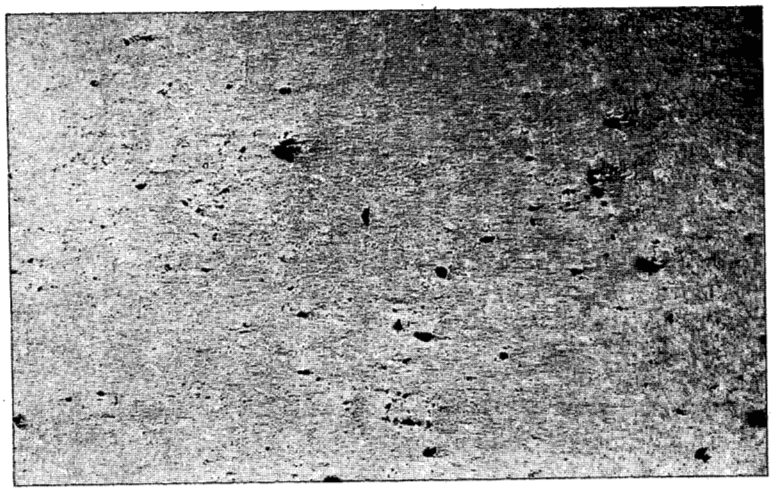

M 3926-1-1 (50×)

(c) Matrix graphite, 25 wt-% pitch, hot-worked to 67% strain, finishing temperature 2900°C

Fig. 22--Microstructure of hot-pressed matrix graphites in several conditions of annealing and hot-working; sections are longitudinal

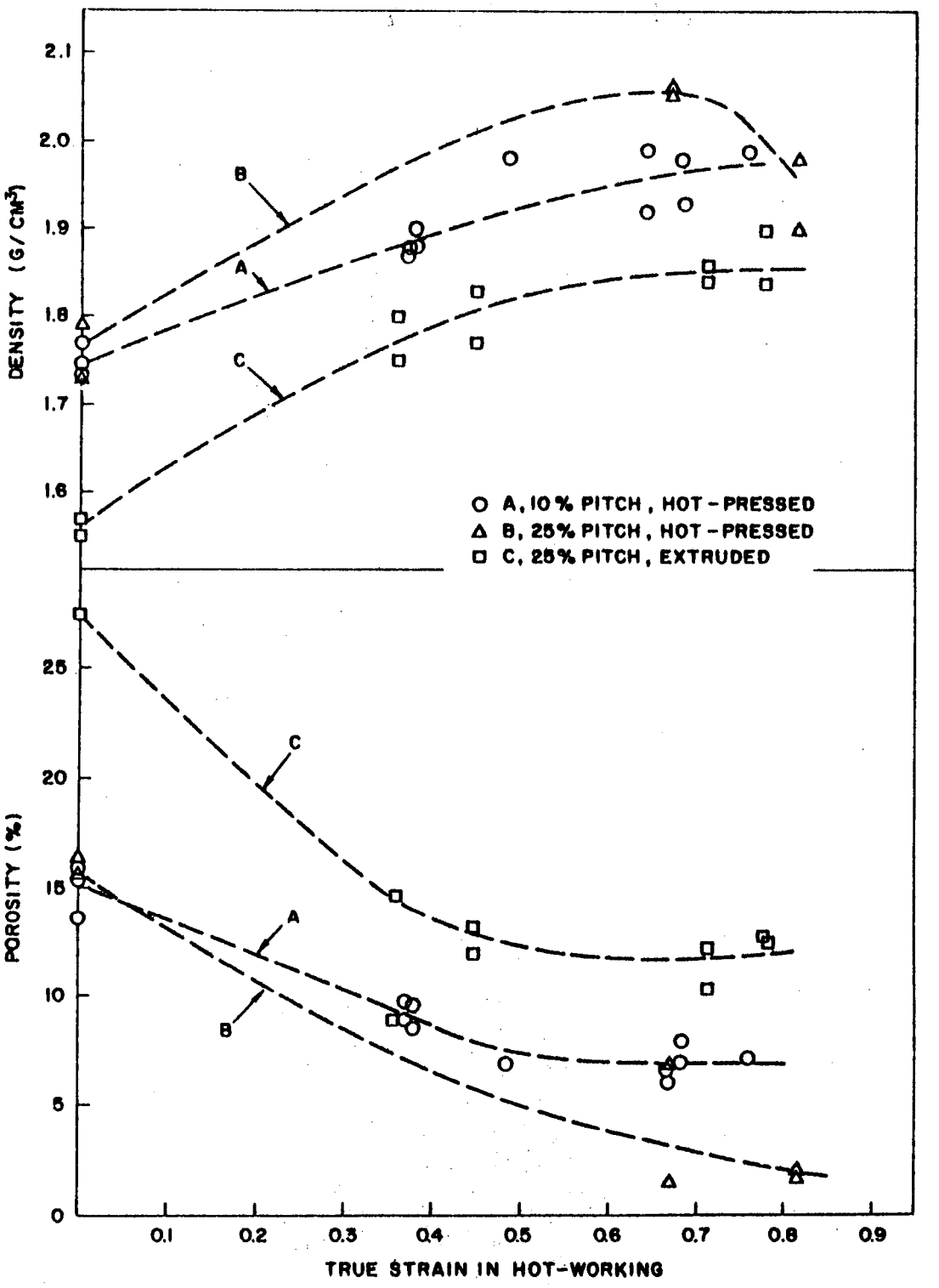

Fig. 23--Density and porosity (for pores greater than 0.086 μ in diameter) of hot-worked fuel-matrix graphite

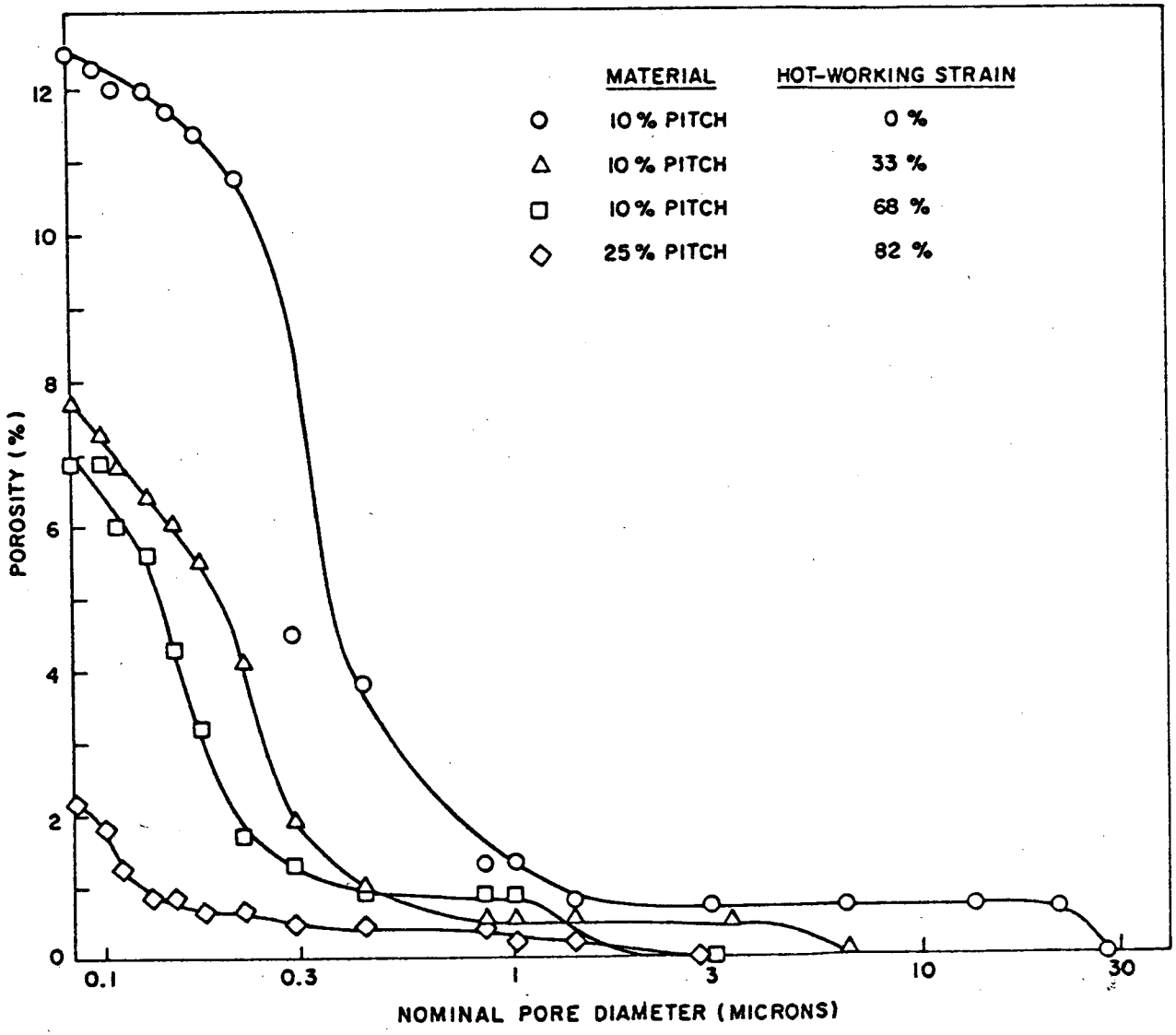

Fig. 24--Typical porosity curves, determined by mercury porosimetry, for annealed and hot-worked fuel-matrix graphites

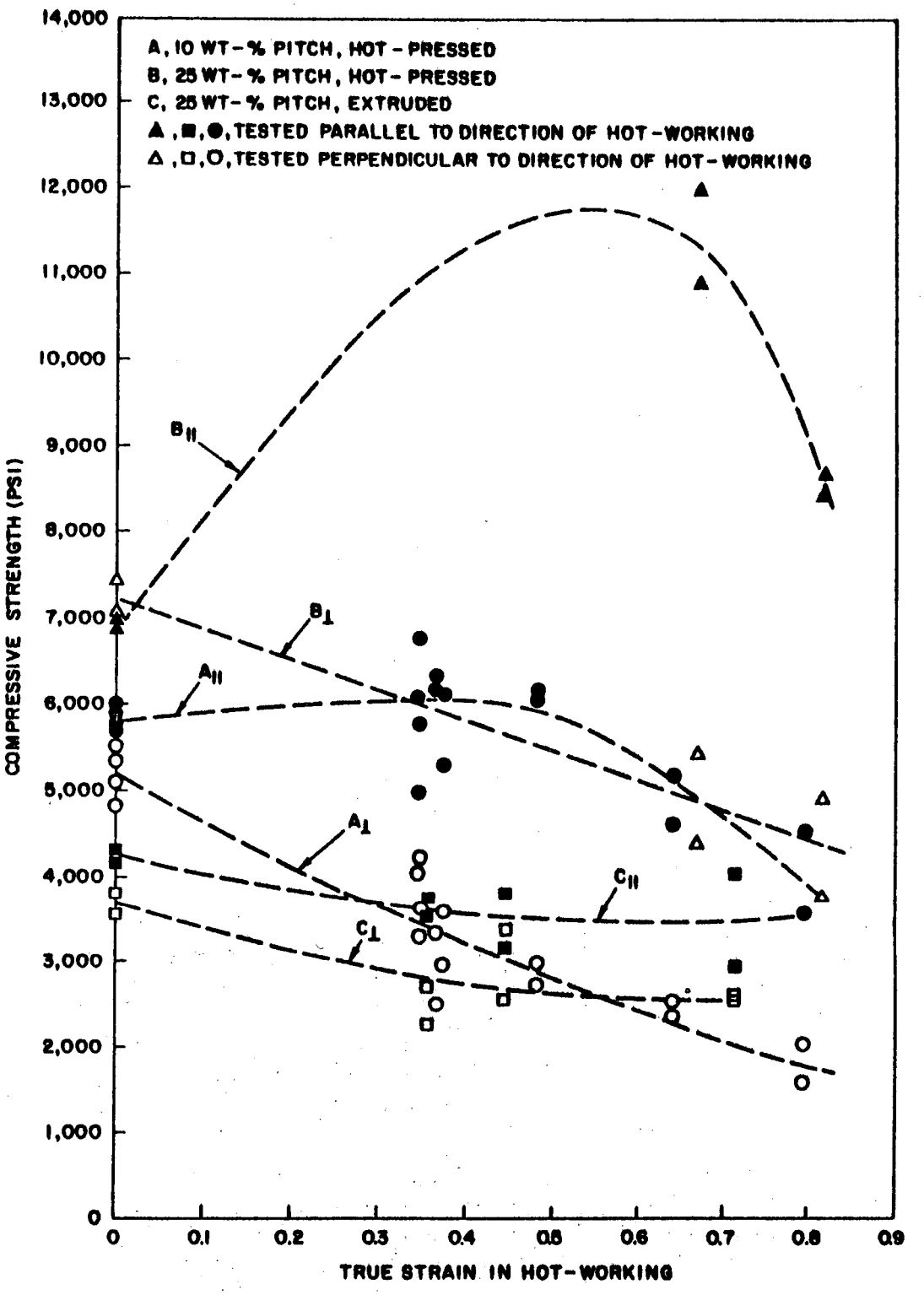

Fig. 25--Compressive strength of hot-worked fuel-matrix graphite

strain during hot-working. The parallel specimens differ widely in behavior. High strengths were observed with hot-pressed specimens prepared with 25 wt-% pitch, and the data suggest the existence of a maximum in the crushing strength at a hot-working strain level below 65%. In all cases the load-deflection curves show low apparent elastic moduli for the hot-worked specimens tested in the parallel direction. For specimens of type B tested parallel with the direction of hot-work, strains in excess of 1% were attained before failure; it may be noted that the apparent modulus, i. e., the slope of the load-deflection curve, increased at the high testing strains.

Typical thermal expansion curves are given in Fig. 26. The results are summarized in Fig. 27 in terms of the mean coefficient of thermal expansion from 22°C to 1000°C. The hot-pressed specimens show a tendency to saturation in the thermal expansion, particularly in the parallel directions. It should be noted that, at high strain levels, the thermal expansion in the perpendicular direction has begun to show the contraction characteristic of the single crystal in the a-direction. The extruded specimens show a crossover in thermal expansion at approximately 40% true strain for parallel and perpendicular specimens, and at higher strain levels the parallel specimens do not reach as high values of thermal expansion as for hot-pressed specimens; these observations are indicative of the more extensive changes in preferred orientation produced by hot-working extruded specimens along the axis of extrusion.

Measurements of the helium permeability in the two principal directions are summarized in Fig. 28. In all cases hot-working is more effective in reducing permeability in the parallel direction. The results for type A, hot-pressed bodies prepared with 10 wt-% pitch, are not impressive; there is considerable scatter in the data and only modest reductions in the parallel direction, and in some cases the permeability in the perpendicular direction is higher for hot-worked specimens than for the annealed reference specimens. In the case of type B specimens prepared with 25 wt-% pitch, the reference specimens are very permeable, and large reductions in permeability are effected by hot-working. The results for the extruded bodies, type C, show a lesser effect of hot-working but suggest the presence of a minimum in permeability near 65% true strain.

Although the trend lines appearing in Figs. 23, 25, 27, and 28 are in some cases only tentative interpolations, the trends found in these exploratory studies are sufficient to provide effective guidance for further work. With the aim of attaining low permeabilities without undue loss in the mechanical properties, it is proposed to investigate the properties as a function of pitch content for a strain level in the neighborhood of 40% and then to study the effect of strain level at the optimum pitch content. No further work with extruded materials is currently contemplated.

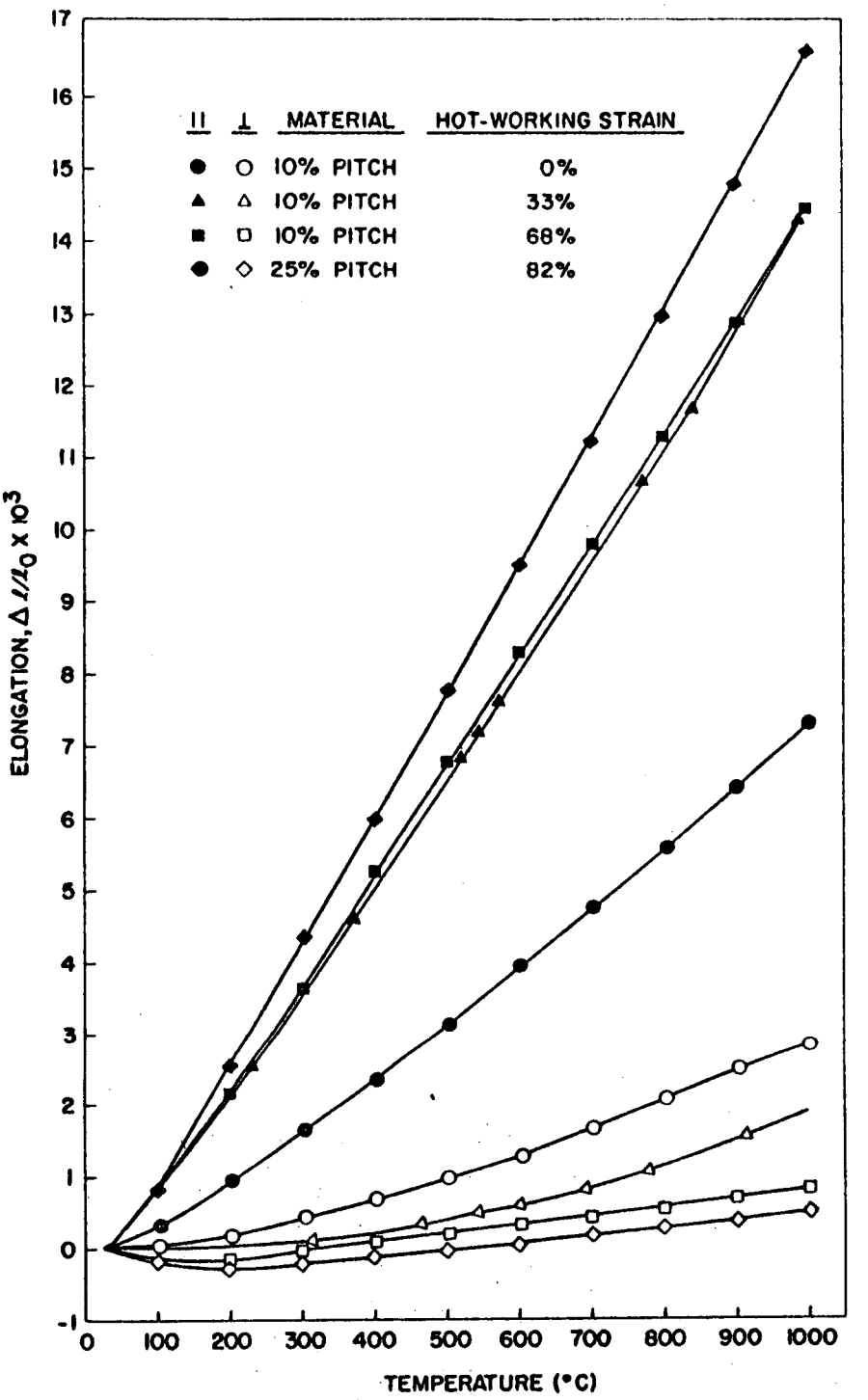

Fig. 26--Typical curves for the thermal expansion of annealed and hot-worked fuel-matrix graphites. Shaded and open symbols refer to measurements made parallel and perpendicular, respectively, to the axis of hot-working or warm-pressing.

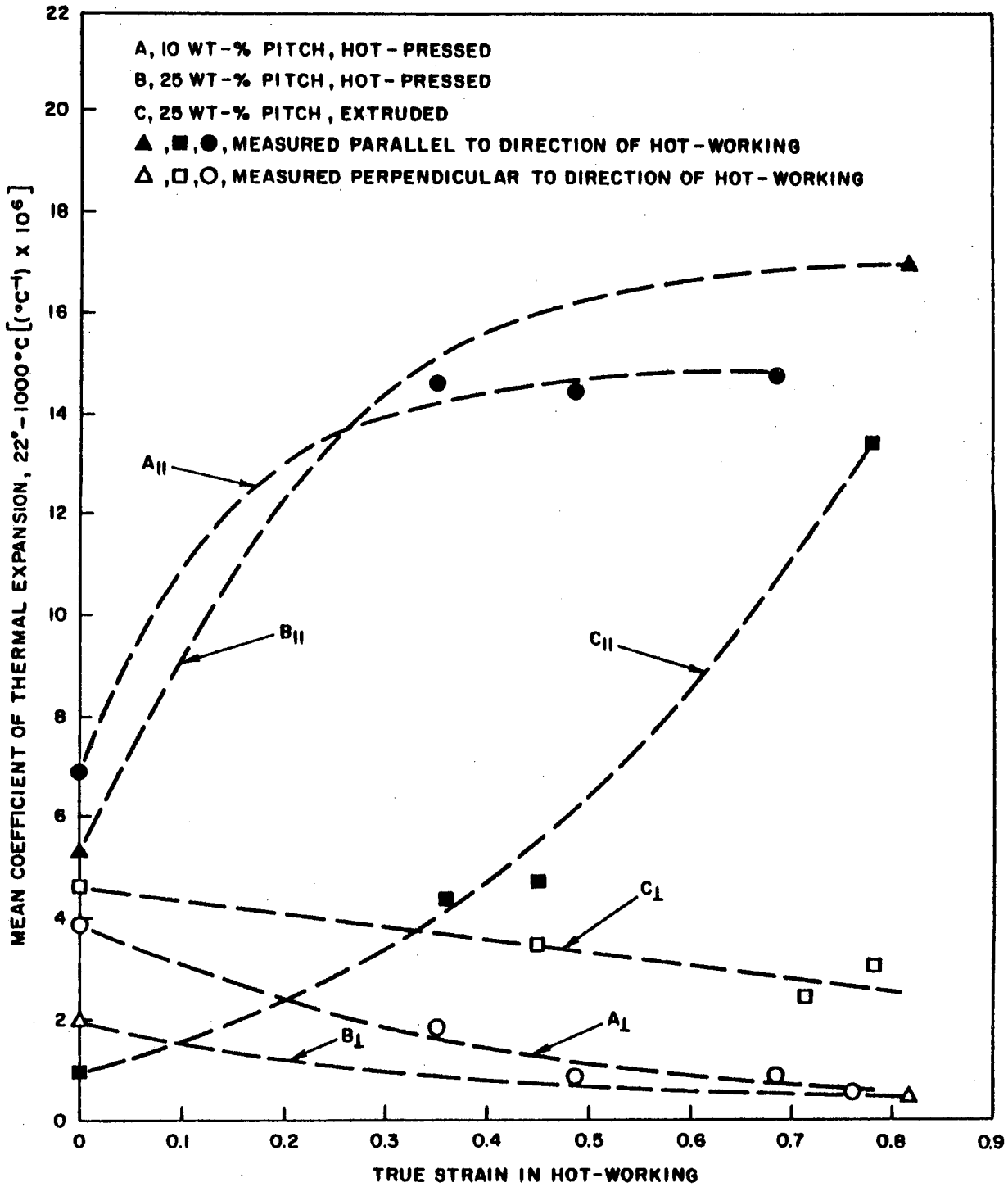

Fig. 27--Thermal expansion of hot-worked fuel-matrix graphite

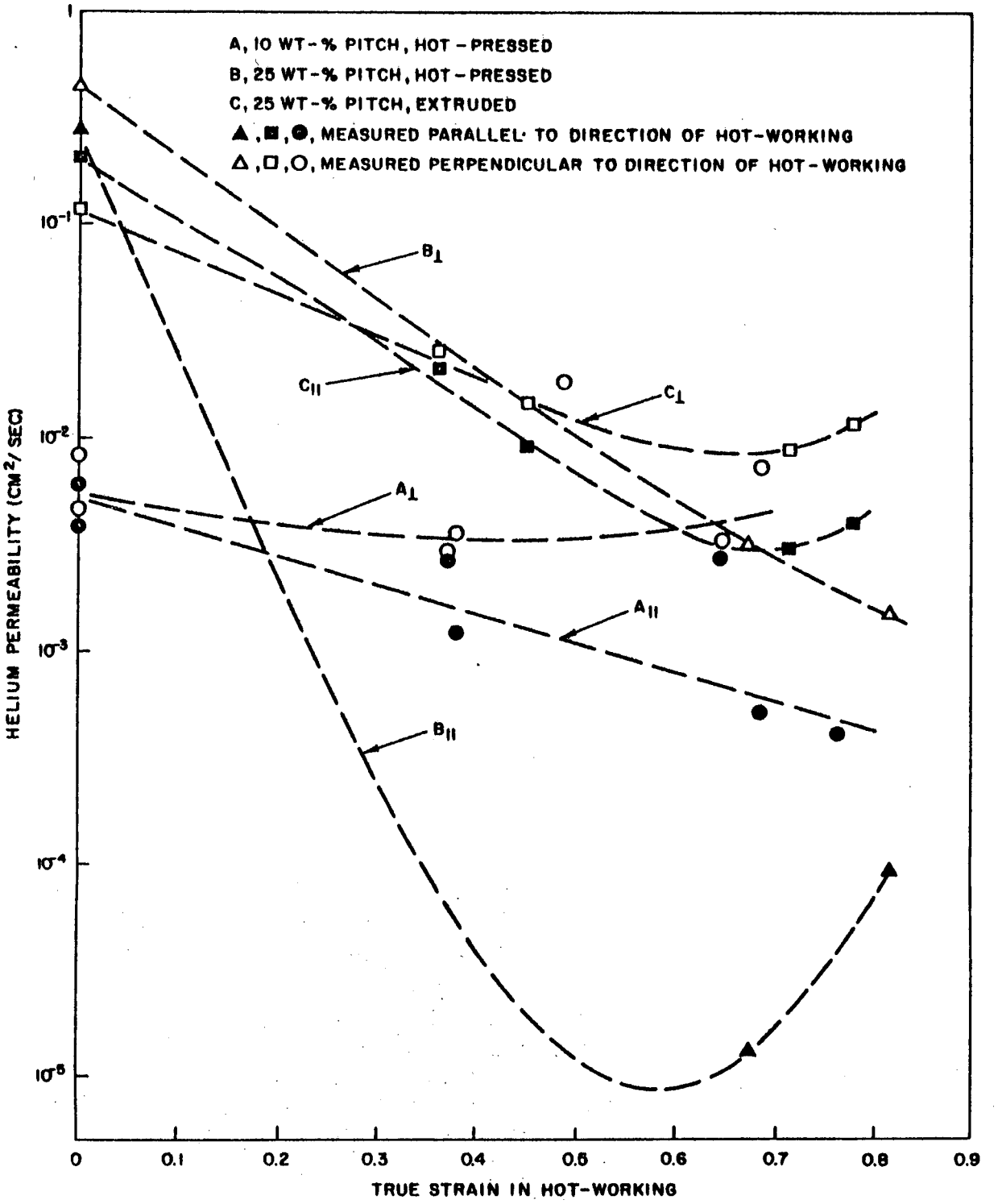

Fig. 28--Helium permeability of hot-worked fuel matrix graphite

3.3. FRACTURE CONDITIONS IN HOT-WORKING
(J. M. Pontelandolfo, J. L. White)

In the course of the work described in Section 3.1, it became apparent that the risk of fracture during hot-working is lower for bodies prepared with higher pitch contents. Some work on the creep of graphite at high temperature indicates that the creep rate is very sensitive to stress.[27] Since the presence of a fuel carbide in a graphite body imposes limitations on the maximum temperature that may be used in hot-working, some experiments have been conducted in support of the companion program on the hot-working of graphite-matrix fuel bodies* to determine the maximum safe hot-working stresses at higher pitch contents than used in the earlier work (i.e., pitch contents greater than 10 wt-%).

Two temperatures were selected for study: 2400°C and 2700°C. Standard hot-working specimens, 1 in. in diameter by 2 in. long, were used. The procedure was to load the specimen rapidly in compression to 5000 lb and then to increase the load in steady increments until fracture occurred. In most cases, appreciable deformation took place before fracture, and in one case fracture did not occur in the period of the run with a maximum load of 10,000 lb.

The results are summarized in Table 1. The ram travel to fracture provides a rough measure of deformation occurring before fracture. These runs verify that appreciably higher hot-working loads can be used without risk of fracture if the pitch content is increased above 10 wt-%. This information has been applied in the hot-working of fueled graphite bodies to reduce the hot-working time markedly.

3.4. X-RAY DIFFRACTION STUDIES ON HOT-WORKED GRAPHITE
(R. J. Price)

X-ray powder photographs were taken of samples of matrix or ZrC-matrix graphite both before and after hot-working. Specimens hot-worked at a number of different temperatures were used.

All the powder patterns showed lines due to highly crystalline graphite having a c-spacing of about 3.36 Å. Well-defined diffraction lines characteristic of a good three-dimensional graphitic structure appeared on all the patterns. There was no difference between the patterns from material before and after hot working. Thus, the diffraction patterns provide no positive evidence for "recrystallization" during hot-working. However, since the starting material itself is highly graphitic, it is doubtful whether

*Contract AT(04-3)-167, Project Agreement 12, Task I.

a further increase in crystalline perfection would produce significant changes in the diffraction pattern.

Table 1

TESTS OF HOT-WORKING LOADS FOR FRACTURE

Pitch Content (wt-%)	Hot-Working Temp. (°C)	Load at Fracture (lb)	Ram Travel at Fracture (in.)
20	2,400	9,800	0.27
20	2,400	10,000	No fracture
20	2,700	10,000	0.45
20	2,700	8,000	0.12
20	2,700	10,000	0.46
30	2,400	10,000	0.20
30	2,400	9,500	0.17
30	2,700	7,500	0.15
30	2,700	9,000	0.35
30	2,700	7,000	0.11

3.5. PREFERRED ORIENTATION IN HOT-WORKED GRAPHITE

(R. J. Price)

Quantitative measurements of the preferred orientation in a number of hot-worked specimens were made using the X-ray technique described in Section 2.2. The following samples were used:

Fuel-matrix graphite prepared with 10 wt-% pitch, annealed at 2500°C

Fuel-matrix graphite prepared with 10 wt-% pitch, hot-worked 28% at 2500°C

Fuel-matrix graphite prepared with 10 wt-% pitch, hot-worked 30% at 2810°C

Fuel-matrix graphite prepared with 10 wt-% pitch, hot-worked 64% at 2850°C

Fuel-matrix graphite prepared with 25 wt-% pitch, hot-worked 82% at 2700° to 2900°C

Fuel-matrix graphite prepared with 10 wt-% pitch containing 23 vol-% irregularly-shaped ZrC particles between 125 and 177 μ in size, annealed at 1850°C

Fuel-matrix graphite prepared with 10 wt-% pitch containing 23 vol-% irregularly-shaped ZrC particles between 125 and 177 μ in size, hot-worked 30% at 2415°C

The resulting curves of $I(\phi)$ against ϕ, where ϕ is the angle between the hot-working direction and the direction in which I is being measured, are shown in Figs. 29 through 32.

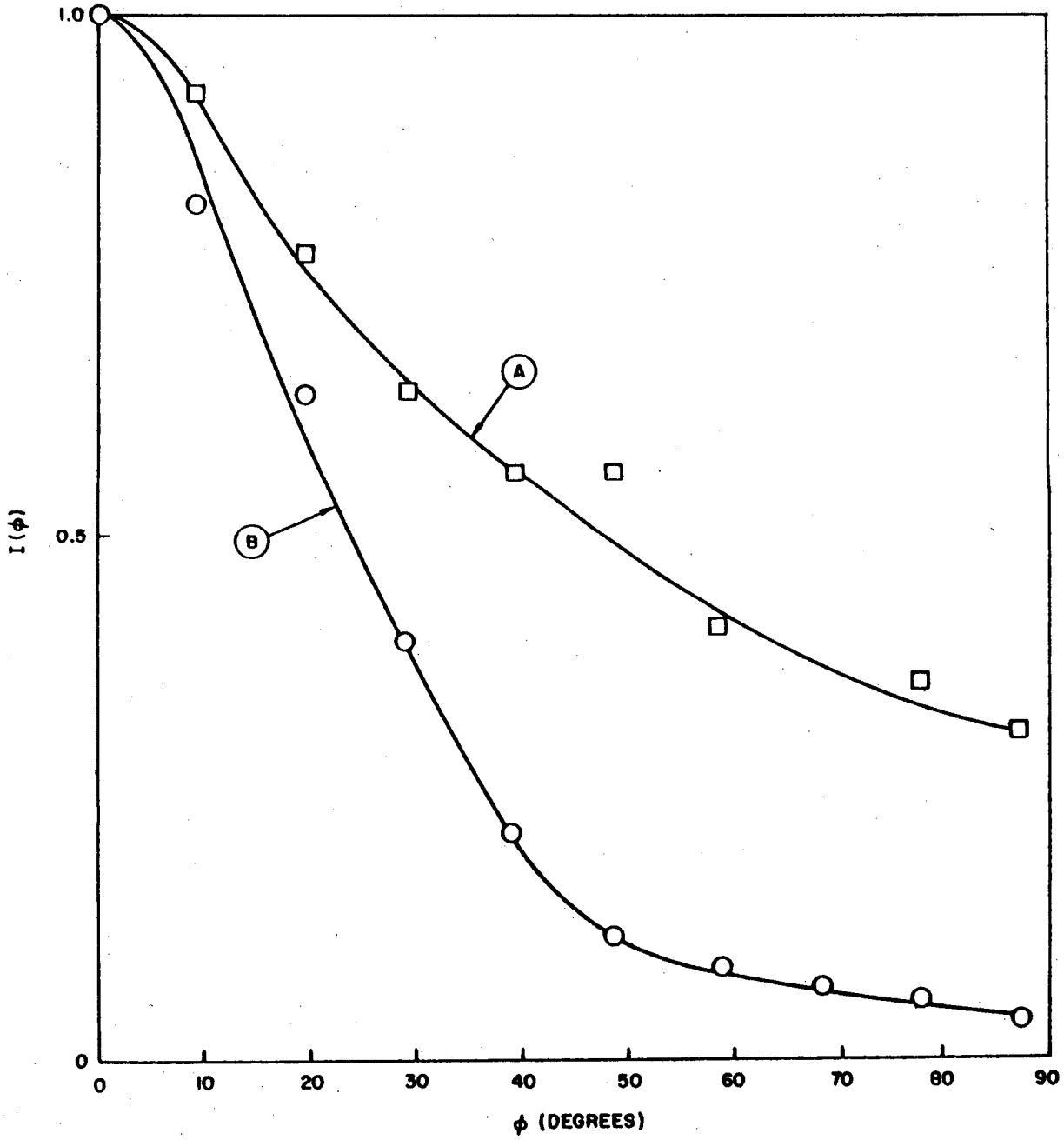

Fig. 29 --Preferred orientation curves for matrix graphite (A) annealed at 2500°C and (B) hot-worked 28% at 2500°C

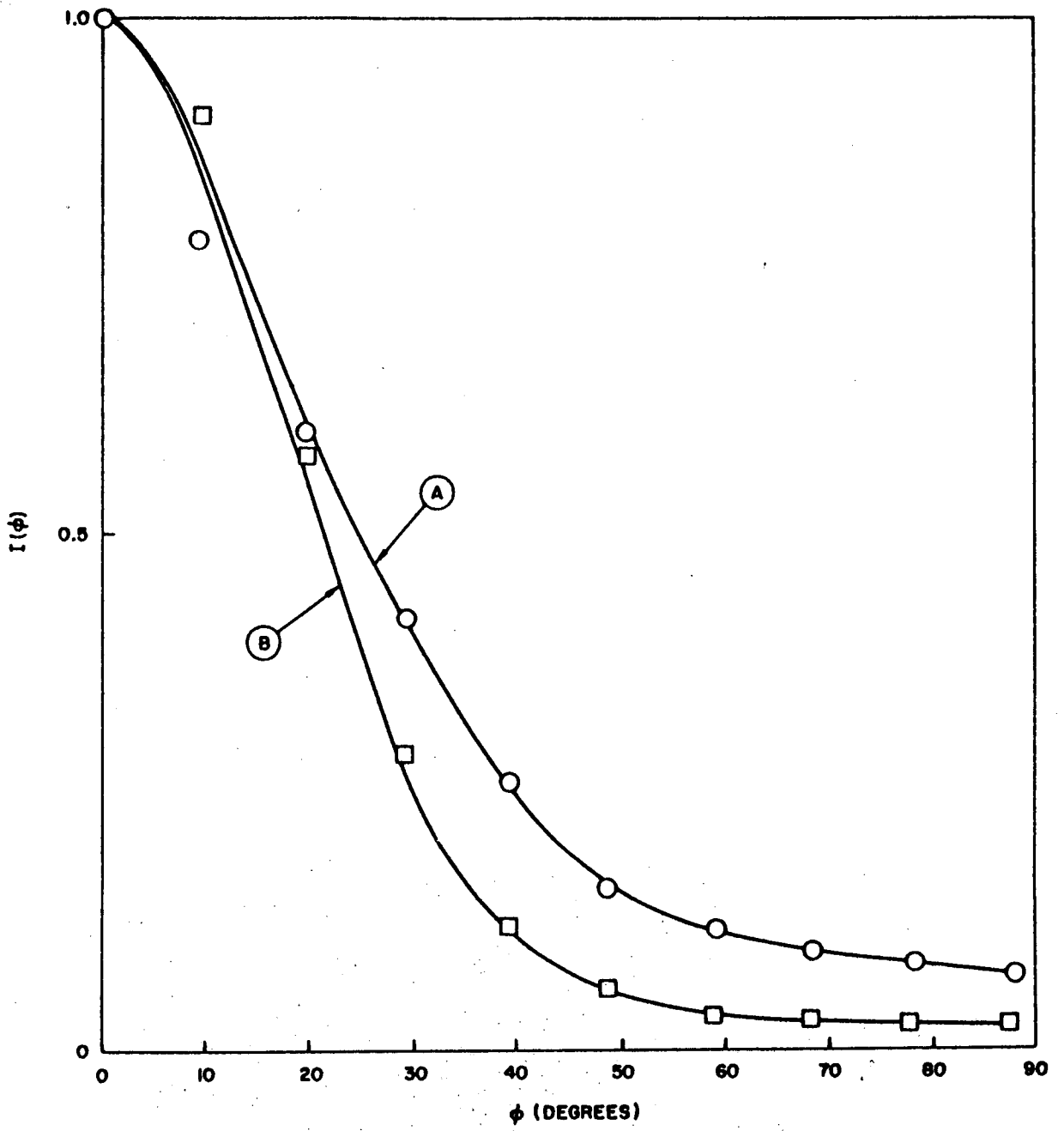

Fig. 30--Preferred orientation curves for matrix graphite hot-worked (A) 30% at 2810°C and (B) 64% at 2850°C

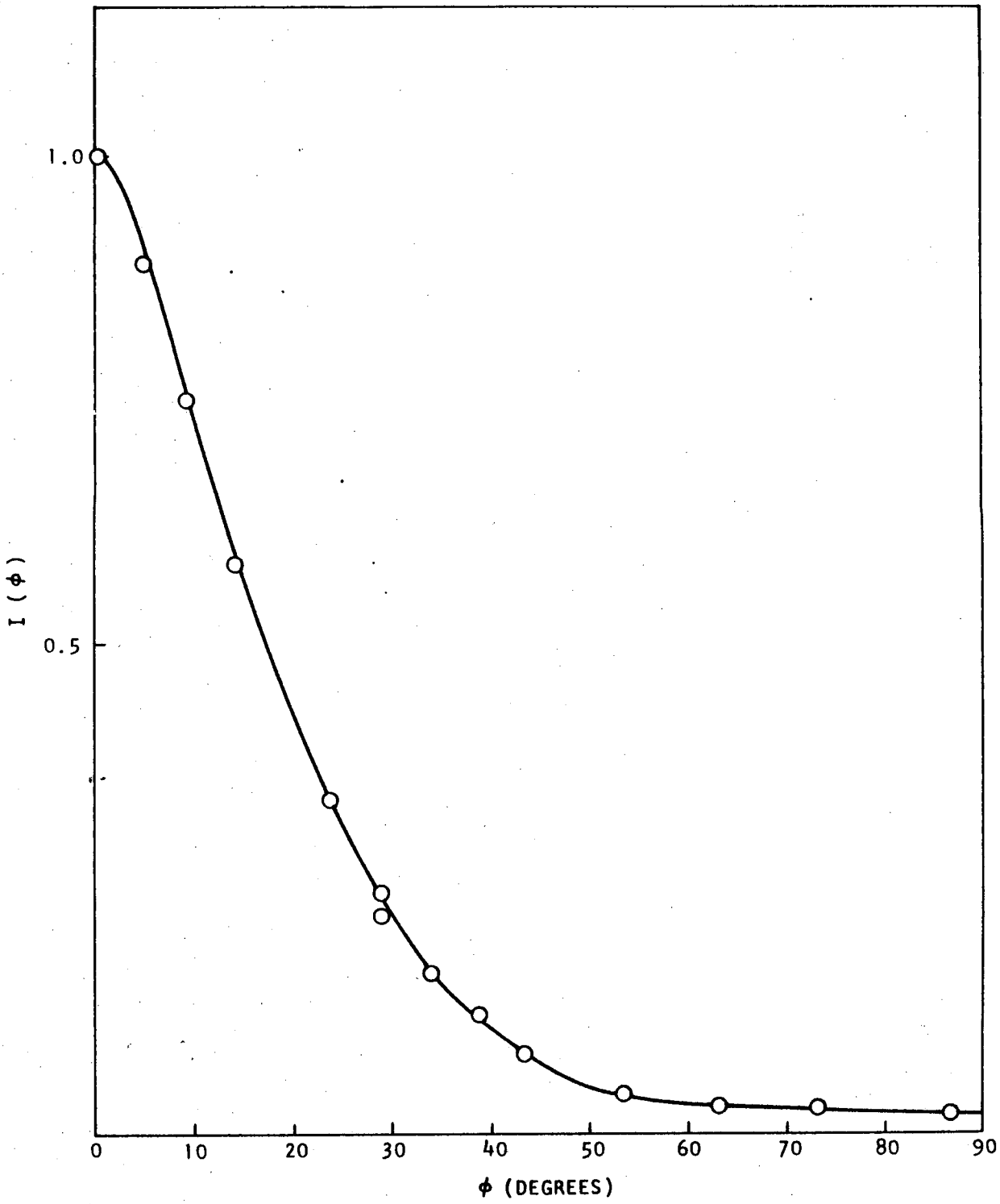

Fig. 31--Preferred orientation curve for matrix graphite (25 wt-% pitch) hot-worked 82% at 2700° to 2900°C

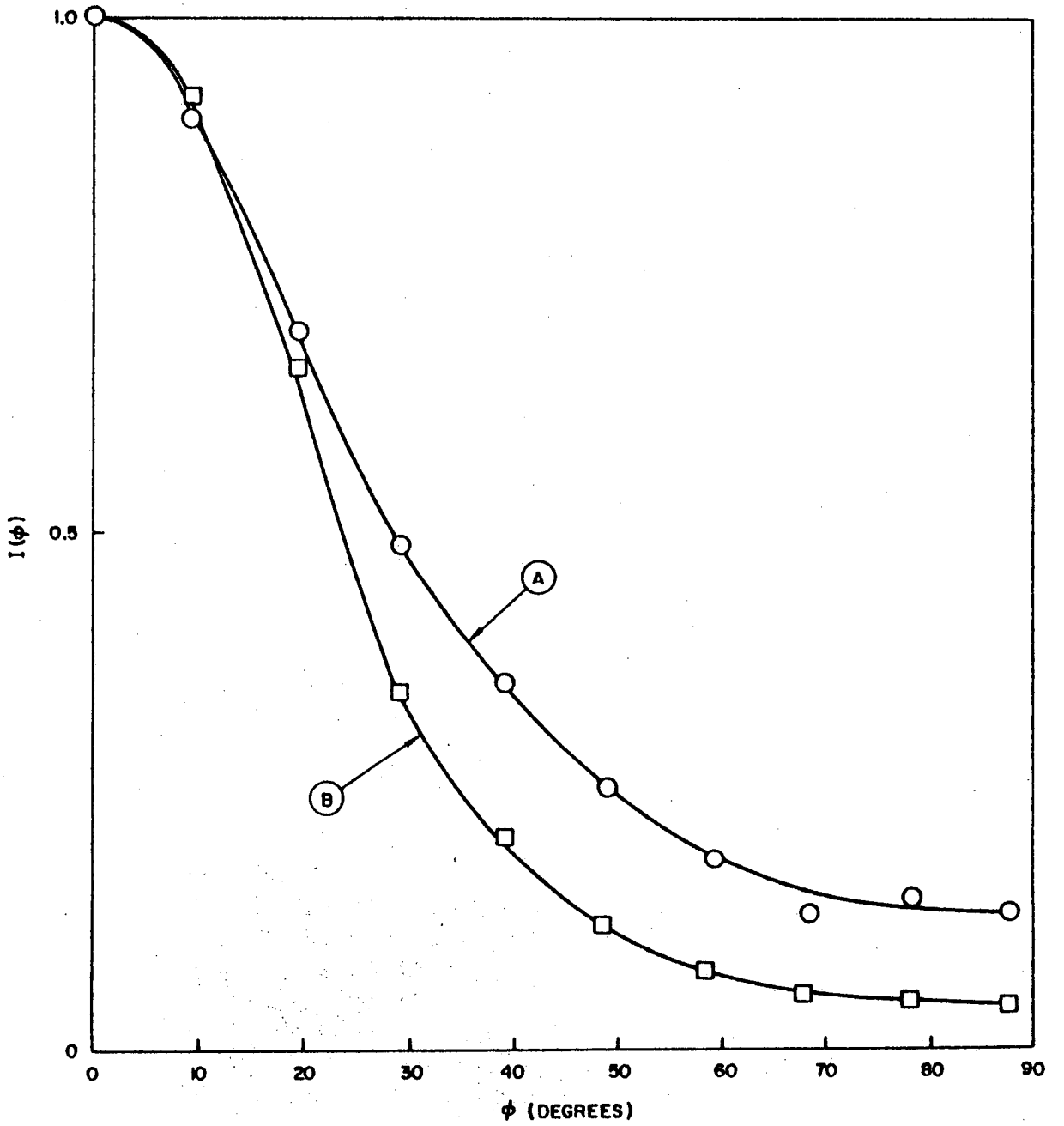

Fig. 32--Preferred orientation curves for ZrC-matrix composites (A) annealed at 1850°C and (B) hot-worked 30% at 2415°C

It can be seen that the starting material has a preferred orientation produced by the warm-pressing operation, the c-axes tending to aline along the pressing direction. Subsequent hot-working in the same direction sharpens the preferred orientation, although it is noticeable that the curves always have a pronounced "tail," $I(\phi)$ remaining at about 0.02 to 0.1 as ϕ approaches 90°. This means that even after extensive hot-working an appreciable number of crystallites have their c-axes perpendicular to the hot-working direction.

The preferred orientation curves for the matrix specimens hot-worked 28% at 2500°C and 30% at 2810°C and for the ZrC-matrix composite hot-worked 30% at 2415°C are almost identical. This indicates that for a given strain the texture is independent of hot-working temperature and is the same whether or not the specimen contains carbide particles. On the other hand, increasing the hot-working strain from 30% to 64% at about 2800°C produces a significantly steeper distribution curve (see Fig. 30). The preferred orientation curve of the specimen prepared with 25 wt-% pitch and hot-worked to 82% strain is only very slightly steeper than the curve of the 10 wt-% pitch specimen hot-worked (64% (see Figs. 31 and 32).

These trends in the relationship between preferred orientation and hot-working strain are closely reflected by the anisotropy of the measured thermal expansion coefficient between the parallel and perpendicular directions.

3.6 RECRYSTALLIZATION OF GRAPHITE FROM LIQUID METAL

(J. M. Pontelandolfo, J. L. White)

Nickel has been chosen as the solvent medium for the initial studies of liquid metal recrystallization because some information exists on the solubility of graphite in nickel[28] and because promising indications of the growth of crystals from nickel melts have been observed by other workers[29] and in previous unpublished work at General Atomic. Two types of experiments have been conducted: simple, single-stage recrystallization by slow cooling of a graphite-saturated melt, and thermal cycling to grow large crystals from less perfectly crystalline material.

Heavy-walled graphite crucibles were used, and the charge consisted of 90 wt-% nickel powder and 10 wt-% graphitized petroleum coke. The maximum temperature was 2200°C. The hot-working furnace, which is now equipped with programmed temperature control, was used to obtain cooling rates of the order of 5°C/min.

Photomicrographs of crystals grown in a single-stage recrystallization run are shown in Figs. 33 and 34. The structure of large proeutectic

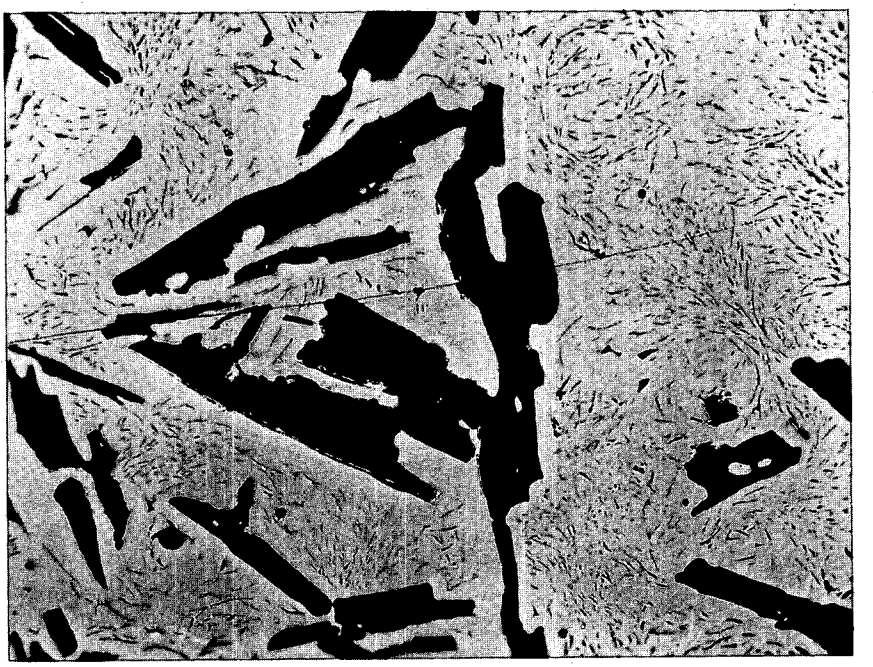

M-6052-1-3 (50×)

Fig. 33--Proeutectic graphite crystals grown in a Ni-C matrix; unetched

M-6052-1-5 (200×)

(a)

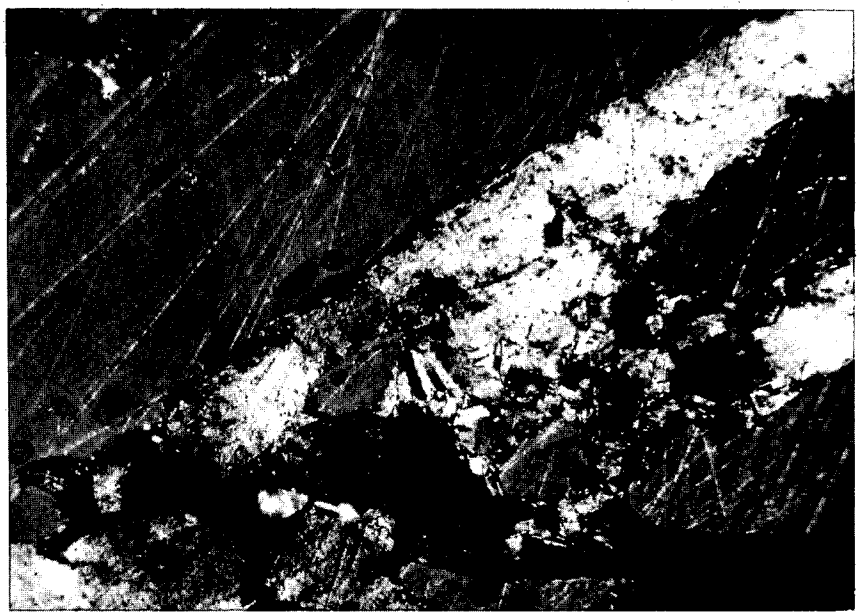

M-6052-1-7 (200×)

(b)

Fig. 34--Structure of a proeutectic graphite dendrite grown in a Ni-C melt; unetched

2

graphite crystals in a eutectic Ni-C matrix is similar to that reported by Minkoff and Einbinder.[29] The individual crystals appear to be relatively free of delamination cracks. However, examination by polarized light or by sensitive-tint microscopy shows that these crystals contain many defects, including twin-like flecks, small-angle boundaries, and bend planes (compare Figs. 34a and 34b). Some relatively perfect crystals were found in the field of section, but even these crystals showed some defects near the edges. The misoriented regions have been observed by Minkoff and Einbinder, who attributed them to growth accidents.

Thermal cycling between 2200°C and 1900°C yielded the unexpected microstructures shown in Fig. 35. In this experiment five thermal cycles were used. Relatively large arrays of polycrystalline aggregates were found in various regions of the crucible. No very large crystals were found; in general the crystals, or grains, were smaller than those found in the single-stage recrystallization run. Most of the crystals in the aggregate regions show extensive delamination cracking; this appears to provide evidence for the existence of accommodation microcracks in other polycrystalline graphite bodies. Bending of the crystals also occurs extensively as indicated by the polarized light photomicrograph (Fig. 35b).

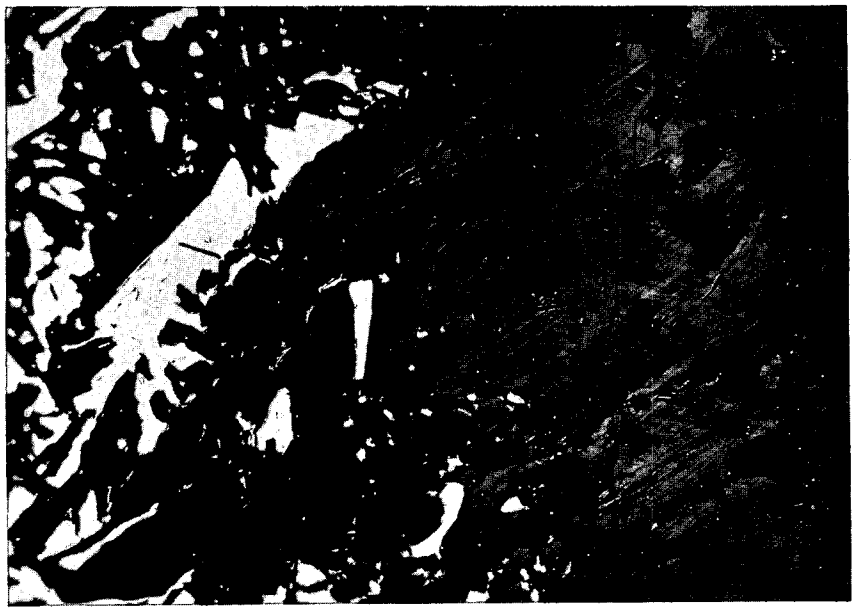

M-6260-1-4 (50×)

(a)

M-6260-1-7 (200×)

(b)

Fig. 35--Graphite crystals grown by thermal cycling of a Ni-C melt in a graphite crucible; unetched

IV. RELATION OF PHYSICAL PROPERTIES TO MICROSTRUCTURE

4.1. PREFERRED ORIENTATION
(J. C. Bokros, R. J. Price)

Because of the extreme anisotropy of the physical properties of a graphite single crystal, the preferred orientation of a polycrystalline body is one of the most important structural parameters for understanding the physical behavior of the body. If preferred orientation measurements could be combined with single-crystal property data to give reliable estimates of physical properties, an important step forward in understanding graphite behavior would result. The work to be described is aimed at bridging this gap.

There are certain directional physical properties of a crystallite that may be averaged to give the over-all properties of a polycrystalline specimen, taking into account the distribution of crystallite orientations. The thermal expansion of a bulk specimen in a given direction is the sum of the contributions of all the crystallites in that direction. Similarly, when a bulk specimen is loaded elastically, the total resulting strain is the sum of strains in the crystallites in the loading direction, and hence the reciprocal of the moduli of the crystallites. If the change in dimensions of graphite with neutron irradiation is seated in the crystallites, the same approach should be applicable to radiation contraction in polycrystals. On the other hand, transport properties (thermal and electrical conductivities, diffusion, etc.), although dependent on orientation, cannot be treated so simply because the flux is free to seek out the easier paths.

To a first approximation the thermal expansion coefficient and the reciprocal modulus of a polycrystalline body may be obtained by averaging out the properties of individual crystallites, using a distribution function to obtain the relative number of crystallites in any orientation. This does not take into account the effect of intercrystalline constraints or of porosity.

Figure 36 represents a group of crystallites in a polycrystal whose c-axes lie within the solid angle between β and $\beta + d\beta$ and between ϕ and $\phi + d\phi$ in a unit sphere. The magnitude of the solid angle is $\sin\phi\, d\phi\, d\beta$ and the number of crystallites within this range is $I(\phi, \beta) \sin\phi\, d\phi\, d\beta$, where I is the intensity function defined in Section 2.2. If these crystallites have an averagable directional property σ whose magnitude at an angle ϕ to the c-axis is $\sigma(\phi)$ then the contribution of the crystallites to the over-all σ in

the OZ direction is proportional to $I(\phi, \beta)\sigma(\phi) \sin \phi \, d\phi \, d\beta$. The bulk property σ in the OZ direction is therefore given by

$$\sigma_{OZ} = \frac{\iint I(\phi,\beta)\sigma(\phi) \sin \phi \, d\phi \, d\beta}{\iint I(\phi,\beta) \sin \phi \, d\phi \, d\beta} . \tag{3}$$

In the case of a graphite body whose texture has cylindrical symmetry (e.g., molded, extruded-rod, hot-worked, or pyrolytic graphite) or orthorhombic symmetry (e.g., the wall of an extruded tube), the limits of integration are 0 and $\pi/2$ for both ϕ and β.

4.2. PREFERRED ORIENTATION AND THERMAL EXPANSION
(J. C. Bokros, R. J. Price)

In a single crystal of a hexagonal material such as graphite, the coefficient of thermal expansion at an angle ϕ to the c-axis is given by

$$\alpha = \alpha_c \cos^2 \phi + \alpha_a \sin^2 \phi , \tag{4}$$

where α_c and α_a are the single-crystal coefficients in the c- and a-directions. When Eq. (4) and Eq. (3) are combined over-all thermal expansion coefficient of a polycrystal in the OZ direction (Fig. 36) is therefore given by

$$\alpha_{OZ} = \frac{\int_0^{\pi/2}\int_0^{\pi/2} I(\phi,\beta) \sin \phi \, (\alpha_c \cos^2 \phi + \alpha_a \sin^2 \phi) \, d\phi \, d\beta}{\int_0^{\pi/2}\int_0^{\pi/2} I(\phi,\beta) \sin \phi \, d\phi \, d\beta} . \tag{5}$$

$$= \alpha_c + (\alpha_a - \alpha_c) \frac{\int_0^{\pi/2}\int_0^{\pi/2} I(\phi,\beta) \sin^3 \phi \, d\phi \, d\beta}{\int_0^{\pi/2}\int_0^{\pi/2} I(\phi,\beta) \sin \phi d\phi \, d\beta} . \tag{6}$$

In the case of a body whose texture has cylindrical symmetry about the OZ

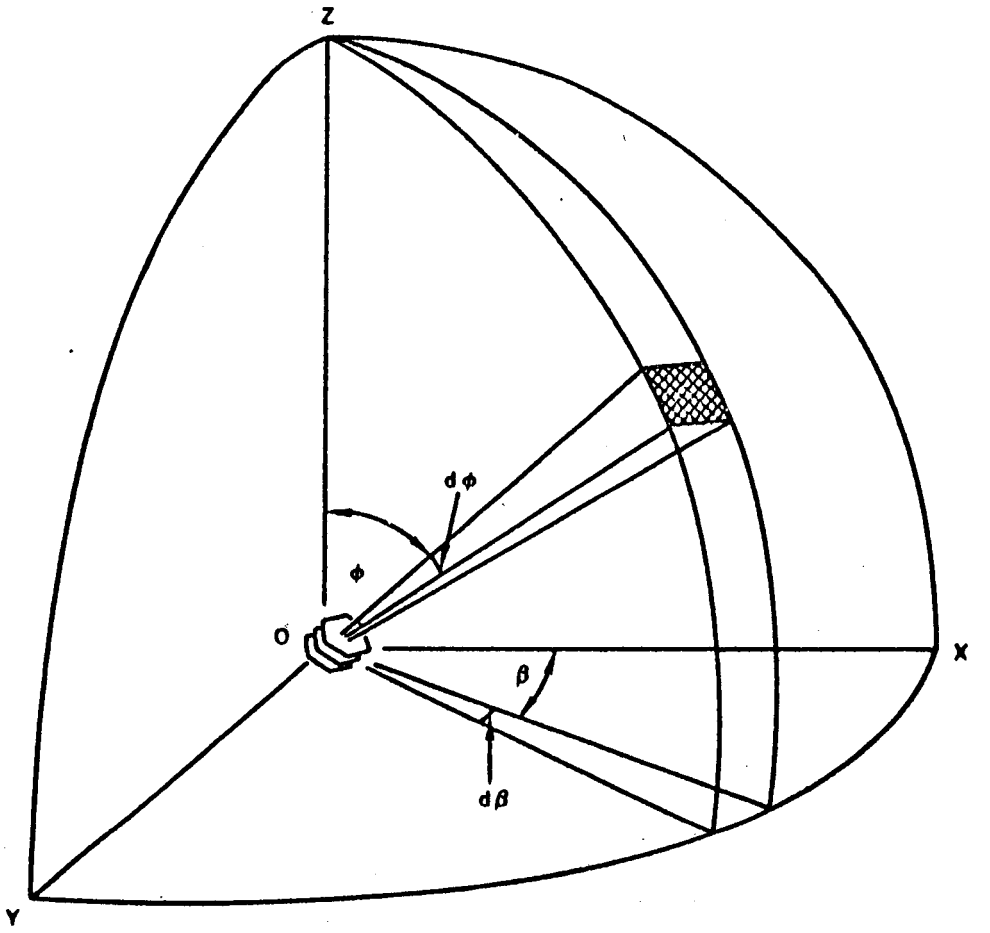

Fig. 36--Angular parameters used in calculating anisotropy of physical properties of polycrystalline graphite

axis this reduces to

$$\alpha_{OZ} = \alpha_c + (\alpha_a - \alpha_c) \frac{\int_0^{\pi/2} I(\phi) \sin^3 \phi \, d\phi}{\int_0^{\pi/2} I(\phi) \sin \phi \, d\phi} . \tag{7}$$

In the OX direction in the same body, the expansion coefficient is

$$\alpha_{OX} = \alpha_a + \frac{\alpha_c - \alpha_a}{2} \frac{\int_0^{\pi/2} I(\phi) \sin^3 \phi \, d\phi}{\int_0^{\pi/2} I(\phi) \sin \phi \, d\phi} . \tag{8}$$

The expressions may be simplified by introducing an orientation parameter R such that

$$R_{OZ} = \frac{\int_0^{\pi/2} \int_0^{\pi/2} I(\phi,\beta) \sin^3 \phi \, d\phi \, d\beta}{\int_0^{\pi/2} \int_0^{\pi/2} I(\phi,\beta) \sin \phi \, d\phi \, d\beta} . \tag{9}$$

R_{OZ} depends on the direction in which OZ is taken in a graphite body and also on the preferred orientation. In a single crystal, it takes the value 1 in the a-direction and 0 in the c-direction, and in a random aggregate it has the value 2/3 in any direction. For a sample whose texture has cylindrical symmetry about the axis OZ, R_{OZ} reduces to

$$R_{OZ} = \frac{\int_0^{\pi/2} I(\phi) \sin^3 \phi \, d\phi}{\int_0^{\pi/2} I(\phi) \sin \phi \, d\phi} , \tag{10}$$

and R_{OX} (perpendicular to the axis of symmetry) is related to R_{OZ} thus:

$$R_{OX} = 1 - \frac{R_{OZ}}{2} . \tag{11}$$

Sutton and Howard [15] have shown that for one grade of reactor graphite substantial accommodation of thermal expansion occurs in the crystallite c-direction, perhaps because of cleavage cracks within the grains, but the a-direction expansion makes a full contribution to the bulk expansion. This means that the c-direction single-crystal expansion coefficient, α_c in the thermal expansion equations, should be multiplied by an "accommodation coefficient" γ, which is the fraction of crystallite c-direction thermal expansion that contributes to the bulk expansion of the sample. The expression for the thermal expansion coefficient α in the direction OZ therefore becomes

$$\alpha_{OZ} = R_{OZ}\alpha_a + (1 - R_{OZ})\gamma\alpha_c \ . \qquad (12)$$

The introduction of the accommodation coefficient γ provides a convenient means of taking into account the effects of intercrystalline restraints and expansion into pores. It is reasonable to postulate that the amount of accommodation of crystallite expansion depends on the preferred orientation of the body, being zero for a single crystal and large for a random aggregate. In the course of relating preferred orientation to thermal expansion, the degree of intercrystalline accommodation during thermal expansion was investigated on an empirical basis as a function of preferred orientation for a wide range of graphites.

The orientation parameter R in Eq. (12) can be calculated from X-ray measurements of preferred orientation (see Section 2.2), using Eq. (9) and performing the integration graphically. For a sample whose preferred orientation has cylindrical symmetry (e.g., pyrolytic, hot-worked, molded, or extruded-rod graphites), a single X-ray measurement can be used to give the orientation parameter R in directions both parallel and perpendicular to the axis of symmetry as expressed in Eqs. (10) and (11).

When the orientation parameter R has been calculated from preferred orientation measurements, the accommodation coefficient γ can be evaluated from the observed thermal expansion coefficient using Eq. (12). The calculation is simplified by using the expansion coefficient at 400°C, where α_a is 0 and α_c is $28 \times 10^{-6}\ {}^{\circ}C^{-1}$. Values of R and γ were worked out in this way for a range of different graphites.

Thermal expansion measurements were made using a Leitz dilatometer. The specimens investigated included the hot-worked samples whose preferred orientation curves are shown in Figs. 29 through 31, and material from the wall of an extruded tube, samples being taken in the radial, tangential, and longitudinal directions. In the latter case values of I were obtained from the relevant pole figure (e.g., Fig. 27) and R was evaluated graphically by double integration using Eq. (9). Samples of extruded

needle-coke graphite (EGCR graphite, Type NC-8) were also tested. A preferred orientation curve, obtained as described in Section 2.2, is shown in Fig. 3. Similar calculations were made in the cases of graphites where sufficient thermal expansion and preferred orientation data have been published in the open literature.[15, 30] The complete results for the measured thermal expansion coefficients at 400°C, orientation parameters R, and accommodation coefficients γ are listed in Table 2.

Figure 37 shows the measured thermal expansion coefficients plotted against the preferred orientation parameter R, with the theoretical line for an accommodation coefficient of unity Eq. (12) marked in. Because of the accommodation effect, the observed values fall below the "no accommodation" line: for any value of R, the ratio of observed expansion coefficient at 400°C to theoretical coefficient is equal to the accommodation coefficient γ. The same data were used to plot γ directly as a function of R in Fig. 38.

From both these plots it is clear that there is a systematic variation of accommodation coefficient with preferred orientation, despite the scatter due to differences in the microstructure, density, and crystallinity of individual graphites. As anticipated, the accommodation coefficient approaches unity in the c-direction in highly oriented samples (R=0) where intercrystalline restraints are at a minimum. The coefficient falls sharply as the sample becomes more random and the intercrystalline restraints increase. As R approaches one (corresponding to the predominantly a-direction in a highly oriented body), the value of the accommodation coefficient seems to depend on the nature of the sample. For example, it is significantly higher for pyrolytic graphite than for a highly hot-worked graphite (Fig. 38).

The explanation may lie in the details in the structure of the two materials as revealed by their preferred orientation curves. Figure 39 shows plots of the relative density of c-axes $I(\phi)$ as a function of the angle ϕ from the normal to the deposit or the hot-working direction for (1) as-deposited pyrolytic graphite and (2) "matrix" graphite hot-worked to 82% strain at 2700° to 2900°C. Although these specimens have very similar R-values in the predominantly a-direction (0.92 and 0.87 respectively), the intensity function for the pyrolytic graphite cuts off sharply, falling to zero at $\phi = 60°$, whereas the intensity function curve for the hot-worked sample has a noticeable "tail," with $I(\phi)$ remaining finite out to $\phi = 90°$. The corresponding structures may be visualized as in Fig. 39. The pyrolytic graphite can be considered as a stack of wrinkled sheets, with the maximum misorientation in the wrinkles being about 60°, while the hot-worked sample still contains a few "islands" where the crystallites are oriented 90° away from the principal texture. It can be seen that the c-direction contributions to the thermal expansion will be much less

Table 2

ORIENTATION PARAMETER, R, AND ACCOMMODATION COEFFICIENT, γ, FOR VARIOUS GRAPHITES

Type of Graphite	Orientation	Measured at 400°C ($\times 10^{-6}$ °C^{-1})	Orientation Parameter, R	Accommodation Coeff., γ
Pyrolytic (Ref. 30)	⊥ Deposit	23.5	0.16	1.00
(1) As-deposited	∥ Deposit	1.2	0.92	0.54
(2) Regenerative; annealed 3 hr at 2800°C	⊥ Deposit	27.0	0.04	1.00
	∥ Deposit	0.6	0.98	0.96
(3) Singularly nucleated; annealed 3 hr at 2800°C	⊥ Deposit	27.0	0.09	1.04
	∥ Deposit	0.8	0.96	0.65
Raytheon pyrolytic carbon, as-deposited	⊥ Deposit	25.0	0.24	1.18
	∥ Deposit	1.8	0.88	0.54
Hot-worked "matrix"				
(1) As-molded	⊥ Molding	2.7	0.71	0.33
	∥ Molding	7.0	0.58	0.64
(2) 28% strain at 2500° C	⊥ Compression	1.4	0.81	0.27
	∥ Compression	14.7	0.38	0.84
(3) 30% strain at 2810°C	⊥ Compression	1.4	0.79	0.24
	∥ Compression	14.5	0.42	0.88
(4) 64% strain at 2850°C	⊥ Compression	1.2	0.86	0.29
	∥ Compression	15.3	0.29	0.77
(5) 83% strain at 2700° to 2900°C	⊥ Compression	0.8	0.87	0.21
	∥ Compression	17.3	0.27	0.85
Extruded EGCR needle-coke graphite (NC-8)	⊥ Extrusion	3.4	0.62	0.32
	∥ Extrusion	1.8	0.77	0.27
Extruded British Reactor Grade A (Ref. 13)				
(1) Ser. I, block 7110	⊥ Extrusion	4.0	0.61	0.37
	∥ Extrusion	1.9	0.79	0.32
(2) Ser. I, block 7113	⊥ Extrusion	4.2	0.60	0.38
	∥ Extrusion	2.2	0.81	0.41
(3) Ser. II, Grade A(1)	⊥ Extrusion	4.8	0.62	0.45
	∥ Extrusion	3.0	0.76	0.45
(4) Ser. II, Grade A(2)	⊥ Extrusion	4.2	0.60	0.37
	∥ Extrusion	2.2	0.79	0.37
(5) Ser. II, experimental, cored Grade A	⊥ Extrusion	3.6	0.60	0.32
	∥ Extrusion	2.0	0.79	0.34
Extruded GA tube stock	Radial	8.8	0.49	0.58
(1) Tube 1	Tangential	4.0	0.65	0.41
	Longitudinal	1.7	0.84	0.39
(2) Tube 2	Radial	8.3	0.50	0.63
	Tangential	4.0	0.63	0.41
	Longitudinal	1.4	0.85	0.33

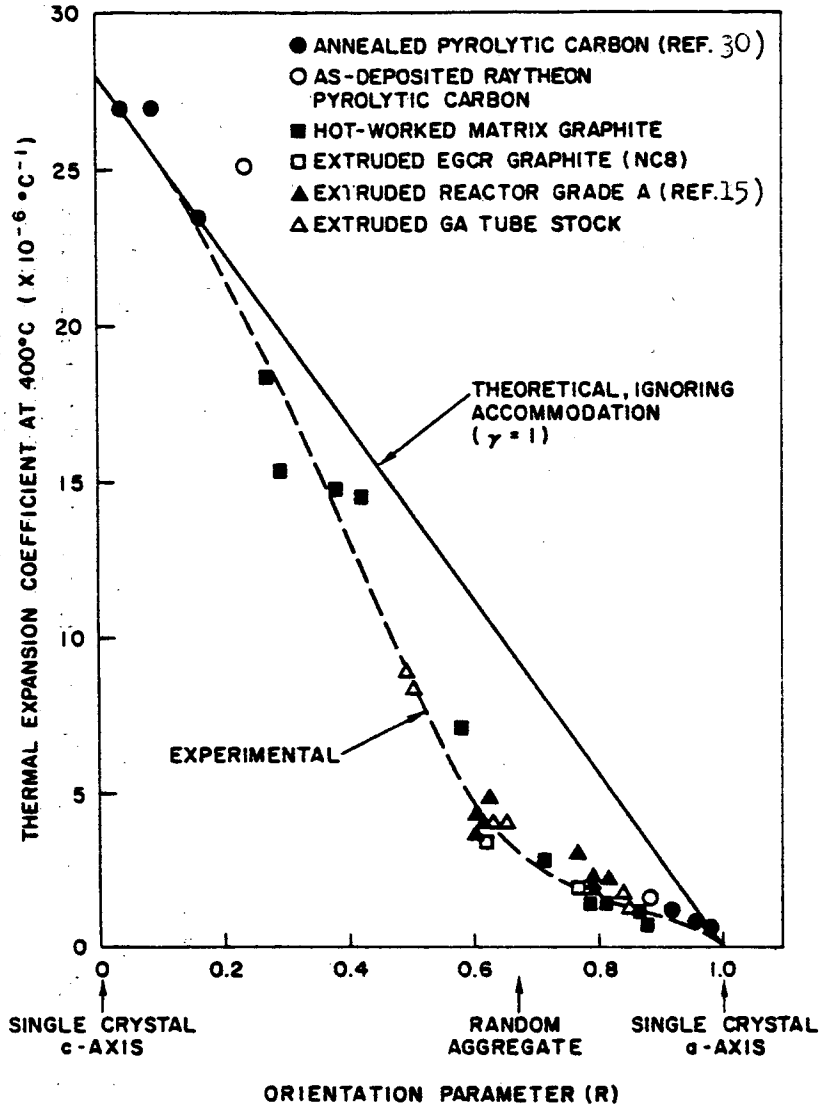

Fig. 37--Thermal expansion coefficient at 400°C versus orientation parameter: (a) theoretical, placing accommodation coefficient $\gamma = 1$; (b) observed for various graphites

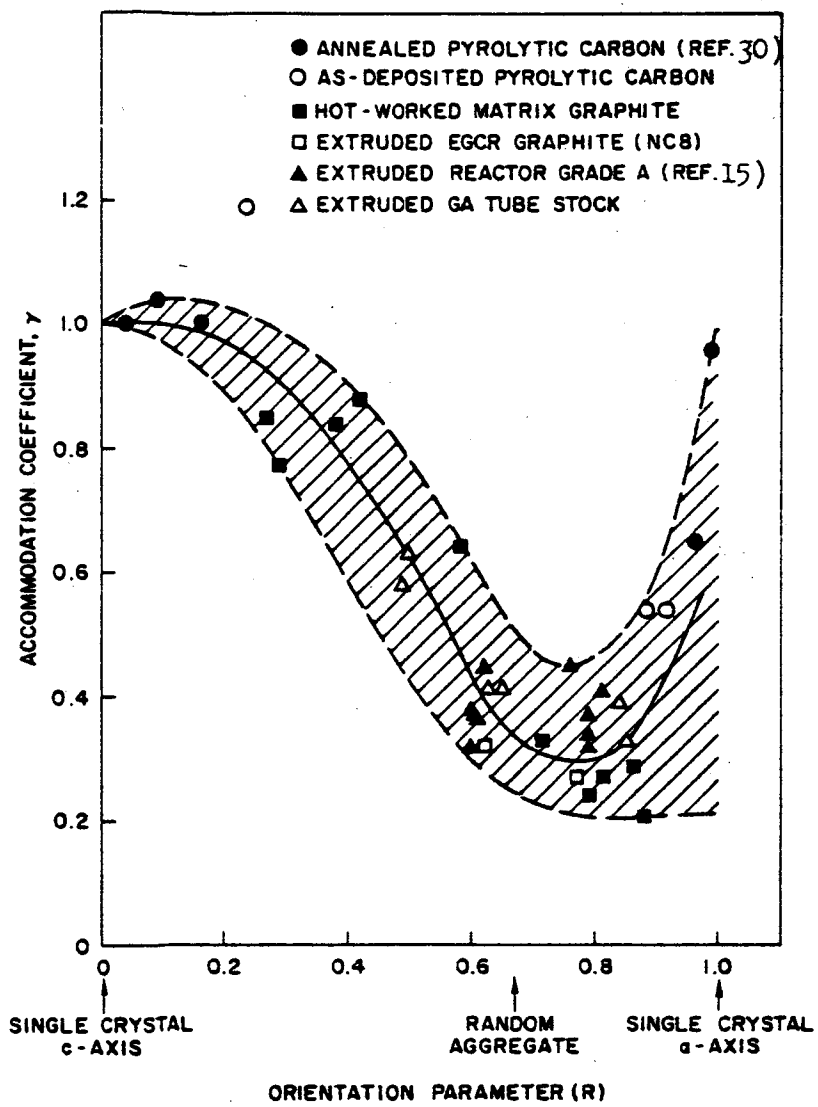

Fig. 38--Accommodation coefficient versus preferred orientation parameter for a number of graphites

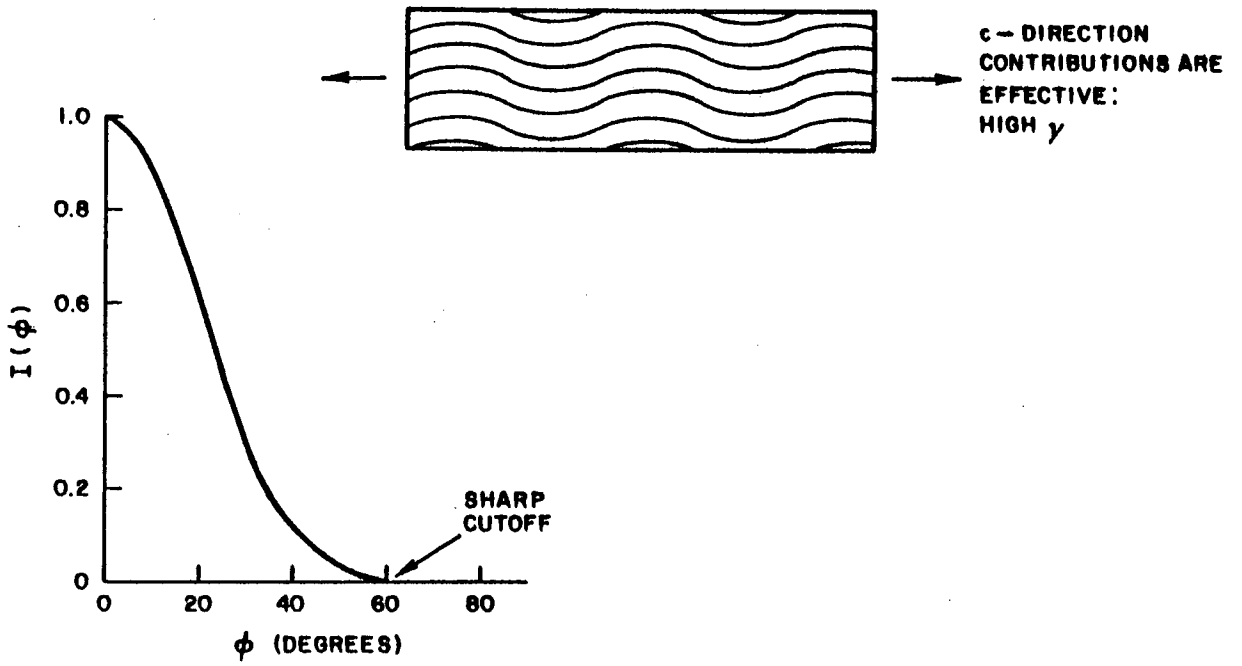

(a) As-deposited pyrolytic carbon; R = 0.92, γ = 0.54

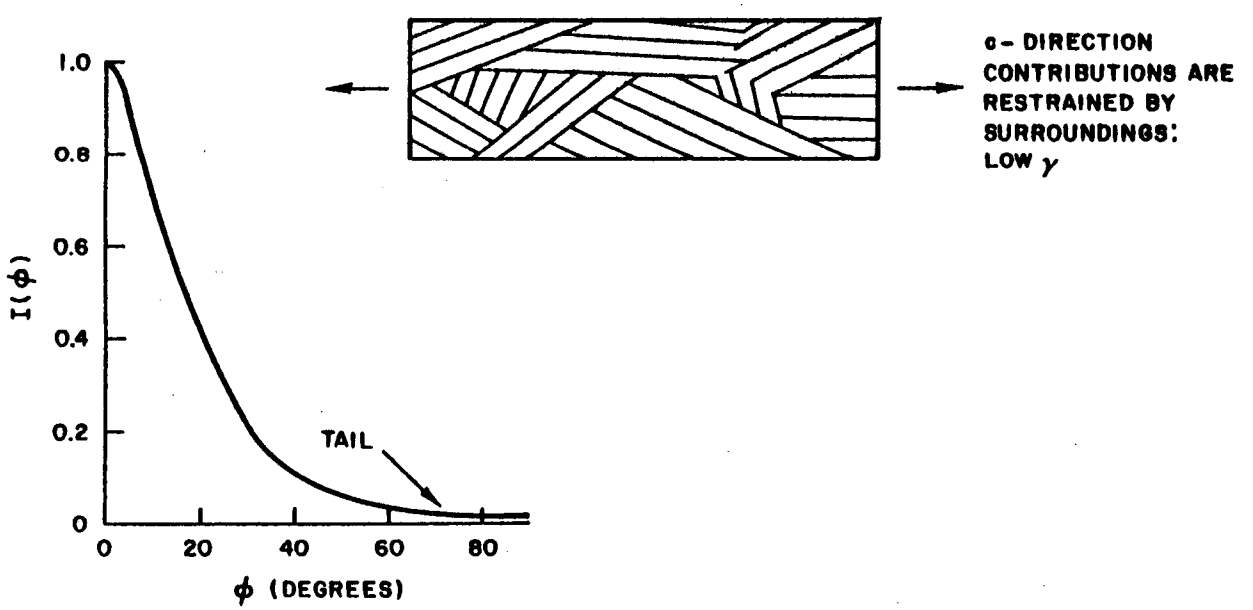

(b) 82% hot-worked graphite; R = 0.87, γ = 0.21

Fig. 39--Schematic illustration of two different kinds of highly-oriented graphite structures and the resulting difference in accommodation coefficient

severely restricted in the "wrinkled-sheet" structure than in the "island" structure, where many of the c-oriented crystallites are restrained by a surrounding matrix of a-oriented crystallites. This may be the reason why the accommodation coefficients at high values of R are systematically higher for pyrolytic graphite than for hot-worked graphite.

In order to use the idea of accommodation coefficients to predict the thermal expansion of a given graphite sample, the R-value is first obtained by making X-ray measurements of the intensity function I as a function of direction in the specimen (see Section 2.2) and using Eqs. (9), (10), or (11). The corresponding mean value of γ may be read off from the solid line in Fig. 38, and the bulk thermal expansion coefficient worked out from Eq. (12). This procedure was followed in the case of an extruded graphite tube. The calculated expansion coefficients were worked out at a series of temperatures, using the data of Nelson and Riley [31] for the single-crystal expansion coefficients as a function of temperature. The results are shown in Table 3, where they are compared with the expansion coefficients measured with a Leitz dilatometer on specimens cut from the tube wall. It can be seen that there is good agreement between the observed and calculated values, except that the coefficients measured in the circumferential direction are systematically higher than calculated. This may be because the nominally circumferential expansion specimens were cut along a chord in the tube wall, and therefore there is a small thermal expansion contribution from the radial direction which raises the expansion coefficient.

Table 3

COMPARISON OF OBSERVED AND CALCULATED THERMAL EXPANSION COEFFIENTS IN THE WALL OF AN EXTRUDED GRAPHITE TUBE
($\times 10^{-6}\ {}^{\circ}C^{-1}$)

Temp. (°C)	Radial		Circumferential		Longitudinal	
	Obs.	Calc.	Obs.	Calc.	Obs.	Calc.
100	7.5	8.4	2.9	2.7	0	0.5
200	8.6	8.8	4.4	3.0	0.8	0.8
300	8.7	9.0	4.0	3.3	1.2	1.2
400	8.8	9.2	4.0	3.5	1.7	1.5
500	9.1	9.4	4.0	3.7	1.9	1.7
600	9.4	9.6	4.6	3.8	2.3	1.9
700	9.4	9.8	4.8	4.0	2.5	2.0

The good agreement between the observed and calculated expansion coefficients over a wide range of temperatures seems to justify the use of Eq. (12) as a model for the thermal expansion in a polycrystalline graphite body. The basic assumptions (i.e., that the bulk thermal expansion is due to the sum of the contributions of the individual crystallites, but the c-expansion is largely accommodated by transgranular cleavage cracks) seem physically reasonable. The fact that the amount of accommodation bears no systematic relation to bulk porosity suggests that gross pores are unimportant in accommodating crystallite expansion, and the porous aggregate expands like a rigid framework.

4.3. RESIDUAL STRESSES IN AN EXTRUDED GRAPHITE TUBE
(L. C. Foster, R. J. Price)

Extruded graphite tubes have been shown to have a pronounced texture in the tube wall, with the basal planes mostly oriented tangentially to the wall surface. The edges of the basal planes are well aligned along the length of the tube, but only roughly aligned circumferentially, apart from a better oriented skin that may be present at the inner and outer surfaces (see Section 2.2). As a result of the texture, the thermal expansion coefficients in the radial, tangential, and longitudinal directions are different (Table 3): typical values at 400°C are 8.8, 4.0, and $1.7 \times 10^{-6}\ {}^{\circ}C^{-1}$, respectively. The anisotropic contraction rates could result in residual internal stresses which might reach an important fraction of the ultimate tensile strength.

A complete analysis of the internal stresses can be made by the Sachs boring-out method,[32] where the longitudinal and tangential strains at the outside surface of the tube are measured as the inside is progressively machined away. This method was applied to a section cut from a General Atomic extruded tube made from GP-38 graphite and Barrett No. 30 pitch and baked out at 900°C. A piece of tubing 9 in. long with an outside diameter of 3.5 in. and an inside diameter of 2.75 in. was used. Strains were measured by resistance strain gauges, each capable of measuring strains in two mutually perpendicular directions, cemented to the outside of the tube at its midpoint in two positions 90° apart. The final measurements were made when the wall thickness was reduced to 0.040 in.

The internal stresses were calculated from the formulae[32]

$$\sigma_L = \frac{E}{1 - \nu^2}\left[(A_o - A)\frac{d\Lambda}{dA} - \Lambda\right], \tag{13}$$

$$\sigma_T = \frac{E}{1 - \nu^2}\left[(A_o - A)\frac{d\theta}{dA} - \frac{A_o + A}{2A}\,\theta\right], \tag{14}$$

$$\sigma_R = \frac{E}{1 - \nu^2} \left[\frac{A_o - A}{2A} \right] \theta \tag{15}$$

where $\Lambda = e_L + \nu e_T$,

$\theta = e_T + \nu e_L$,

σ_L = longitudinal stress,

σ_T = tangential stress,

σ_R = radial stress,

e_L = measured longitudinal strain,

e_T = measured tangential strain,

E = Young's modulus,

ν = Poisson's ratio,

$A_o = \pi/4 \times (OD)^2$

$A = \pi/4 \times (ID)^2$

E was measured from a bend test and ν from a compression test on specimens cut from the same tube. In both cases, strains were measured by resistance strain gauges. The measurements were 1.3×10^6 psi and 0.195, respectively. No allowance was made for the different elastic properties of the material in different directions. These differences are probably small, since Young's modulus is relatively insensitive to preferred orientation (refer to Section 4.4).

The internal stresses calculated from Eqs. (13) through (15) are given in Figs. 40 and 41. No data are available on the stresses within 0.040 in. of the outer surface because this was the amount of material remaining after the last cut. It can be seen that maximum stresses of about 300 psi are present in both the longitudinal and tangential directions. Radial stresses are very small. The tangential stress distributions are qualitatively similar for strain gauges A and B, but the longitudinal distributions are mutually inverted between the two positions, suggesting the presence of a locked-in flexural stress.

Strain gauges A and B both reveal the presence of a small region of tangential compressive stress near the inner surface, then a larger zone of tensile stress, and finally a compressive region near the outer surface.

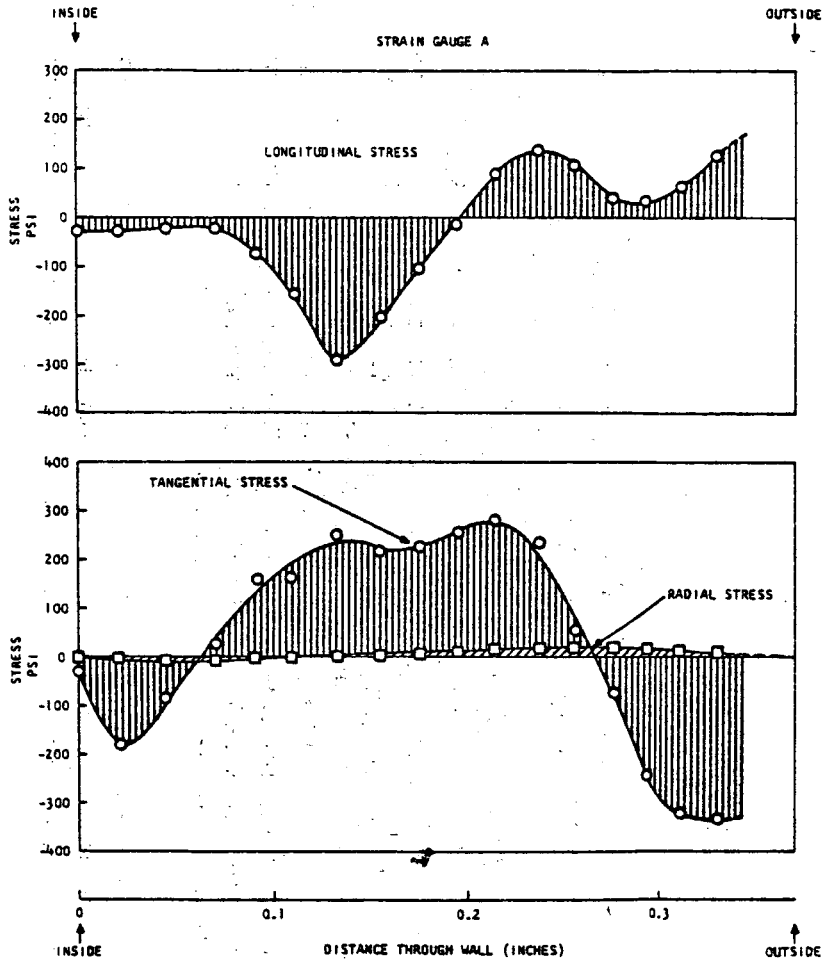

Fig. 40--Residual stresses in tube wall at position A

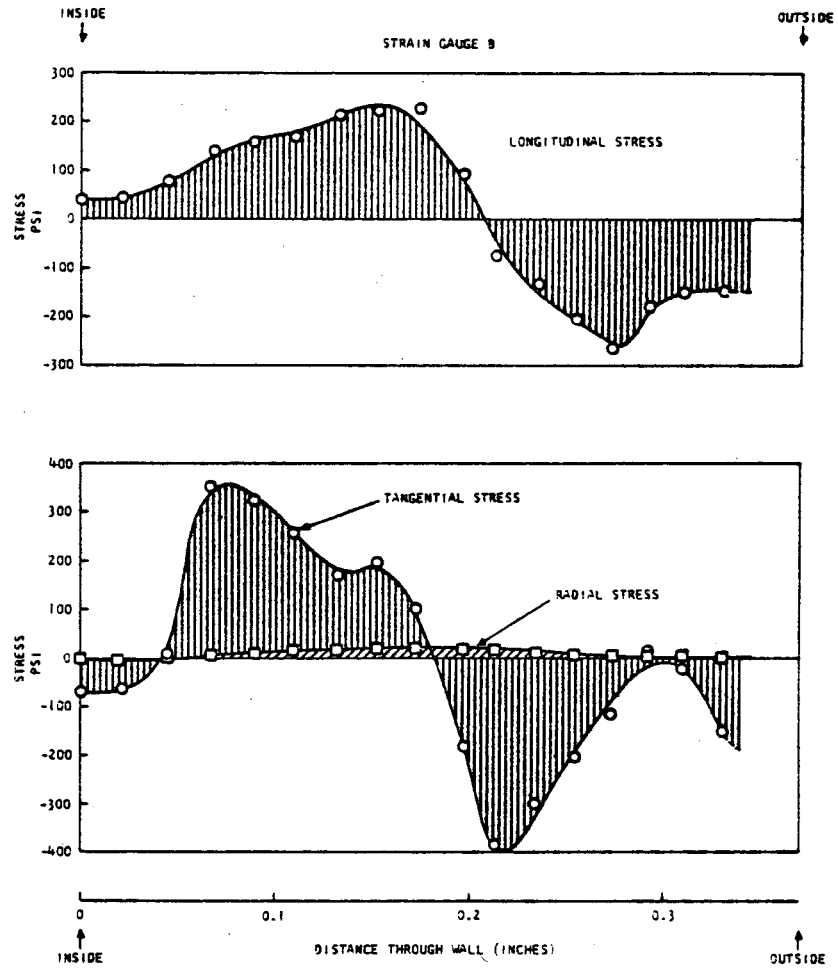

Fig. 41--Residual stresses in tube wall at position B (90° from position A)

This pattern can be qualitatively explained in terms of the thermal expansion coefficients in various directions in the tube wall, assuming that the body is stress-free at its heat treatment temperature and the stresses develop on cooling. Consider a segment of the tube wall subtending a fixed angle at the center (Fig. 42a). Since the radial expansion coefficient is higher than the circumferential coefficient, the inner and outer arcs try to contract very little on cooling, while the radial width of the segment decreases much faster. This would result in the situation shown in Fig. 42b. In actual fact the segment is constrained to stay the same shape on cooling, resulting in a compressive stress at the outside and a tensile stress on the inside (Fig. 42c).

This simple stress pattern is modified by the presence of the more highly oriented inner and outer skins, in which the anisotropy of the thermal expansion coefficients is higher than in the bulk of the wall material. The unrestrained length changes on cooling in the three layers are shown schematically in Figs. 42d and 42e. Since the three layers actually remain joined together during cooling, a stress pattern of the type shown in Fig. 42f is produced. If this skin-effect stress pattern is superimposed upon the pattern expected in the anisotropic wall without oriented skins (Fig. 42c), the result (Fig. 42g) is qualitatively similar to the one observed. It therefore seems probable that the tangential residual stresses are due to differential contractions on cooling.

The observed diffrerence in longitudinal stress pattern between the two positions A and B cannot be explained by preferred orientation effects. The stress pattern (Figs. 40 and 41) suggests internal stresses of a flexural nature. It is significant that extruded green stock normally exhibits a considerable bow, possibly connected with uneven flow from top to bottom of the horizontal extrusion dies. This shape is maintained during baking by firmly packed alumina powder.[33] If the amount of bow has any tendency to increase or decrease during heat treatment, the restraints imposed by the packing may cause localized flow, resulting in residual longitudinal stresses when the body is cooled down.

4.4. PREFFERRED ORIENTATION AND YOUNG'S MODULUS

(J. C. Bokros, R. J. Price, J. Schultz)

When an aggregate of crystallites with anisotropic elastic properties is loaded elastically, each crystallite will contain a different stress and strain depending on its orientation with respect to the applied load. The stresses and strains will depend to some extent on the neighboring crystallites, since certain boundary conditions must be obeyed at the crystallite boundaries. As in the case of thermal expansion, the boundary interactions are very difficult to treat theoretically. However, two extremely simplified

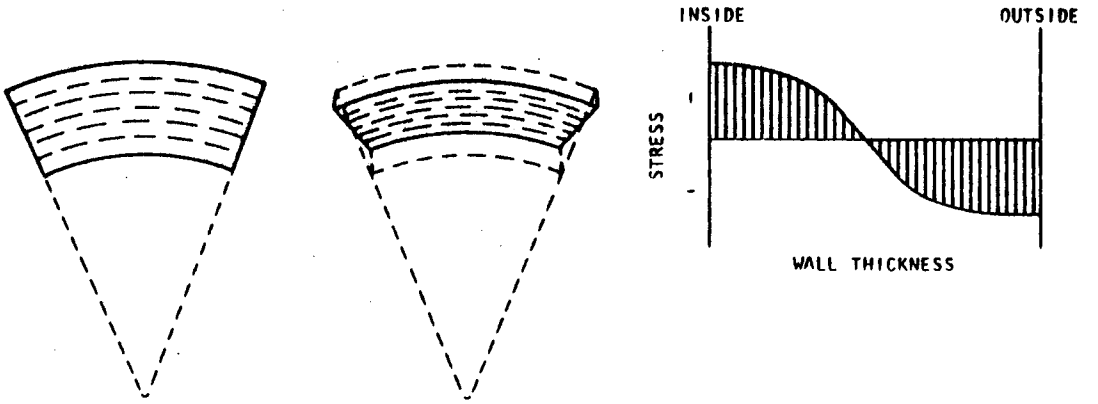

A: SEGMENT OF TUBE WALL, STRESS-FREE AT HEAT TREATMENT TEMPERATURE

B: SAME SEGMENT AFTER COOLING (IF UNRESTRAINED)

C: STRESSES DEVELOPED IN SEGMENT IF IT IS FORCED TO RETAIN ITS SHAPE

A-C DEVELOPMENT OF RESIDUAL STRESS DUE TO UNEQUAL RADIAL AND CIRCUMFERENTIAL CONTRACTION RATES

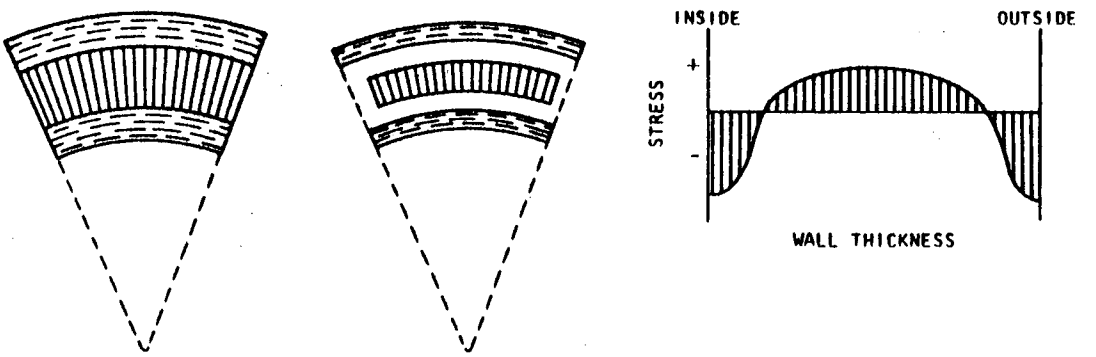

D: SEGMENT WITH HIGHLY ORIENTED INNER AND OUTER "SKINS"; STRESS-FREE

E: SEGMENT AFTER COOLING (SKINS DETACHED FROM REST OF WALL)

F: STRESS PATTERN IN SEGMENT IF THREE LAYERS REMAIN JOINED TOGETHER.

D-F: DEVELOPMENT OF RESIDUAL STRESS DUE TO HIGHLY ORIENTED INNER AND OUTER "SKINS"

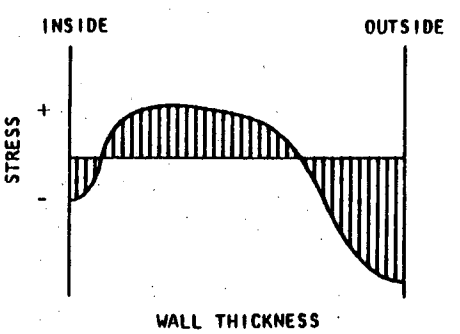

G: FINAL STRESS DISTRIBUTION IN TUBE WALL, TAKING "SKIN EFFECT" INTO ACCOUNT (PATTERN C PLUS PATTERN F)

Fig. 42--Schematic diagram of formation of residual stresses in wall of an extruded graphite tube

models may be considered (Fig. 43). In the first model, the crystallites are treated as being pinned tightly together so that the strain in each is the same and equal to the bulk strain. The stress in each crystallite is different and depends on its orientation (Fig. 43a). In the second model (Fig. 43b), the crystallite boundaries are free to slide, with the result that the stress in each crystallite is the same as the applied bulk stress but the strain is different, depending on whether the crystallite is in a "hard" or a "soft" orientation. The true behavior lies somewhere between the two extremes.

The elastic anisotropy of a graphite crystal is extremely large, with Young's modulus varying from 130×10^6 psi to 1.3×10^6 psi between the two extreme directions. If a loaded aggregate behaved as though the crystallite boundaries were rigid (Fig. 43a), the crystallites in a graphite polycrystal loaded to 0.1% elastic strain would contain tensile stresses ranging from 1,300 psi to 130,000 psi. This situation is physically unreasonable. It is more probable that the stresses tend to even out, inconsistencies in strain between neighboring crystallites being accommodated in the boundary layer, resulting in a situation much closer to the sliding-boundary model shown in Fig. 43b. The following calculations are based on this latter model, which implies a constant tensile stress in each crystallite and assumes that the crystallite boundary effects are confined to narrow layers and that their effect on the bulk stress-strain relationships is small.

If an aggregate of this type is loaded elastically to an over-all tensile stress σ, then the tensile stress in each crystallite is also σ. The over-all strain is ϵ, and is equal to the average of the strains ϵ_x in the individual crystallites contained in one end-to-end column (Fig. 43b). The over-all Young's modulus E is therefore given by

$$E = \frac{n\sigma}{\sum \epsilon_x} \tag{16}$$

where n is the number of crystallites in a column. The strain in an individual crystallite ϵ_x is related to its Young's modulus in the direction of the applied stress E_x thus:

$$\epsilon_x = \frac{\sigma}{E_x}, \tag{17}$$

$$E = \frac{n\sigma}{\sum (\sigma/E_x)} = \frac{n}{\sum (1/E_x)}, \tag{18}$$

$$\frac{1}{E} = \frac{\sum (1/E_x)}{n} \tag{19}$$

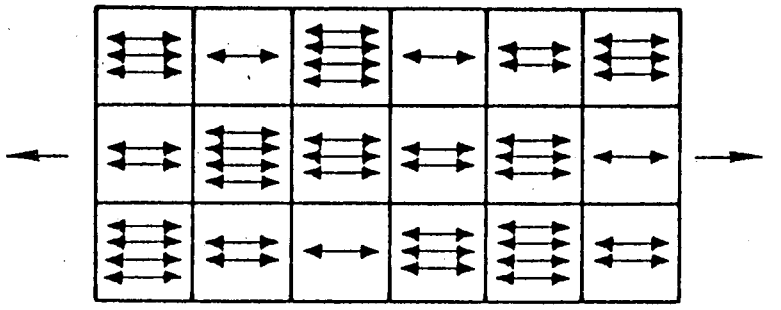

(a) Crystallites pinned together; the strain is the same on all crystallites, but the stress depends on the individual moduli

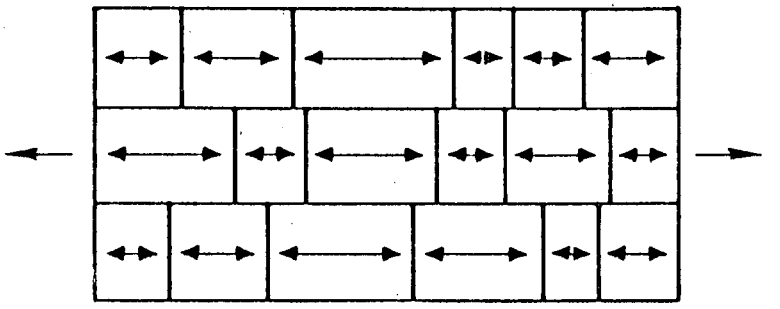

(b) Crystallite boundaries free to slide; the stress in each crystallite is the same, but the strains are different

Fig. 43--Schematic illustration of the behavior of an elastically loaded aggregate of anisotropic crystallites

Thus, the reciprocal of Young's modulus is an averagable quantity, and the reciprocal modulus of a bulk specimen can be obtained from the single-crystal elastic properties using the averaging equation Eq. (3); i.e.,

$$\frac{1}{E_{OZ}} = \frac{\iint I(\phi,\beta)\,\frac{1}{E_x(\phi)}\,\sin\phi\,d\phi\,d\beta}{\iint I(\phi,\beta)\,\sin\phi\,d\phi\,d\beta}\,, \tag{20}$$

using the notation shown in Fig. 36.

$E_x(\phi)$, Young's modulus for a single crystal at an angle ϕ to the c-axis, can be obtained from the standard equation for a hexagonal crystal:[34]

$$\frac{1}{E_x(\phi)} = S_{11}\sin^4\phi + S_{33}\cos^4\phi + (2S_{13} + S_{44})\sin^2\phi\cos^2\phi\,. \tag{21}$$

For present purposes, the elastic coefficients used by Spence[35] were employed, since these represent an average of the available data. These elastic coefficients were transformed to elastic constants,[34] with the following results:

$$S_{11} = 1.11 \times 10^{-13}\ \mathrm{cm}^2\ \mathrm{dyne}^{-1}\,,$$
$$S_{12} = -0.04 \times 10^{-13}\ \mathrm{cm}^2\ \mathrm{dyne}^{-1}\,,$$
$$S_{13} = -2.5 \times 10^{-13}\ \mathrm{cm}^2\ \mathrm{dyne}^{-1}\,,$$
$$S_{33} = 33.3 \times 10^{-13}\ \mathrm{cm}^2\ \mathrm{dyne}^{-1}\,,$$
$$S_{44} = 435 \times 10^{-13}\ \mathrm{cm}^2\ \mathrm{dyne}^{-1}\,,$$

Placing these numbers in Eq. (21), we obtain

$$\frac{1}{E_x(\phi)} = 1.11\sin^4\phi + 33.3\cos^4\phi + 430\sin^2\phi\cos^2\phi(\times 10^{-13}\ \mathrm{cm}^2\ \mathrm{dyne}^{-1})\,. \tag{22}$$

Plots of E and 1/E versus ϕ based on this equation are shown in Figs. 44 and 45. It can be seen from Fig. 44 that the very high modulus (about 130×10^6 psi) associated with the a-direction influences only a narrow range of orientations around the a-axis. On the other hand, there is a wide range of orientations between 10° and 70° from the c-axis, where the

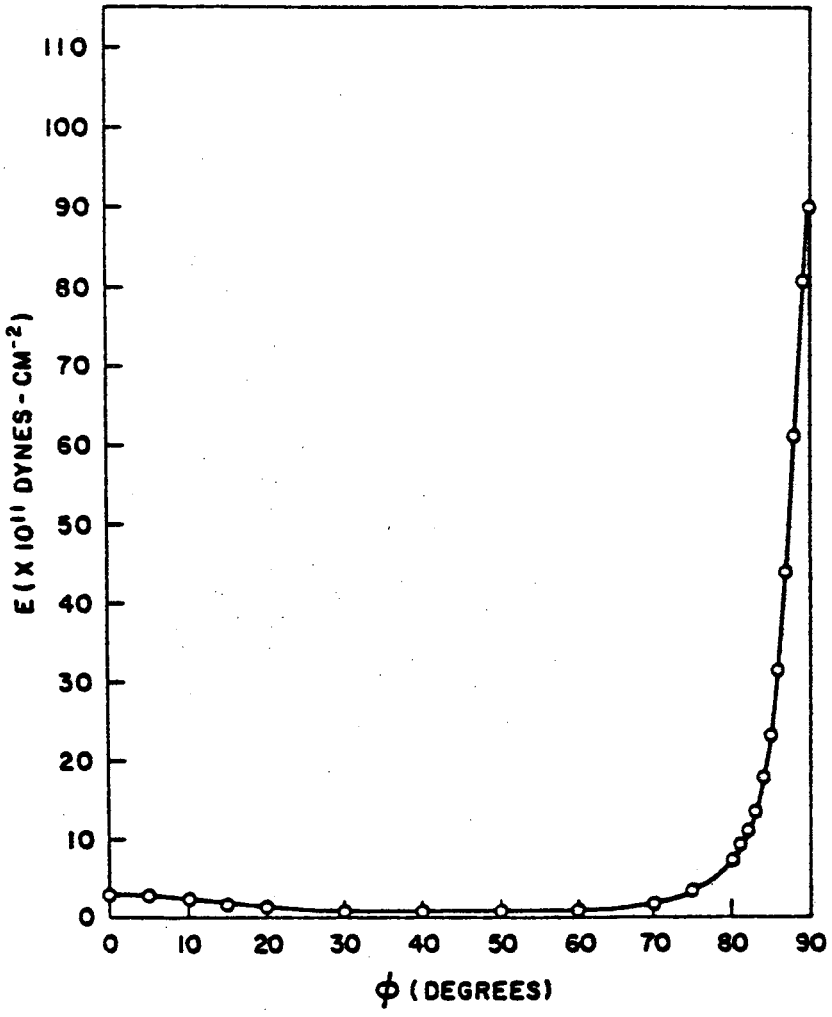

Fig. 44--Variation of Young's modulus with angle ϕ, from the c-axis in a graphite single crystal

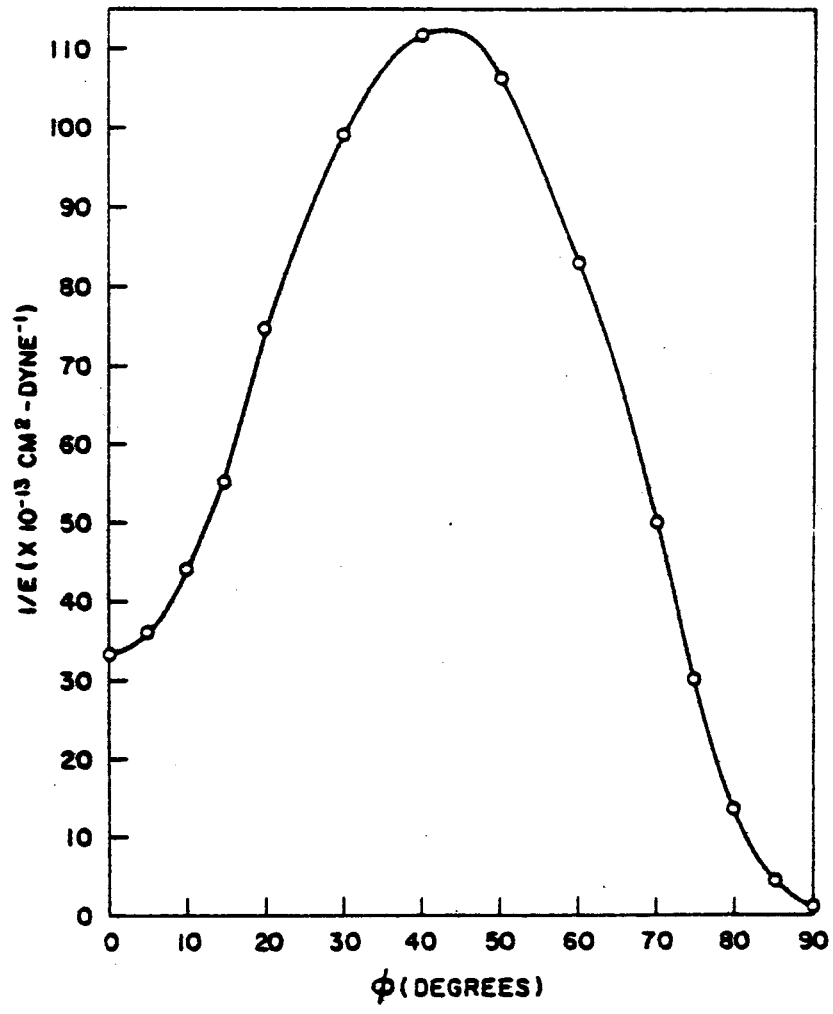

Fig. 45--Variation of reciprocal of Young's modulus with angle ϕ, from the c-axis in a graphite single crystal

modulus is very low (1 to 2 × 10^6 psi), because it is dominated by the low shear modulus parallel to the basal planes.

The expression for Young's modulus in any graphitic body whose preferred orientation has been measured can be evaluated from Eq. (20); values of $1/E(\phi)$ are read from Fig. 45. For a body whose texture has cylindrical symmetry, I is independent of β in Eq. (20). This fact, together with Eq. (22) for $1/E_x(\phi)$, can be used to derive the following expressions for the modulus parallel and perpendicular to the symmetry axis:

$$\frac{1}{E_{\parallel}} = 33.3 + 363 \frac{\int_0^{\pi/2} I(\phi) \sin^3 \phi \, d\phi}{\int_0^{\pi/2} I(\phi) \sin \phi \, d\phi} - 397 \frac{\int_0^{\pi/2} I(\phi) \sin^5 \phi \, d\phi}{\int_0^{\pi/2} I(\phi) \sin \phi \, d\phi} \; (\times 10^{-13} \text{ cm}^2/\text{dyne}); \tag{23}$$

$$\frac{1}{E_{\perp}} = 1.11 + 214 \frac{\int_0^{\pi/2} I(\phi) \sin^3 \phi \, d\phi}{\int_0^{\pi/2} I(\phi) \sin \phi \, d\phi} - 148 \frac{\int_0^{\pi/2} I(\phi) \sin^5 \phi \, d\phi}{\int_0^{\pi/2} I(\phi) \sin \phi \, d\phi} \; (\times 10^{-13} \text{ cm}^2/\text{dyne}) . \tag{24}$$

These calculations ignore effects of porosity and the anelastic strains due to limited slip on the basal planes during loading, which make the measured modulus lower than these equations predict. The latter effect can be very important in well graphitized materials of large crystallite size, as is shown by the marked increase in modulus after the low-temperature irradiation of such samples. The defects produced by low-temperature irradiation effectively pin the basal dislocations and eliminate anelastic strains during subsequent modulus measurements.

The equations were checked using samples of pyrolytic graphite deposited at 2200°C, where the porosity is small and the crystallite size low. The preferred orientation curve was measured by the technique described in Section 2.2 and is shown in Fig. 46. Young's modulus for the same material was measured by the sonic method, using samples cut either parallel or perpendicular to the deposition plane. The measured values are compared in Table 4 with values calculated from Eqs. (23 and (24), using the measured preferred orientation curve and evaluating the integrals graphically.

Table 4

YOUNG'S MODULUS OF PYROLYTIC GRAPHITE DEPOSITED AT 2200°C
($\times 10^{11}$ dynes/cm^2)

Orientation	Measured	Calculated
Parallel to deposition plane	1.92	2.7
Perpendicular to deposition plane	0.71	1.2

The measured values are considerably lower than calculated, but the ratio between the moduli in the two directions is about the same as expected. The discrepancy may be due to anelastic strains within the crystallites or to errors in the single crystal elastic constants used. The accuracy claimed in the original measurement[36] of S_{44} (the most important elastic constant) allows for an error of 20% to 50%.

It is important to note that Young's modulus is a much less sensitive function of preferred orientation than is, for example, the thermal expansion coefficient. Despite the strong preferred orientation of the pyrolytic graphite used, Young's modulus varies only by a factor of about 2.5 between the two mutually perpendicular orientations, whereas the ratio of the thermal expansion coefficients at 400°C is 14.

It is proposed to extend the comparison of observed and calculated Young's modulus to pyrolytic graphite plastically extended at high temperatures (which has a very high preferred orientation) and to annealed pyrolytic graphite before and after a low-temperature irradiation to pin the basal dislocations and thus remove the anelastic error from the modulus measurements.

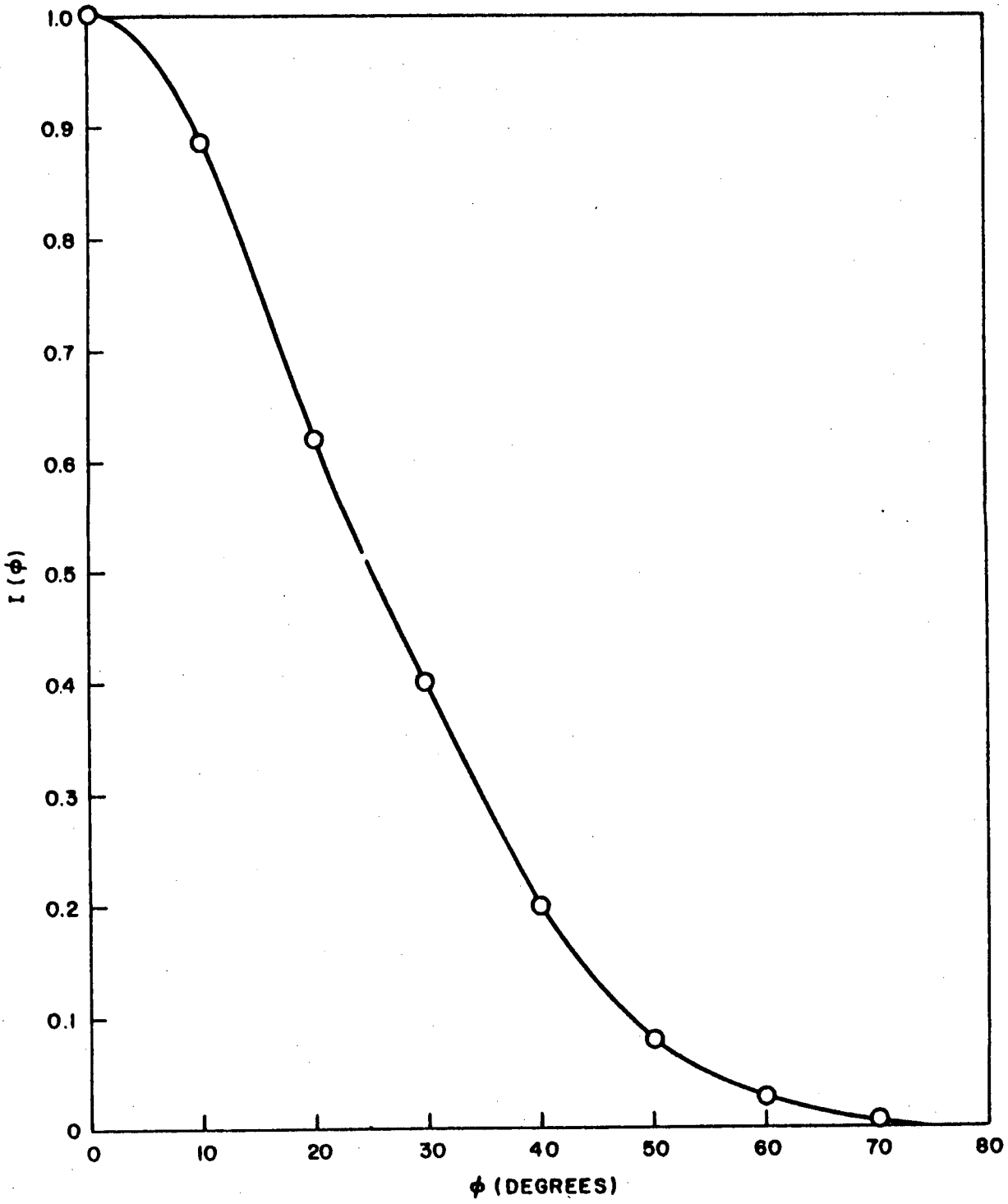

Fig. 46--Preferred orientation cuved for pyrolitic carbon deposited at 2200°C

4.5. PREFERRED ORIENTATION AND RADIATION-INDUCED DIMENSIONAL CHANGES

(J. C. Bokros, R. J. Price)

Transmission electron microscopy on graphite single crystals irradiated with fast neutrons has shown that carbon atoms are displaced from their lattice sites and condense as sheets of interstitial atoms inserted between the basal planes.[37] This process must produce growth in the c-direction and contraction in the a-direction, the growth rate depending on the flux, temperature, and the density of traps where interstitials and vacancies can be annihilated. If it is assumed that such dimensional changes within the crystallites are the principal factor responsible for the gross dimensional changes observed in neutron-irradiated graphite, then the dimensional changes in fully graphitic material can be rationalized in terms of crystallite dimensional changes.

The rate of dimensional change as a function of fast neutron exposure will have the same type of dependence on direction within the crystallite as the thermal expansion coefficient, since both properties relate strain to a scalar quantity. It is reasonable to assume that the dimensional changes of the crystallites can be integrated, taking their preferred orientation into account, to give the over-all dimensional changes in the bulk sample in the same way as may be done for thermal expansion (Section 4.2). If it is assumed that a proportion γ of the crystallite c-direction expansion is accommodated by microcracks (as for thermal expansion), then, following Eqs. (11) and (12), the bulk dimensional change rates β in directions parallel and perpendicular to the symmetry axis OZ (axis of extrusion or molding force) can be expressed as

$$\beta_{OZ} = R_{OZ}\beta_a + (1 - R_{OX})\gamma_{OZ}\beta_c , \tag{25}$$

$$\beta_{OX} = \left(1 - \frac{R_{OZ}}{2}\right)\beta_a + \frac{R_{OZ}}{2}\gamma_{OX}\beta_c , \tag{26}$$

where β_a and β_c are the rates of dimensional change in the crystallites in the a- and c-directions, respectively, and the other quantities are defined in Section 4.2. Two assumptions are made about accommodation of crystallite dimensional changes: first, the a-direction contraction is assumed to be fully effective, with no accommodation effects; this is reasonable because the microcracks which are presumed to be responsible for accommodation effects lie parallel with the layer planes, and also the a-direction Young's modulus is extremely high; and second, the accommodation coefficient in the crystallite c-direction is assumed to be the same as during thermal expansion, enabling the values of γ obtained during thermal expansion investigations (Section 4.2) to be used for interpreting dimensional effects on irradiation.

The model represented by Eqs. (25) and (26) explains many of the characteristics of the irradiation behavior of fully graphitized nuclear graphites. The difference between the parallel and perpendicular directions in extruded and molded graphites is clearly associated with the preferred orientation of the crystallites, with directions containing a large density of a-directions showing the most rapid contraction. During low-temperature irradiation, a sudden increase in the expansion rate of extruded graphites perpendicular to the extrusion axis is noted at moderate exposures ("breakaway"), accompanied by an increase in the thermal expansion coefficient at about the same exposure. This may be interpreted as happening at the point where crystallite c-axis expansion closes up the accommodation microcracks and γ becomes equal to one.

Equations (25) and (26) are similar in outline to those derived by Simmons[38] by generalized arguments, except that Simmons' equations do not contain the accommodation coefficient γ, and the R-factors are not defined explicitly but are deduced from thermal expansion measurements. In the present equations the R-factors are properly defined functions of orientation, and it is not necessary to assume that they change during irradiation to explain breakaway, as is the case with Simmons' equations.[38]

In order to apply the equations, it is necessary to obtain values for the basic crystallite dimensional change rates, β_a and β_c. In principle, these could be obtained from direct measurements on single-crystal graphite or highly annealed pyrolytic graphite, but the irradiation data on this type of material are too limited to be employed usefully. However, extensive measurements are available on British Reactor Grade A graphite,[39] and data on the preferred orientation and thermal expansion in this material have been published.[15] It was therefore decided to calculate the basic crystallite distortion rates from the Reactor Grade A data, using the measured growth rates for both parallel and perpendicular samples[39] and solving Eqs. (25) and (26) for β_a and β_c. The values used for R_{OZ} and γ were 0.79 and 0.39 respectively, these being averages calculated from data on several batches of Reactor Grade A quoted in Ref. 15. It was assumed that γ changed to 1.0 at the point at which breakaway occurred during irradiation at 200°C and 250°C. The calculated values for β_a and β_c are shown in Table 5. The growth rates are given in terms of fast flux measured with nickel monitors ($E > 1$ Mev). As expected, the calculated crystallite dimensional changes are all positive in the c-direction and negative in the a-direction. In general, the rates of change decrease with increasing temperature.

The validity of Eqs. (25) and (26) was checked for EGCR needle-coke graphite (NC-8) and a sample of molded nuclear graphite heat-treated at 2700°C. Irradiation contraction data for these graphites are given in Refs. (40) and (41). Samples of these graphites obtained from Hanford were

Table 5

RATES OF CRYSTALLITE DIMENSIONAL CHANGE WITH FAST-NEUTRON EXPOSURE FOR NUCLEAR GRAPHITE (β_a AND β_c)

Temp. (°C)	Exposure ($\times 10^{20}$ nvt)	Strain/10^{20} nvt, E> 1 Mev	
		β_a ($\times 10^4$)	β_c ($\times 10^4$)
200	0	-24	+122
	5	-90	+245
250	0	-10	+45
	5	-12	+42
	10	-25	+45
	15	-34	+66
	20	-38	+70
350	0	-4.4	+20
	5	-5.7	+11
	10	-5.9	+9.2
	15	-6.1	+8.8
	20	-6.1	+8.8
	25	-6.1	+8.8
450	0	-3.5	+12.3
	5	-5.2	+7.0
	10	-6.9	+9.6
	15	-7.1	+10.0
	20	-7.1	+10.0
650	0	-0.7	+6.0
	5	-1.7	+4.9
	10	-2.0	+4.2
	15	-3.3	+6.4
	20	-3.3	+6.4

used for preferred orientation determinations, using the techniques described in Section 2.2. The preferred orientation curve of the NC-8 graphite is given in Fig. 3 and that of the molded graphite in Fig. 47. The values of R_{OZ} for the two graphites, calculated from Eq. (9), were 0.77 and 0.59, respectively. Values of γ for the NC-8 graphite were measured as described in Section 4.2, and for the molded graphite appropriate values were taken from Fig. 38. The values used were: NC-8, $\gamma_{\parallel} = 0.27$ and $\gamma_{\perp} = 0.32$; molded graphite, $\gamma_{\parallel} = 0.45$, $\gamma_{\perp} = 0.32$. The corresponding contraction rates were worked out from Eqs. (25) and (26) in conjunction with Table 5 for temperatures of 450°C for the molded sample and 450°C and 650°C for

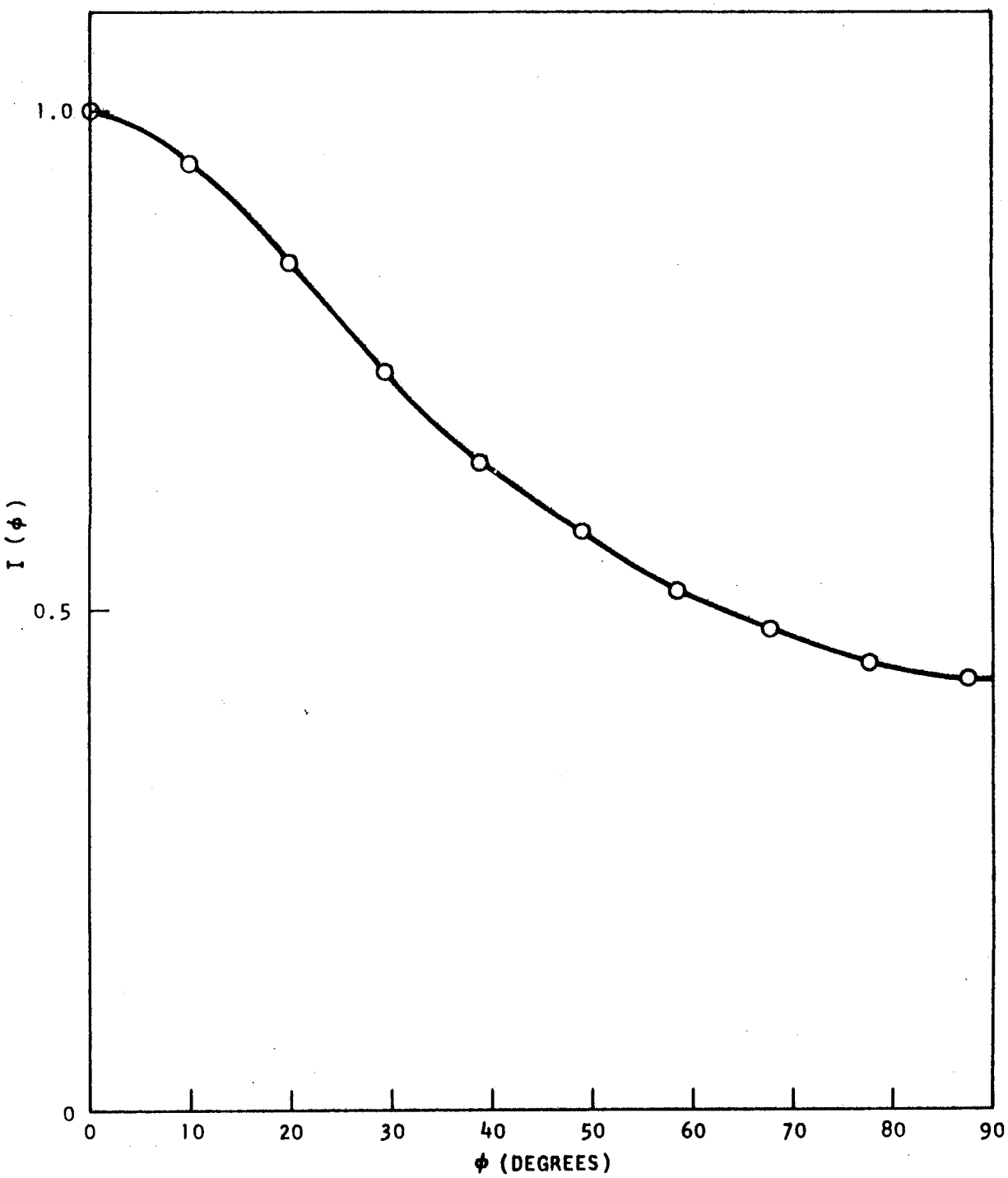

Fig. 47--Preferred orientation curve for molded reactor graphite heat-treated at 2700°C

the NC-8. The calculated curves of dimensional change with fast neutron exposure are shown in Figs. 48 through 50, together with the changes observed at comparable temperatures taken from Refs. 40 and 41. The quoted exposures were converted to nvt (E > 1 Mev) by multiplying exposures in nvt (E > 0.18 Mev) by 1.7 and exposures in Mwd/adjacent ton by 7.6×10^{16}. Bearing in mind the scatter in the experimental data, the differences in temperature, and the uncertainties involved in comparing neutron exposures obtained in different reactors, the agreement between the observed and calculated contraction rates is encouraging.

Similar comparisons between calculated and observed dimensional changes were made for ZTA hot-worked graphite, isotropic graphite, and annealed pyrolytic graphite, using recent British data which have not yet been published in the open literature. Again the agreement was very encouraging.

Values for β_a and β_c were calculated for pyrolytic carbon at 2200°C, using published dimensional changes on irradiation at 650°C[42] and preferred orientation measurements on a sample of the same material. The results are shown in Table 6. β_a and β_c are almost an order of magnitude higher for the pyrolytic carbon than for the fully graphitized nuclear graphite irradiated at 650°C, showing that crystallite dimensional changes are a sensitive function of the degree of graphitization. Using the measured values of β_a and β_c in conjunction with Eqs. (25) and (26) leads to the conclusion that a randomly oriented pyrolytic carbon (R = 0.67) should nevertheless be fairly stable on irradiation.

Table 6

RATES OF CRYSTALLITE DIMENSIONAL CHANGE WITH FAST-NEUTRON EXPOSURE AT 650°C (β_a AND β_c) FOR PYROLYTIC CARBON DEPOSITED AT 2200°C

Exposure (10^{20} nvt)	(Strain/10^{20} nvt, E > 1 Mev)	
	β_a ($\times 10^4$)	β_c ($\times 10^4$)
0	-3.4	+9.5
5	-17	+37

4.6. HIGH-TEMPERATURE DEFORMATION MECHANISMS
(J. O Gardner, R. J. Price)

Below about 2400°C, polycrystalline graphite is a brittle material, showing extensions of less than 1%. This lack of plasticity is a result of

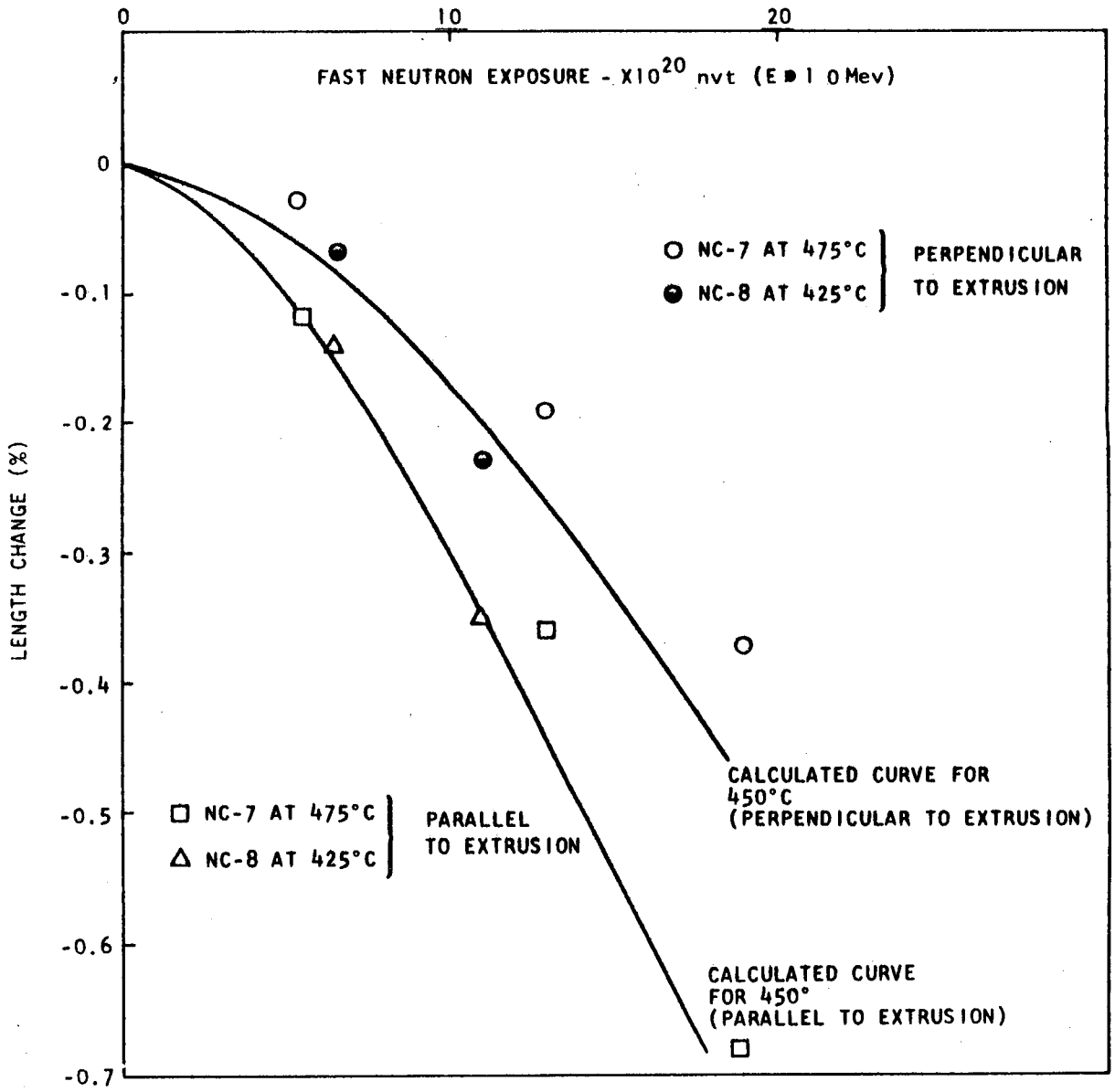

Fig. 48--Observed and calculated contraction of EGCR graphite at ~450°C as a function of exposure

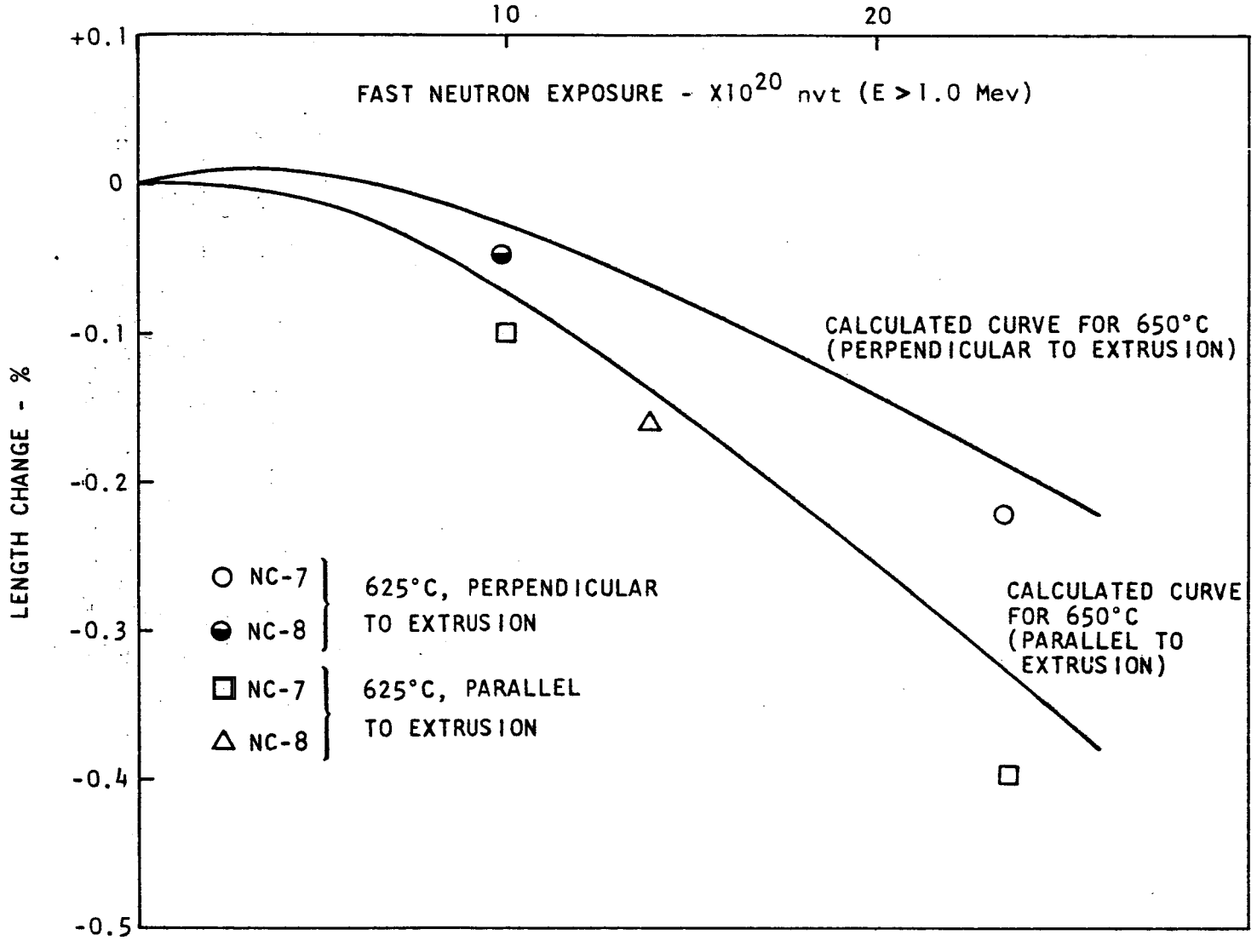

Fig. 49--Observed and calculated contraction of EGCR graphite at ~650° C as a function of exposure

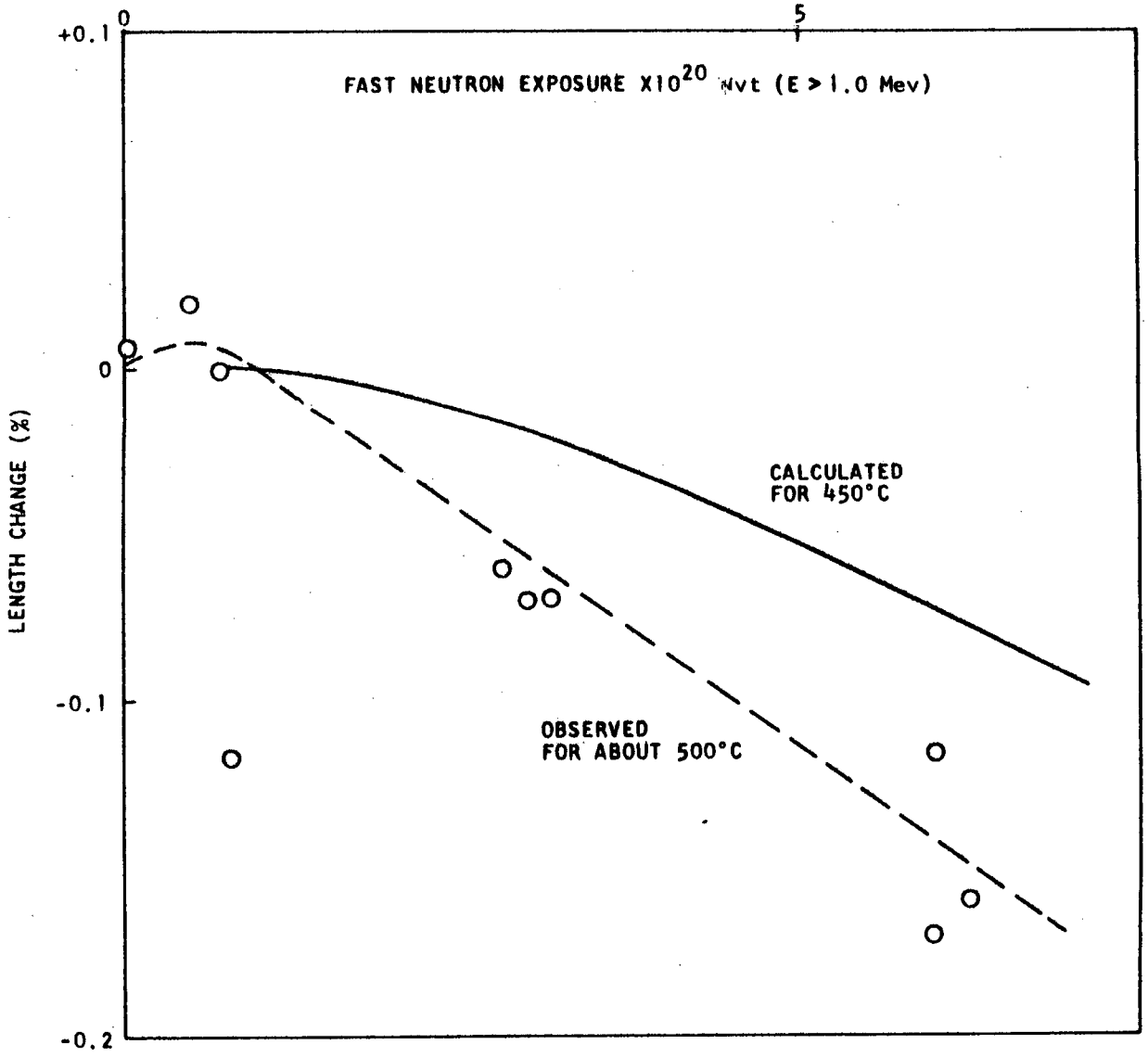

Fig. 50--Observed and calculated contraction of molded nuclear graphite parallel with the molding direction as a function of exposure at ~500°C

slip in the crystallites being limited to the basal plane, which necessarily precludes any extensive plastic flow. Single-crystal experiments show that the only low-temperature mechanisms operative are basal slip and twinning about an axis in the basal plane,[26] both via basal dislocations.[43]

Above 2400°C, graphite becomes appreciably plastic, and at 2800°C extensions of nearly 100% have been observed in pyrolytic graphite.[44] This suggests that another basic deformation mechanism comes into play at high temperature, but apart from suggestions that "dewrinkling" of basal planes may be important[45] or that deformation occurs by a stress-aided flow of vacancies (Nabarro-Herring creep),[46] little work has been done on high-temperature flow mechanisms.

An understanding of the basic aspects of high-temperature deformation is important for augmenting the knowledge of flow and fracture of graphite in general and for the development of hot-working techniques in particular. Accordingly some preliminary investigations of high-temperature deformation, using electron transmission microscopy, have been made.

4.6.1. Electron Transmission Microscopy

The material used in the investigation by electron transmission microscopy was Madagascar single-crystal graphite. The only satisfactory technique for preparing transmission specimens of graphite is by cleaving, but this has the disadvantage that specimens are usually deformed further in preparation. Consequently a technique was devised wherein the freshly cleaved surface of a graphite crystal is cemented onto a hard backing and allowed to dry. Successive layers are cleaved from the crystal with Scotch tape until the film remaining on the cement backing is thin enough to transmit electrons, whereupon the cement is dissolved away in acetone. Suitable films are thin enough to be translucent and are dark grey in color. This technique ensures that the microscope specimen receives a minimum of deformation in preparation.

Specimens were examined after deforming in bending either at room temperature or at 2800°C in a graphite jig incorporated into the hot-working device.[1] Room-temperature deformation was used to provide a comparison with the samples bent at 2800°C.

Both sets of specimens contained networks of basal dislocations, whose density varied widely from region to region of the sample. The dislocations were glissile and were frequently seen to move under stresses induced by contamination buildup. Room-temperature deformed specimens are characterized by networks of extended dislocations, normally joined

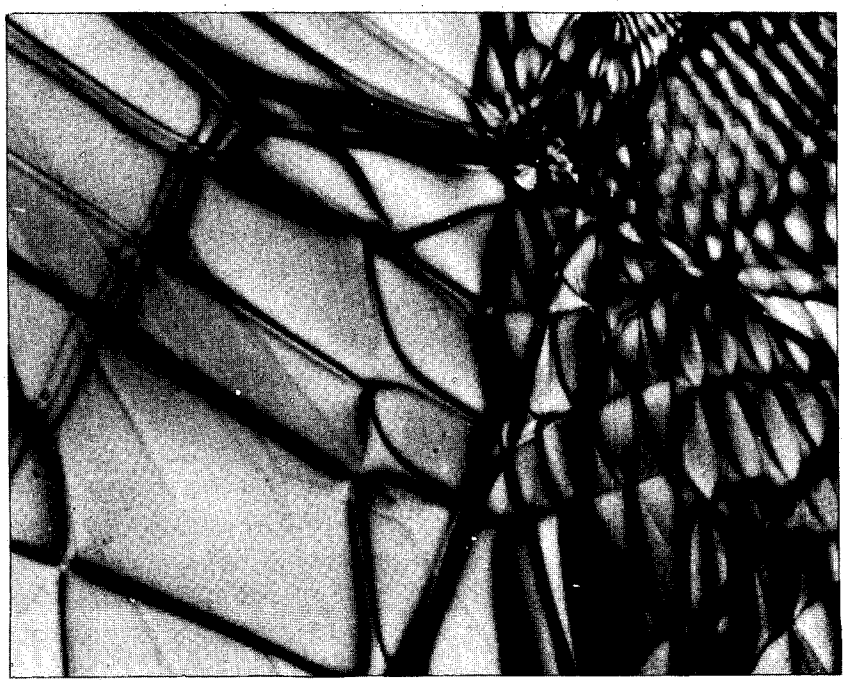

P 2041 (1800×)

Fig. 51--Transmission electron micrograph of single-crystal graphite deformed at room temperature, showing various dislocation interactions

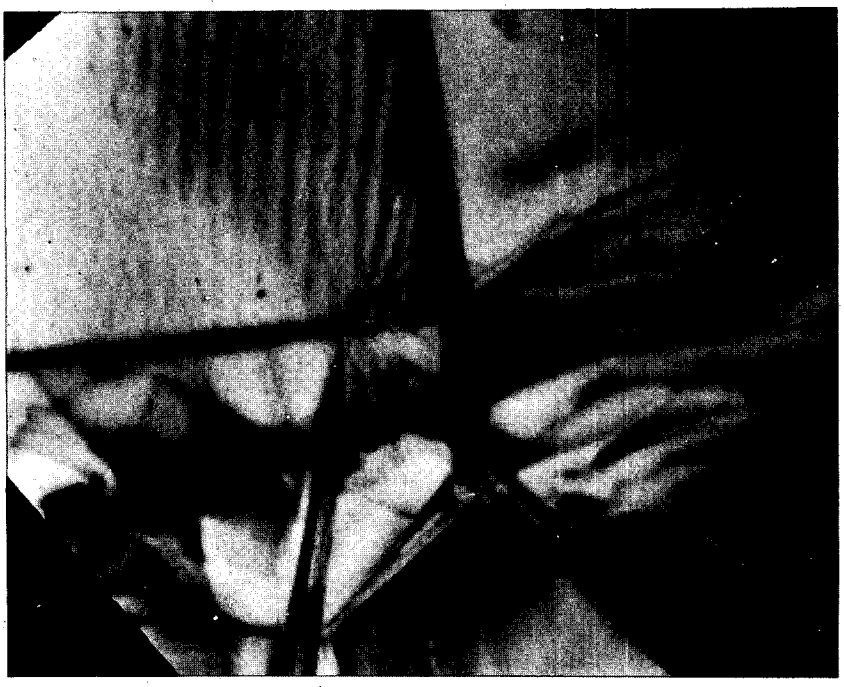

P 2056 (1800×)

Fig. 52--Transmission electron micrograph of single-crystal graphite deformed at room temperature, showing narrow kink bands

P 2292 (15,000×)

Fig. 53--Transmission electron micrograph of single-crystal graphite deformed at 2800°C, showing very closely spaced dislocation networks

P 2291 (15,000×)

Fig. 54--Transmission electron micrograph of single-crystal graphite deformed at 2800°C, showing dislocation networks with local dense clusters

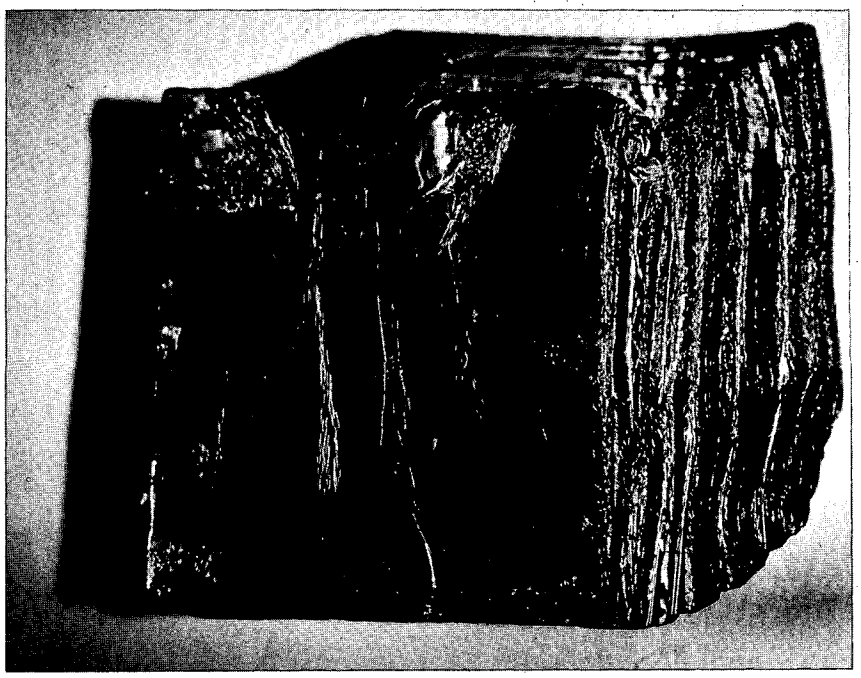

M-6604 (5×)

Fig. 55--Pyrolytic graphite deformed in compression perpendicular to the deposition plane at 3000°C after failure by sideway shearing (looking down onto the deposition plane)

at expanded or contracted nodes (see Fig. 51). The triangular regions in the expanded nodes show the type of contrast typical of stacking faults. Figure 51 also shows strong elastic interactions between crossing dislocations on neighboring planes, a triple dislocation,[43] and a faint network of very narrow ghost dislocations. The latter are probably very close to one free surface, which would account for the small separation of the partials[47] and the faint contrast. Measurements of the widths of double and triple extended dislocations[47] give a value of 0.5 to 0.7 ergs/cm for the stacking fault energy, in good agreement with other workers. Another interesting feature is the presence of "bubbles" ("hohlstelle") between the basal planes (Fig. 51) at which large numbers of dislocations are held up, suggesting that a high density of these defects should make graphite harder to deform. In addition, narrow kink bands are also seen (Fig. 52); the material inside these bands is tilted about an axis in the basal plane. These bands are almost certainly small-scale versions of the twins and kinks observed optically in large single crystals[26] and by electron microscopy on replicas taken from polycrystalline graphite (Section 2.5).

Specimens deformed at 2800°C show similar features to those deformed at room temperature, except that the dislocation networks are often more closely spaced (see Figs. 53 and 54). Very dense local clusters of dislocations are also present (Fig. 54), suggesting the presence of obstacles introduced by the high-temperature deformation. However, the poor contrast resulting from the strain fields of the dense networks makes it impossible to identify the obstacles. In future work it is hoped to look at specimens deformed at high temperatures by extension in the basal planes rather than by bending. This should minimize the generation of basal dislocations in favor of alternative deformation mechanisms, which should simplify identification of these mechanisms by electron transmission microscopy.

4.6.2. High-temperature Compression Test

A sample of commercially manufactured pyrolytic carbon (deposited at 2200°C and having a Bacon anisotropy factor[22] of 6.2 and a density of 2.195 g/cm^2) was loaded in compression perpendicular to the deposition plane at a temperature of 3000°C. There was no measurable compressive strain until the stress reached 6000 psi, when the specimen failed by shearing sideway, like a deck of cards (Fig. 55). This suggests that even at this high temperature slip parallel to the basal planes is still the easiest deformation mechanism, and the secondary mechanisms need a much higher stress to activate them.

The material in the sheared zone of the deformed sample had physical characteristics similar to those of a single crystal of graphite. It was very easily cleaved and thin slices were sufficiently flexible to be

plastically bent at room temperature. This material appeared to be much closer to a perfect single crystal than a comparison sample heated to 3300°C without deformation.

4.6.3. High-temperature Testing Facility

A high-temperature furnace has been fitted to an existing Baldwin testing machine for use in studies of deformation mechanisms and to provide better data on the deformation characteristics of both graphite and carbide-loaded graphite in the hot-working temperature range. Provision is being made for testing in either compression or tension at temperatures up to 3000°C either in an inert atmosphere or in a vacuum.

Heating will be accomplished by a cylindrical graphite heating element powered by an 80-kva saturable-core reactor. In compression the load will be transmitted by water-cooled rams with graphite end-pieces and in tension by carbon pull-rods. In both cases the load will be recorded by the Baldwin load cell arrangement. Temperature will be controlled and measured by radiometric methods. Initially strain will be measured with extensometer rods from the specimen to external strain gauges, but the sight ports are large enough to allow optical strain measurement if this should become necessary.

REFERENCES

1. Goeddel, W. V., J. L. White, and L. R. Zumwalt (eds.) "Advanced, Graphite Matrix, Dispersion-Type Fuel Systems," Parts 1 and 2, Annual Report, April 1, 1962, through March 31, 1963, General Atomic Report GA-4022, May 1, 1963.

2. Bokros, J. C., W. V. Goeddel, J. R. Hooker, H. K. Lonsdale, J. L. White, and L. R. Zumwalt (eds.), "Advanced, Graphite-Matrix, Dispersion-Type Fuel Systems," Annual Report, April 1, 1963, through March 31, 1963, General Atomic Report GA-5016.

3. Price, R. J., and J. L. White, "Research on Graphite," Quarterly Progress Report for Period Ending September 30, 1963, General Atomic Report GA-4675, October 31, 1963.

4. Price, R. J., and J. L. White, "Research on Graphite," Quarterly Progress Report for Period Ending December 31, 1963, General Atomic Report GA-4901, February 13, 1964.

5. Clark, T. J., "Metallographic Studies of Reactor Graphite Materials. Part I, Cokes," Hanford Laboratories Report HW-68182, Part 1, February 10, 1961.

6. Coy, W. J., "An Electron Microscope Study of Pyrolytic Graphite," J. Amer. Ceram. Soc. 45, 223 (1962).

7. Hales, R. L., and E. M. Woodruff, "Technique for Microscopic Studies of Graphite," Proc. Fifth Carbon Conf. 1, 456 (1962).

8. Kotlensky, W. V., and H. E. Martens, "Structural Transformation in Pyrolytic Graphite Accompanying Deformation," Jet Propulsion Laboratory Report 32-360, November 1, 1962.

9. Martens, H. E., and W. V. Kotlensky, "Structural and High-Temperature Tensile Properties of Special Pitch-Coke Graphites," Jet Propulsion Laboratory Report 32-181, November 30, 1961.

10. Peters, G. L., and H. D. Shade, "Photomicrographic Techniques for Carbon and Graphite," Sixth Carbon Conference, Pittsburgh, June, 1963 (to be published).

11. Pincus, I., and N. J. Gendron, "Microscopy in Structures of Brush Carbons," Proc. Fourth Carbon Conf., 687 (1959).

12. Susich, G., and L. M. Dogliotti, "The Microscopic Comparison of the Structure of Pyrographite with That of Natural Graphite and Graphite Whiskers," Quartermaster Research and Engineering Command, Technical Report PR-4, May, 1962.

13. Tarpinian, A., and G. B. Gazza, "A Technique for the Microstructural Examination of Polycrystalline Graphites," Watertown Arsenal Laboratory Technical Report WAL-TR-132.5/1, February, 1959.

14. Tarpinian, A., "Crystallographic and Microstructural Changes Occurring during the Graphitization of a Petroleum Coke," Watertown Arsenal Laboratory Technical Report WAL-TR825.5/1, January, 1960.

15. Sutton, A. L., and V. C. Howard, "The Role of Porosity in the Accommodation of Thermal Expansion in Graphite," J. Nucl. Matls. 1, 58 (1962).

16. Thrower, P. A., and W. N. Reynolds, "Microstructural Changes in Neutron-Irradiated Graphite," J. Nucl. Matls. 8, 221 (1963).

17. Jenkins, G. M., "Fracture in Reactor Graphite," J. Nucl. Matls. 5, 280 (1962).

18. Mrozowski, S., "Mechanical Strength and Structure of Carbons," Proc. First and Second Carbon Confs., 31 (1956).

19. Loch, L. D., A. B. Austin, R. D. Harrison, and W. H. Duckworth, "Effect of Constitution of Graphites on Their Stability Under Low-Temperature Irradiation," Battelle Memorial Institute Report BMI-1042, September 30, 1955.

20. Bierlein, T. K., H. W. Newkirk, Jr., and B. Mastel, "Etching of Refractories and Cements by Ion Bombardment," J. Amer. Ceram. Soc. 46, 196 (1958).

21. Oberlin, M., J. Rappeneau, and M. Yvars, "Kinetics of the Oxidation in Liquid Phase of Non-irradiated and Irradiated Nuclear Graphites," Sixth Carbon Conference (to be published).

22. Bacon, G. E., "A Method for Determining the Degree of Orientation of Graphites," J. Appl. Chem. 6, 477 (1956).

23. Neel, E. A., A. A. Kellar, and J. J. Zeitsch, "High-Density Recrystallized Graphite by Hot Forming," National Carbon Company Report WADD-TR-61-72, Vol. VII, June, 1962.

24. Bushong, R. M., and E. A. Neel, "Properties of High-Density, Recrystallized Graphite," Proc. Fifth Carbon Conf. 1, 595 (1962).

25. Nightingale, R. E., "Structure," in Nuclear Graphite, R. E. Nightingale (ed.), Academic Press, New York, 1962, Chap. 5.

26. Freise, E. J., and A. Kelly, "Twinning in Graphite," Proc. Roy. Soc. (London) A264, 269 (1961).

27. Seldin, E. J., "High-Temperature Tensile Creep of Graphite," Sixth Carbon Conference (to be published).

28. Hansen, M., and K. Anderko, Constitution of Binary Alloys, McGraw-Hill, New York, 1958.

29. Minkoff, I., and I. Einbinder, "Dendritic Growth of Graphite from Melts," Nature 194, 765 (1962).

30. Pappis, J., C. Cvikevich, L. Hagen, and N. Viola, "The Thermal Expansion of Pyrolytic Graphite," in High Temperature Materials II (G. M. Ault, et al., eds.) Interscience, New York, 1962, p. 419.

31. Nelson, J. B., and D. P. Riley, "The Thermal Expansion of Graphite from 15°C to 800°C," Proc. Phys. Soc. (London) 57, 477 (1945).

32. Lynch, J. J., "The Measurement of Residual Stresses," in Residual Stress Measurements, A.S.M., Cleveland, 1952, pp. 42 ff.

33. Tully, G. R., private communication.

34. Schmid, E., and W. Boas, Plasticity of Crystals, F. A. Hughes, London, 1950.

35. Spence, G. B., "Application of Anisotropic Elastic Continuum Theory to Dislocations in Graphite," National Carbon Company Report WADD-TR-61-72, Vol. II, 1962.

36. Bowman, J. C., and J. A. Krumhansl, "Low Temperature Specific Heat of Graphite," J. Phys. Chem. Solids 6, 367 (1958).

37. Baker, C. and A. Kelly, "Studies of Radiation in Single Crystal Graphite," Sixth Carbon Conference (to be published).

38. Simmons, J. H. W., "The Effects of Irradiation on the Mechanical Properties of Graphite," Proc. Third Carbon Conf., 559 (1960).

39. Bridge, H., B. T. Kelly, and P. T. Nettley, "The Effect of High-Flux Fast-Neutron Irradiation on the Physical Properties of Graphite," UKAEA, TRG-Report-567(C), 1963.

40. Nightingale, R. E., "Summary of Recent Hanford Irradiations," Hanford Atomic Products Operation Report HW-SA-2467, 1962.

41. Helm, J. W., and J. M. Davidson, "Effect of Massive Neutron Exposure on the Distortion of Reactor Graphite," Hanford Atomic Products Operation Report HW-SA-2926, 1963.

42. Yoshikawa, H. H., "The Effect of Radiation on Pyrolytic Graphite," Hanford Atomic Products Operation Report HW-78645, 1964.

43. Delavignette, P., and S. Amelinckx, "Dislocation Patterns in Graphite," J. Nucl. Matls. 5, 17 (1962).

44. Kotlensky, W. V., and H. E. Martens, "Tensile Properties of Pyrolytic Graphite to 5000°F," Jet Propulsion Laboratory Technical Report 32-71, 1961.

45. Stover, E. R., "Mechanisms of Deformation and Fracture in Pyrolytic Graphite," General Electric Research Laboratory Report 61-RL-2745M, 1961.

46. Jenkins, G. M., and G. K. Williamson, "Deformation and Creep Mechanisms in Graphite," C. E. G. B., Berkeley Nuclear Laboratories Report RD/B/N. 113, 1963.

47. Spence, G. B., "Theory of Extended Dislocations in Symmetry Directions in Anisotropic Infinite Crystals and Thin Plates," J. Appl. Phys. 33, 729 (1962).